THE UNIVERSITY OF QUEENSLAND

AUSTRALIA

Modelling Spin-Crossover Lattices with Machine-Learned Force Fields

Huiwen Tan

Under the supervision of Professor Ben Powell

and Dr Carla Verdi

A thesis submitted for

the degree of Bachelor of Advanced Science with Honours

at The University of Queensland in October 2024

School of Chemistry and Molecular Biosciences

Abstract

Machine learning force fields (MLFF) have received increasing attention recently due to their ability to describe interatomic potentials with quantum-level accuracy while scaling to classical systems. The accuracy of the machine-learned potentials highly depends on the choice of the underlying *ab initio* reference method. However, modelling spin-crossover (SCO) lattices using density functional theory (DFT) still presents difficulties, especially in balancing accuracy and efficiency when predicting the energy difference between the high- and low-spin states at 0 K, known as the enthalpy difference.

In this thesis, a semi-empirical DFT method was employed to train MLFFs for $[Fe(ptz)_6](BF_4)_2$ (ptz = 1-propyltetrazole) on the fly during molecular dynamics (MD) simulations. The developed MLFFs achieved DFT-level accuracy with high efficiency across a series of benchmarks and successfully predicted the thermal expansion effect of the SCO system using quasi-harmonic approximations. This study provides key insight into modelling SCO with DFT, highlighting the critical role of zero-point effects in the enthalpy difference calculation. Combining a reliable DFT reference with MLFF provides a promising strategy for accurately and efficiently simulating the lattice dynamics of SCO systems. Additionally, a potential scheme for MLFF-driven MD simulations was proposed.

Declaration by author

This research report is composed of my original work, and contains no material previously published or written by another person except where due reference has been made in the text. I have clearly stated the contribution by others to jointly-authored works that I have included in my report.

I have clearly stated the contribution of others to my research report as a whole, including statistical assistance, survey design, data analysis, significant technical procedures, professional editorial advice, and any other original research work used or reported in my report. The content of my report is the result of work I have carried out since the commencement of my honours research project and does not include a substantial part of work that has been submitted to qualify for the award of any other degree or diploma in any university or other tertiary institution. I have clearly stated which parts of my research report, if any, have been submitted to qualify for another award.

I acknowledge that copyright of all material contained in my research report resides with the copyright holder(s) of that material. Where appropriate I have obtained copyright permission from the copyright holder to reproduce material in this thesis and have sought permission from co-authors for any jointly authored works included in the thesis.

Signature of Author:

Huiwen Tan 21/10/24

Principal Supervisor Agreement

I have read the final report and agree with the student's declaration.

Signature of Principal Supervisor:

21/10/24

Acknowledgments

First, I would like to sincerely thank my supervisor, Professor Ben Powell, for providing extensive theoretical guidance for my project. Thanks to him for selecting me from the summer research program two years ago and always supporting me to do my favourite and exciting projects, which has greatly improved my research skills.

I deeply appreciate my co-supervisor, Dr. Carla Verdi. She's so nice, responsible, and patient. She was the first teacher who gave me hands-on guidance on how to do calculations. I appreciate that she always took the time to write long emails and answer my questions carefully.

Thanks also to Dr. Muhammad Nadeem for patiently answering my questions. I've learned much from him about paper writing, plotting figures, and using LaTeX. I also want to thank the people in the Powell group for their helpful talks, which allowed me to learn new knowledge at the weekly Cake Meeting.

To my friends at UQ, especially Liyuan Zhu, Ben Jiang, and Xie He, thank you for inviting me out for meals every week and discussing science and first-year tutoring with me. I'm so glad I met you guys in CHEM3011.

Finally, thanks to UQ for providing many undergraduate research opportunities and making every day of my undergraduate life meaningful.

Thanks to chemistry for lighting up my life!

Contents

Abstract ii

Contents **v**

List of Figures **viii**

List of Tables **xii**

List of abbreviations **xiii**

1 Introduction **1**

1.1 Spin Crossover Materials 3

1.2 Experimental Characterisations of Spin Crossover Properties 7

1.3 Modelling Approaches for Spin Crossover Systems 13

2 Theory **17**

2.1 Density Functional Theory 17

2.1.1 The Schrödinger equation and Born-Oppenheimer approximation 18

2.1.2 Hohenberg-Kohn theorems 19

2.1.3 Kohn-Sham DFT 20

2.1.4 Exchange-correlation functionals 21

2.1.5 DFT+U: adding a Hubbard U term to localised functional . . . 24

2.2 Lattice Dynamics . . . 24

2.2.1 Harmonic lattice dynamics . . . 25

2.2.2 Quasi harmonic approximations . . . 26

3 Method **27**

3.1 Software . . . 27

3.2 Choice of DFT Method . . . 28

3.3 Reference Data . . . 29

3.4 Training Data . . . 30

3.5 Quasi-Harmonic Approximation Based on Machine Learning Force Fields . . . 32

4 Results and Discussion **33**

4.1 Overview of Reference *Ab Initio* Method . . . 34

4.2 Parameterisation of Machine-learned Force Fields . . . 35

4.3 Benchmarking: Prediction of Energies and Forces . . . 37

4.4 Benchmarking: Crystallography and Enthalpy Differences . . . 38

4.5 Benchmarking: Phonons . . . 40

4.6 Force Field-Predicted Quasi-Harmonic Approximation Calculations . . . 42

5 Conclusion **47**

5.1 Future Work . . . 48

5.1.1 Machine Learning-Driven Molecular Dynamics Simulations . . . 48

Bibliography **51**

A Appendix **63**

A.1 Time Information 63

A.2 Starting Geometries in POSCAR Format 64

A.3 Relaxed Geometries in POSCAR Format 79

A.4 KPOINTS 93

A.5 POTCAR 94

A.6 INCAR 94

A.6.1 Full relaxations under PBE-D3(BJ)+U 94

A.6.2 Self-consistent calculations under PBE-D3(BJ)+U 96

A.6.3 Phonon calculations under PBE-D3(BJ)+U 98

A.6.4 On-the-fly training of MLFF 101

A.7 Python Script for ML-Driven MD simulations 104

List of Figures

1.1 The chemical structure of $[Fe(ptz)_6](BF_4)_2$ (ptz = 1-propyltetrazole), all hydrogen atoms are omitted for clarity. 2

1.2 Energy level diagram of the Fe(II) ion in an octahedral crystal field, demonstrating the influence of the crystal field on taking the two possible states: low-spin (LS) or high-spin (HS) state. Δ_o is the crystal field splitting energy and P is the pairing energy. This figure is taken from Vallone *et al.*[1] 4

1.3 Temperature dependence of (a) vibrational enthalpy ΔH^{vib}_{HL} and (b) vibrational entropy ΔS^{vib}_{HL} in a single-molecule model of $[Fe(dppen)_2X_2]\cdot Sol$ (X = {Br, Cl}, Sol = {vacuum, chloroform, dichloromethane}, dppen = bis(diphenylphosphino)ethene), computed using the PBE functional. This figure is taken from Tan *et al.*[2] 5

1.4 Diagram of the Gibbs free energy surface G variation of Fe(II) materials in the respective spin states with temperature, where $T_2 > T_1$. The relationships between the octahedral crystal field splitting energy are $\Delta_{LS}(T_1) > \Delta_{LS}(T_2)$ and $\Delta_{HS}(T_1) > \Delta_{HS}(T_2)$. This figure is reprinted from Shelest *et al.*[3] 7

1.5 The SQUID magnetic measurements of the $[Fe(ptz)_6](BF_4)_2$ single crystal include slow cooling (black) and heating after slow (blue) and fast (red) cooling, as well as the LIESST (green) at 10 K. The inserts illustrate the temperature derivatives of the relaxation curves in the low-temperature range and the time dependence of magnetisation×temperature after irradiation. This figure is taken from Kusz *et al.*[4] 12

1.6 At various U_{eff} values, the error between the ΔH_{HL} predicted by PBE+U using the Dudarev approximation and the experimental values. This figure is reprinted from Ohlrich and Powell.[5] 14

4.1 (a) U_{eff}-dependence of the enthalpy difference ΔH_{HL}. The unit cells of $[Fe(ptz)_6](BF_4)_2$ in LS and HS states were fully relaxed using the PBE-D3(BJ)+U method with different U_{eff} values. The calculated ΔH_{HL} at each U_{eff} was obtained from self-consistent calculations on the optimised structures using the same functional. The experimental ΔH_{HL} is 63.2 meV; (b) The absolute error between the calculated and experimental values of ΔH_{HL} under different U_{eff} values. The optimal U_{eff} of 1.9 eV was obtained at the minimum absolute error. 33

4.2 (a) Fluctuations in total energy, free energy, and temperature in the LS state system during 8000 timesteps of MD simulations. For the first 5000 MD steps, the temperature was controlled at 300 K. In the subsequent 3000 steps, the system temperature was set to 100 K for further training to capture more configurations within the SCO temperature range. (b) Evolution of the real errors in forces (ERR), Bayesian error estimations in forces (BEEF), and learning threshold (CTIFOR) during the training of the LS state MLFF; (c) Changes in total energy, free energy, and temperature in the HS state system over 14000 MD steps. The first 5000 steps were performed at 300 K, followed by 9000 steps at 100 K to sample a comparable number of configurations to the LS state; (d) Evolution of ERR, BEEF, and CTIFOR in forces during HS state MLFF training. 36

4.3 Regression results comparing the force field data with the *ab initio* data in the final refitting step for (a) total energies of the LS state, (b) forces on atoms in the LS state, (c) total energies of the HS state and (d) forces on atoms in the HS state. The diagonal grey line represents a perfect fit, indicating that the MLFF and *ab initio* data are identical. The closer the data points are to this line, the better the fit. 37

4.4 The comparison of phonon density of states by DFT calculations (lines) and MLFF predictions (shaded areas) for (a) LS states and (b) HS states. 41

4.5 (a) The electronic energy surfaces $E(V)$ of the LS and HS states constructed by quadratic fitting of data points; (b) The Helmholtz free energy surfaces $F(V)$ at 0 K, which also represent the surfaces of electronic energy E plus zero-point motion energy F^{ZP}. 42

4.6 The Helmholtz free energy F of the LS and HS states versus volume at temperatures from 0 K to 290 K in 10 K intervals. The Helmholtz free energy surfaces of the LS state (solid lines) and HS state (dotted lines) were obtained by quadratic fitting of the plus-sign and circle data points, respectively. The data points were generated by QHA calculations based on MLFFs. 44

4.7 (a) Equilibrium volume V_{eq} of $[Fe(ptz)_6](BF_4)_2$ unit cell as a function of temperature in LS and HS states; (b) Variation of the thermal expansion coefficient α_V with the temperature predicted by the MLFFs. 45

5.1 Flowchart of molecular dynamics simulations driven by machine learned force fields. . . 48

List of Tables

1.1 Fe-N stretching frequency changes upon SCO in iron(II) compounds, where ω_{LS} and ω_{HS} are Fe-N stretching force constants of LS and HS states. This table is reproduced from Tuchagues *et al.*[6] 9

1.2 Experimental data for $[Fe(ptz)_6](BF_4)_2$. This table is taken from Kusz *et al.*[7] 11

3.1 Datasets used in MLFF training. 31

4.1 Final root mean square errors (RMSEs) of MLFFs. 38

4.2 Crystallographic and energy information of $[Fe(ptz)_6](BF_4)_2$ obtained by experiments[7] and calculations. 39

A.1 Computational time and the number of CPUs used for various job types. 63

List of abbreviations

AIMD	*Ab initio* molecular dynamics
ASE	Atomic Simulation Environment
BEEF	Bayesian error estimations in forces
BJ	Becke-Johnson
CTIFOR	Learning threshold
DFT	Density functional theory
DSC	Differential scanning calorimetry
dppen	Bis(diphenylphosphino)ethene
ELM	Electron energy minimisation
ERR	Real errors in forces
FF	Force field
GGA	Generalised gradient approximation
HF	Hartree-Fock
HS	High-spin
IOM	Ionic optimisation minimisation
IS	Intermediate spin
LDA	Local density approximation

LIESST	Light-induced excited spin state trapping
LS	Low-spin
MBD	Many-body dispersion
MD	Molecular dynamics
ML	Machine learning
MLFF	Machine learning force field
Meta-GGA/mGGA	Meta-generalised gradient approximation
NMR	Nuclear magnetic resonance
PAW	Projector augmented wave
PBE	Perdew-Burke-Ernzerhof
pDoS	Phonon density of states
ptz	1-propyltetrazole
QHA	Quasi-harmonic approximation
RMSE	Root mean square error
SCO	Spin crossover
SOC	Spin-orbit coupling
SQUID	Superconducting quantum interference device
TS-vdW	Tkatchenko-Scheffler van der Waals
VASP	Vienna *Ab initio* Simulation Package
VESTA	Visualisation for Electronic and Structural Analysis
XC	Exchange-correlation
XDM	Exchange-dipole moment

Chapter 1

Introduction

Some first-row transition metal complexes with d^4 to d^7 electronic configurations in octahedral molecular geometries exhibit a crossover or phase transition in the solid state between low-spin (LS) and high-spin (HS) states under external perturbations such as temperature,[8,9] light irradiation,[10,11] pressure,[12] and magnetic field.[13] Dramatic variations in the physical properties of materials, like magnetism,[14] volume,[15] crystal structure,[16] conductivity,[17,18] and colour,[19] usually accompany such spin crossover (SCO). Consequently, the SCO phenomenon can be characterised by various experimental techniques, including X-ray diffraction,[20] calorimetry,[21,22] vibrational spectroscopy,[6] and magnetic susceptibility measurements.[23] SCO materials have been extensively studied over recent decades because of their potential applications as molecular switches[24] in nanoscale devices for memory,[25] sensing,[26,27] display,[28] and actuation.[29] The realisation of these applications relies on the successful design and synthesis of SCO compounds that can undergo spin-state switching under ambient conditions.[30]

Screening SCO materials with desired properties in the laboratory is labour-intensive and time-consuming. First principle calculations, starting from quantum mechanics, can establish the relationship between structure and properties without relying on empirical parameters, thus providing crucial

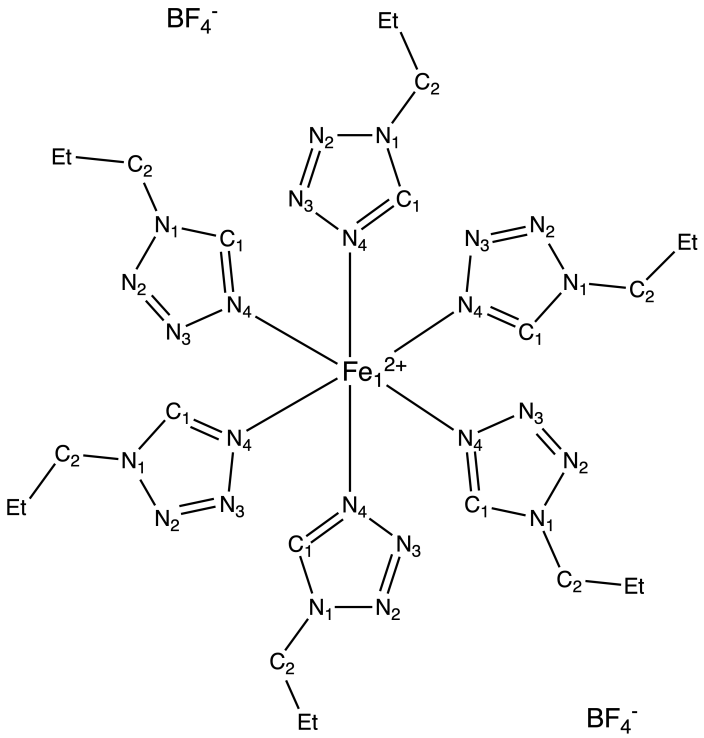

Figure 1.1: The chemical structure of $[Fe(ptz)_6](BF_4)_2$ (ptz = 1-propyltetrazole), all hydrogen atoms are omitted for clarity.

insights into the experimental design of materials with desired properties.[31] Whilst first-principle methods, represented by density functional theory (DFT), can offer accurate predictions, they still face challenges in scaling up to large systems and long timescales owing to current computational limitations. In recent years, machine learning (ML) has been reported as a promising complement to first-principles calculations for accelerating the discovery of candidate materials.[32–34]

The main objective of this thesis is to develop on-the-fly machine learning force fields (MLFFs) for an extensively studied d^6 SCO system, $[Fe(ptz)_6](BF_4)_2$ (ptz = 1-propyltetrazole), whose chemical structure is shown in figure 1.1. We show that MLFFs can achieve an accuracy comparable to DFT in predicting spin crossover-related properties. The thermal effects in the SCO phenomenon can be accurately captured by calculating the vibrational contributions to free energy using the quasi-harmonic approximation (QHA). This calculation would be time-consuming with DFT.

In this chapter, we first provide a brief introduction to SCO complexes in section 1.1, followed by

a discussion of commonly used experimental characterisation techniques in section 1.2, along with a thorough review of the experimental literature referred to in this thesis. In section 1.3, we review molecular modelling methods utilised in previous SCO studies.

1.1 Spin Crossover Materials

The failure of traditional valence bond theory[35] on transition metal complexes revealed that understanding the origin of the SCO phenomenon requires consideration of the impact of ligands on the *d*-electrons of the central metal ion. As the simplest approach to this system, crystal field theory assumes that the metal-ligand interactions are purely electrostatic.[36] In a molecule with an octahedral ligand geometry, the ligands are treated as negative charges located at the vertices of the octahedron, thus generating a negative potential field known as the crystal field, with the metal cation placed at the centre of the octahedron. As a result of unequal repulsion from the octahedral crystal field, the five-fold degeneracy of the *d* orbitals (d_{z^2}, d_{xz}, d_{yz}, d_{xy}, and $d_{x^2-y^2}$) in the free metal ion is broken, splitting into two orbital sets with different energies, the lower energy three-fold degenerate t_{2g} orbital set (d_{xz}, d_{yz}, and d_{xy}) and the higher energy two-fold degenerate e_g orbital set (d_{z^2} and $d_{x^2-y^2}$).

In simple terms, the spin state of the metal centre hinges on the relative size of the crystal field splitting energy Δ_o and the pairing energy P, where Δ_o is the energy gap between the two orbital sets, whose magnitude depends on the crystal field strength, and P is the energy compensation that forces two electrostatically repulsive electrons to occupy the same orbital. Schematic electronic configurations of the Fe(II) complex, which is the focus of this project, are shown in figure 1.2. Under a strong crystal field, the splitting energy is greater than the pairing energy. So in the ground state, all six electrons occupy the t_{2g} orbitals, and the Fe(II) ion is in the LS singlet state (total spin angular

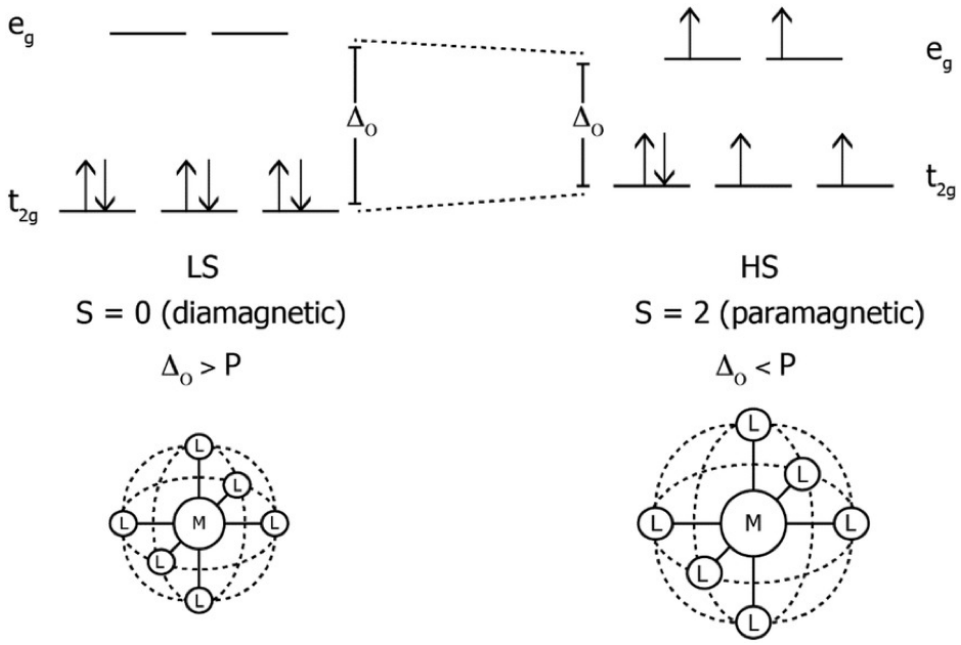

Figure 1.2: Energy level diagram of the Fe(II) ion in an octahedral crystal field, demonstrating the influence of the crystal field on taking the two possible states: low-spin (LS) or high-spin (HS) state. Δ_o is the crystal field splitting energy and P is the pairing energy. This figure is taken from Vallone *et al.*[1]

momentum S = 0 and spin multiplicity 2S + 1 = 1). If the crystal field strength is weaker than the pairing energy, the *d* electrons tend to be unpaired, and two electrons occupy the e_g orbitals of higher energies, resulting in the Fe(II) ion in the HS quintuplet state (S = 2 and 2S + 1 = 5) with four unpaired electrons. If the energies of LS and HS states are close, the molecule displays the bistable spin-state switching characteristics, which is the theoretical basis of the SCO phenomenon.

The transitions between spin states result in subtle changes in various properties of the compound. One of the most notable properties is magnetism. The HS state, which contains unpaired electrons, is paramagnetic, while the LS state, in which all electrons are paired, is diamagnetic. This makes the HS complexes have stronger magnetic susceptibilities than the LS complexes. The other is structural, the spin switching from the LS to the HS state involves the promotion of two electrons from the non-bonding t_{2g} orbitals into the anti-bonding e_g orbitals, which lengthens the metal-ligand bonds and usually accompanies distortions in bond angles.[37] The variations in molecular structure are

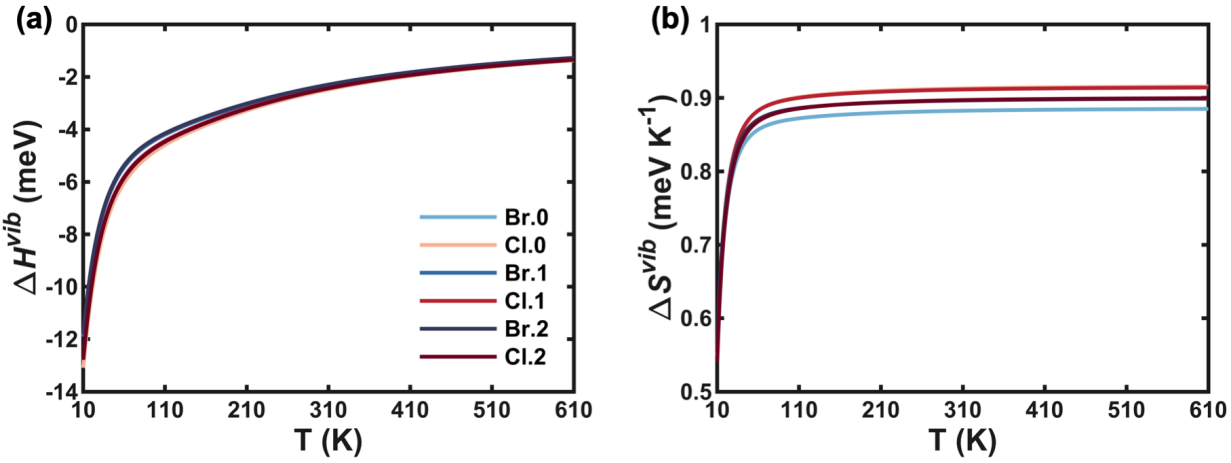

Figure 1.3: Temperature dependence of (a) vibrational enthalpy $\Delta H^{vib}_{\mathrm{HL}}$ and (b) vibrational entropy $\Delta S^{vib}_{\mathrm{HL}}$ in a single-molecule model of $[\mathrm{Fe(dppen)_2X_2}]\cdot\mathrm{Sol}$ (X = {Br, Cl}, Sol = {vacuum, chloroform, dichloromethane}, dppen = bis(diphenylphosphino)ethene), computed using the PBE functional. This figure is taken from Tan *et al.*[2]

cooperatively transmitted in solids through elastic interactions,[38] explaining the enormous changes in the size and shape of crystals observed in the SCO phenomenon. Also, the weakening of the Fe(II)-ligand bonds from the LS to HS states leads to a prominent decrease in the associated vibrational frequencies ω.[6]

Thermally-induced SCO is the crossover or phase transistion from the LS state at low temperature to the HS state at high temperature. This phenomenon is driven by the Gibbs free energy. The difference in the Gibbs free energy of the two spin states can be expressed as,

$$\Delta G_{\mathrm{HL}} = G_{\mathrm{HS}} - G_{\mathrm{LS}} = \Delta H_{\mathrm{HL}} - T\Delta S_{\mathrm{HL}} \tag{1.1}$$

where the enthalpy change of the system $\Delta H_{\mathrm{HL}} = H_{\mathrm{HS}} - H_{\mathrm{LS}}$ and the entropy change $\Delta S_{\mathrm{HL}} = S_{\mathrm{HS}} - S_{\mathrm{LS}}$. For a particular spin state, the enthalpy can be further expressed as,

$$H_{\mathrm{HS/LS}} = H^{elec}_{\mathrm{HS/LS}} + H^{vib}_{\mathrm{HS/LS}} \tag{1.2}$$

In SCO molecules, the difference between the temperature-independent electronic term $H^{elec}_{\mathrm{HS/LS}}$ of the HS state and LS state, $\Delta H^{elec}_{\mathrm{HL}}$, must be greater than zero to ensure that the LS state is realised

at cryogenic temperatures. For a single molecule, the vibrational term $H^{vib}_{\mathrm{HS/LS}}$ is described by the frequency ω of vibrational modes,[39]

$$H^{vib}_{\mathrm{HS/LS}}(T) = \sum_{i=1}^{3N-6}\left(\frac{\hbar\omega_{i,\mathrm{HS/LS}}}{2} + \frac{\hbar\omega_{i,\mathrm{HS/LS}}\exp\left(-\frac{\hbar\omega_{i,\mathrm{HS/LS}}}{k_{\mathrm{B}}T}\right)}{1-\exp\left(-\frac{\hbar\omega_{i,\mathrm{HS/LS}}}{k_{\mathrm{B}}T}\right)}\right) \tag{1.3}$$

where N is the number of atoms in the molecule, k_{B} is the Boltzmann constant, and $\hbar$ is the reduced Planck constant. The first term is called zero-point vibrational energy,

$$H^{\mathrm{ZP}}_{\mathrm{HS/LS}} = \sum_{i=1}^{3N-6}\left(\frac{\hbar\omega_{i,\mathrm{HS/LS}}}{2}\right) \tag{1.4}$$

which arises from the vibrational motion of molecular systems, even at 0 K. In single SCO molecules, H^{vib}_{LS} is greater than H^{vib}_{HS}, and their difference decreases with increasing temperature, as shown in figure 1.3 (a). Similarly, the entropy for HS/LS state can be represented as,

$$S_{\mathrm{HS/LS}} = S^{elec}_{\mathrm{HS/LS}} + S^{vib}_{\mathrm{HS/LS}} \tag{1.5}$$

The electronic entropy $S^{elec}_{\mathrm{HS/LS}}$ has contributions from both the orbital part, $S^{orb}_{\mathrm{HS/LS}} = R\ln(2L_{\mathrm{HS/LS}}+1)$, and the spin part, $S^{spin}_{\mathrm{HS/LS}} = R\ln(2S_{\mathrm{HS/LS}}+1)$, where R is the ideal gas constant. This indicates that $\Delta S^{elec}_{\mathrm{HL}} = S^{elec}_{\mathrm{HS}} - S^{elec}_{\mathrm{LS}}$ arises from the difference in the degeneracies of the total orbital momentum $L_{\mathrm{HS/LS}}$ and the total spin momentum $S_{\mathrm{HS/LS}}$ between two spin states.[40] Hence, $\Delta S^{elec}_{\mathrm{HL}} = \Delta S^{orb}_{HL} + \Delta S^{spin}_{HL} = R\ln(3) + R\ln(5) = 0.23\ \mathrm{meV\,K^{-1}}$ for perfectly octahedral Fe(II) complexes.[41] For a single molecule, the vibrational entropy is[6]

$$S^{vib}_{\mathrm{HS/LS}}(T) = \sum_{i=1}^{3N-6}\left(\frac{\hbar\omega_{i,\mathrm{HS/LS}}}{2T\tanh\left(\frac{\hbar\omega_{i,\mathrm{HS/LS}}}{2k_{\mathrm{B}}T}\right)} - k_{\mathrm{B}}\ln\left[2\sinh\left(\frac{\hbar\omega_{i,\mathrm{HS/LS}}}{2k_{\mathrm{B}}T}\right)\right]\right) \tag{1.6}$$

Using the low-frequency approximation ($\hbar\omega_i \ll k_{\mathrm{B}}T$), it can be deduced that $\Delta S^{vib}_{\mathrm{HL}} = S^{vib}_{\mathrm{HS}} - S^{vib}_{\mathrm{LS}}$ is always positive and increases with temperature, as shown in figure 1.3 (b). This change is always, numerically, more remarkable than $\Delta S^{elec}_{\mathrm{HL}}$, generally between 0.42 and 0.83 $\mathrm{meV\,K^{-1}}$ for octahedral Fe(II) compounds with N-coordinated ligands.[42]

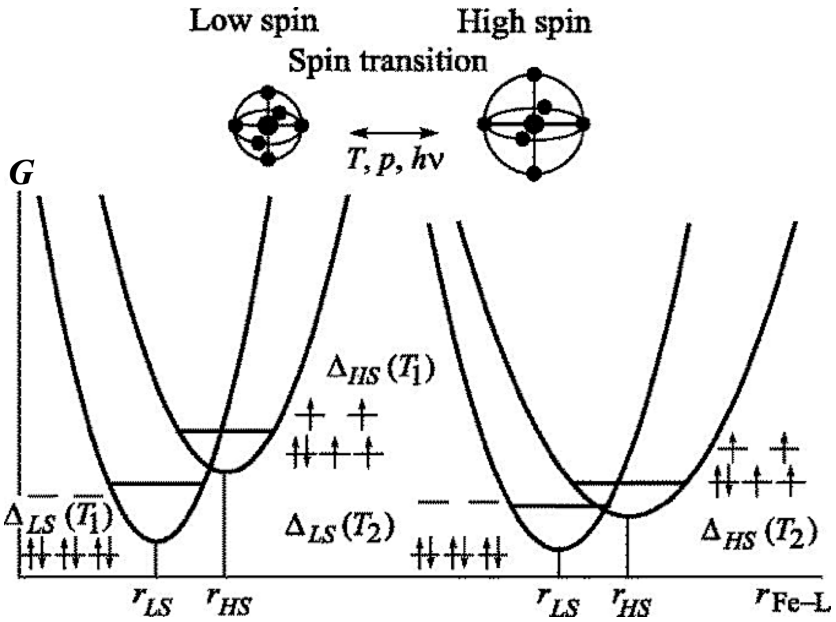

Figure 1.4: Diagram of the Gibbs free energy surface G variation of Fe(II) materials in the respective spin states with temperature, where $T_2 > T_1$. The relationships between the octahedral crystal field splitting energy are $\Delta_{LS}(T_1) > \Delta_{LS}(T_2)$ and $\Delta_{HS}(T_1) > \Delta_{HS}(T_2)$. This figure is reprinted from Shelest *et al.*[3]

Therefore, $T\Delta S_{\mathrm{HL}}$ increases significantly with temperature compared with ΔH_{HL} and exceeds ΔH_{HL} at the thermal transition temperature $T_{1/2}$, where the system crossovers from the LS to the HS state. More explicitly, $T_{1/2}$ is defined as the temperature where the HS and LS states are in thermodynamic equilibrium ($\Delta G_{\mathrm{HL}} = 0$),

$$T_{1/2} = \frac{\Delta H_{\mathrm{HL}}}{\Delta S_{\mathrm{HL}}} \tag{1.7}$$

At this temperature, half of the molecules in the system are in the LS state, and half are in the HS state. Figure 1.4 demonstrates that as the temperature rises, the free energy surface of the HS state gradually stabilises relative to the LS state.

1.2 Experimental Characterisations of Spin Crossover Properties

Established experimental studies are often the benchmark for assessing the accuracy of computational models. Before proceeding with computational work, a thorough understanding of the experimental

details presented in the literature is essential. In this section, we will first provide an overview of the experimental techniques used to characterise the properties of SCO materials and then highlight relevant experimental studies on the specific material of interest.

Experimentally, changes in structural, thermal, vibrational, and magnetic properties associated with spin state conversion can be detected by crystal structure determination, heat capacity measurements, vibrational spectroscopy, and magnetic susceptibility measurements. A precise description of the structural changes in the SCO phenomenon can be provided by X-ray crystallography. This technique can quantify the change in metal-ligand bond lengths due to the rearrangement of valence electrons. For Fe(II) SCO compounds with $[FeN_6]$ coordination cores, the average Fe-N bond lengths increase by 0.19 ± 0.05 Å in the HS state compared to the LS state, resulting in a volume expansion of $3.8 - 6.0\%$.[7] Additionally, crystal space group symmetry changes for some SCO complexes can be observed using X-ray diffraction. For instance, Kusz *et al.*[4] reported that $[Fe(ptz)_6](BF_4)_2$ undergoes ferroelastic transitions from the space group $R\bar{3}$ in the HS phase to the space group $P\bar{1}$ in the LS phase upon slow cooling.

Calorimetric measurements, in most cases using differential scanning calorimetry (DSC), give the enthalpy change, entropy change, transition temperature and other thermodynamic information of SCO compounds by measuring the heat capacity as a function of temperature. At constant pressure, heat capacity C_p can be expressed as the partial derivative of enthalpy with respect to temperature, i.e.,

$$C_p = \left(\frac{\partial H}{\partial T}\right)_p \tag{1.8}$$

When the system temperature approaches $T_{1/2}$, the SCO phenomenon induces a significant change in enthalpy, resulting in excess heat capacity, ΔC_p. This is obtained by subtracting the normal heat capacities from the heat capacity curve observed in the DSC measurement.[43] The ΔH_{HL} is derived

Table 1.1: Fe-N stretching frequency changes upon SCO in iron(II) compounds, where ω_{LS} and ω_{HS} are Fe-N stretching force constants of LS and HS states. This table is reproduced from Tuchagues *et al.*[6]

Compound	Fe-N stretching frequencies (cm^{-1})		ω_{LS}/ω_{HS}
	HS state	LS state	
$[Fe(X\text{-}bzimpy)_2](ClO_4)_2$ (X=H, OH, Cl)	220, 215, 212	436, 436, 436	2.0–2.1
$[Fe(X\text{-}bzimpyH_{-1})_2]$ (X=H, OH, Cl)	229, 217, 213	440, 436, 435	1.9–2.0
$[Fe(ptz)_6](BF_4)_2$	167, 231	261/279, 412	1.6, 1.8
$[Fe(phen)_2(NCS)_2]$	220, 252	368, 376	1.7, 1.5
$[Fe(phen)_2(^{15}N^{13}CS)_2]$	220, 248	368, 374	1.7, 1.5
$[Fe(phen)_2(NCSe)_2]$	218	363	1.7
$[Fe(bpy)_2(NCS)_2]$	235	384	1.6
$[Fe(HB(pz)_3)_2]$	223, 258	400, 434	1.8, 1.7
$[Fe(CH_3O\text{-}phen)_3](ClO_4)_2{\cdot}H_2O$	227, 237	341, 352	1.5
$[Fe(tpa)(NCS)_2]$	241, 242, 284	344, 375, 424	1.5
$[Fe(pz)(M(CN)_4)]{\cdot}2H_2O$ (M: Ni, Pd, Pt)	231, 223, 226	394, 390, 402	1.7–1.8
$[Fe(py)_2(M(CN)_4)]$ (M: Pd, Pt)	217, 221	383, 395	1.8

by integrating ΔC_p over T and the ΔS_{HL} is determined by integrating ΔC_p over $\ln(T)$.[40] It should be noted that when discussing ΔH_{HL} in the SCO systems, especially experimental ΔH_{HL}, the extrapolated energy difference between HS and LS states at 0 K is often used.

The spin transition affects specific ligand vibrational modes and metal-ligand stretching modes, which can be characterised using vibrational spectroscopy to investigate the vibrational contribution to the SCO process.[6] In infrared and Raman spectra, the weakening of the metal-ligand stretching modes in the LS-HS transition is observable through the band shift from high to low frequencies. Table 1.1 summarises the noteworthy change in Fe-N vibrational frequencies upon spin state switching.

Magnetic susceptibility measurements commonly involve using superconducting quantum interference device (SQUID), magnetometer or Faraday balance for solids and the Evans nuclear magnetic resonance (NMR) method for solutions.[23] The magnetic susceptibility χ of the sample as a function of temperature can be expressed as,[44]

$$\chi(T) = \gamma_{HS}(T)\chi_{HS} + (1 - \gamma_{HS}(T))\,\chi_{LS} \tag{1.9}$$

where γ_{HS} represents the proportion of HS molecules, χ_{LS} and χ_{HS} are the magnetic susceptibilities of the sample in the pure LS and HS states. In the heating and cooling modes, the temperatures at which $\gamma_{HS} = 0.5$ are defined as $T_{1/2\uparrow}$ and $T_{1/2\downarrow}$, respectively.[45] This gives the thermal SCO temperature,

$$T_{1/2} = \frac{1}{2}(T_{1/2\uparrow} + T_{1/2\downarrow}) \tag{1.10}$$

$[Fe(ptz)_6](BF_4)_2$ was reported by Decurtins *et al.*[46] in 1984 as the first example of the light-induced excited spin state trapping (LIESST) effect, wherein green light irradiation induces a transition from the ground LS phase to the long-lived metastable HS phase at low temperatures. A thermally induced spin transition from the LS to HS state was also observed at around 135 K. Hauser[47] later reported the reverse-LIESST, in which the HS state can be depopulated via red light irradiation. The combination of the reverse-LIESST and LIESST effects allows $[Fe(ptz)_6](BF_4)_2$ to undergo spin state switching through light stimulation, making it a highly promising molecular switch.[10]

In this project, we use the crystal structures of $[Fe(ptz)_6](BF_4)_2$ in both low- and high-spin states determined by Kusz *et al.*,[7] as the experimental reference structures and the starting structures for calculations. In the experiment, rapid cooling ($> 10\ \mathrm{K\,min^{-1}}$) of $[Fe(ptz)_6](BF_4)_2$ single crystals from room temperature prevents the phase transition accompanying the spin state switching from the HS to the LS state, thus remaining in the structural space group $R\bar{3}$. The structure of the supercooled-ordered LS phase was determined using an Xcalibur four-circle diffractometer at 10 K, while the HS structure data were collected after irradiating the LS phase sample at 10 K with a 514 nm Ar laser. The LS and HS crystal structure data are deposited in the Cambridge Crystallographic Data Centre[48] with CSD identifiers JANSAS06 and JANSAS05, respectively. The bond lengths of Fe-N are the key bond lengths for this system, which are 1.99 Å in the LS state and 2.18 Å in the HS state. The crystallographic information for the two spin states of $[Fe(ptz)_6](BF_4)_2$ is listed in table 1.2.

Table 1.2: Experimental data for $[Fe(ptz)_6](BF_4)_2$. This table is taken from Kusz *et al.*[7]

	Experimental	
	LS	**HS**
Chemical formula	$C_{24}H_{48}B_2F_8N_{24}Fe$	
M_W	902.33	
Temperature (K)	10 (1)	
Laser wavelength (Å)	0.7093	
Z	3	3
a (Å)	10.70	10.88
b (Å)	10.70	10.88
c (Å)	31.90	31.48
α (°)	90	90
β (°)	90	90
γ (°)	120	120
V (Å^3)	3163.5	3227.8
$d_{\text{Fe-N}}$ (Å)	1.99	2.18
$\Delta d_{\text{Fe-N}}$ (Å)	0.19	
ΔH_{HL} (meV)	63.2	
Space group	$R\bar{3}$	$R\bar{3}$
Colour	red	colourless
CSD	JANSAS06	JANSAS05

There is no literature reporting direct thermodynamics measurements using the DSC mentioned above. Hauser *et al.*[49] measured the $^1A_1 \rightarrow {}^1T_1$ $d-d$ transition region in the single-crystal absorption spectra of $[Fe(ptz)_6](BF_4)_2$ at different temperatures and plotted the SCO curve of the relative intensity (interpreted as LS proportion γ_{LS}) with temperature, thereby linearly fitting the $\Delta H_{\text{HL}} = 63.2$ meV and $\Delta S_{\text{HL}} = 0.63\ \text{meV}\,\text{K}^{-1}$ at the spin state equilibrium according to

$$\Delta G_{\text{HL}} = \Delta H_{\text{HL}} - T\Delta S_{\text{HL}} = -k_{\text{B}}T \ln K_{\text{HL}} = -k_{\text{B}}T \ln \frac{1-\gamma_{\text{LS}}}{\gamma_{\text{LS}}} \tag{1.11}$$

where K_{HL} is the relaxation rate from the HS to LS states.

Kusz *et al.*[4] have performed SQUID magnetic measurements in the study of structural phase transition in $[Fe(ptz)_6](BF_4)_2$, reproduced in figure 1.5. The single crystal sample of $[Fe(ptz)_6](BF_4)_2$ in the HS phase was recrystallised from nitromethane. As previously described, slow cooling at 1 $\text{K}\,\text{min}^{-1}$ yielded a disordered LS phase that belongs to a space group different from the HS phase. In figure 1.5, the cooling and heating processes are shown in black and blue, respectively. However, this

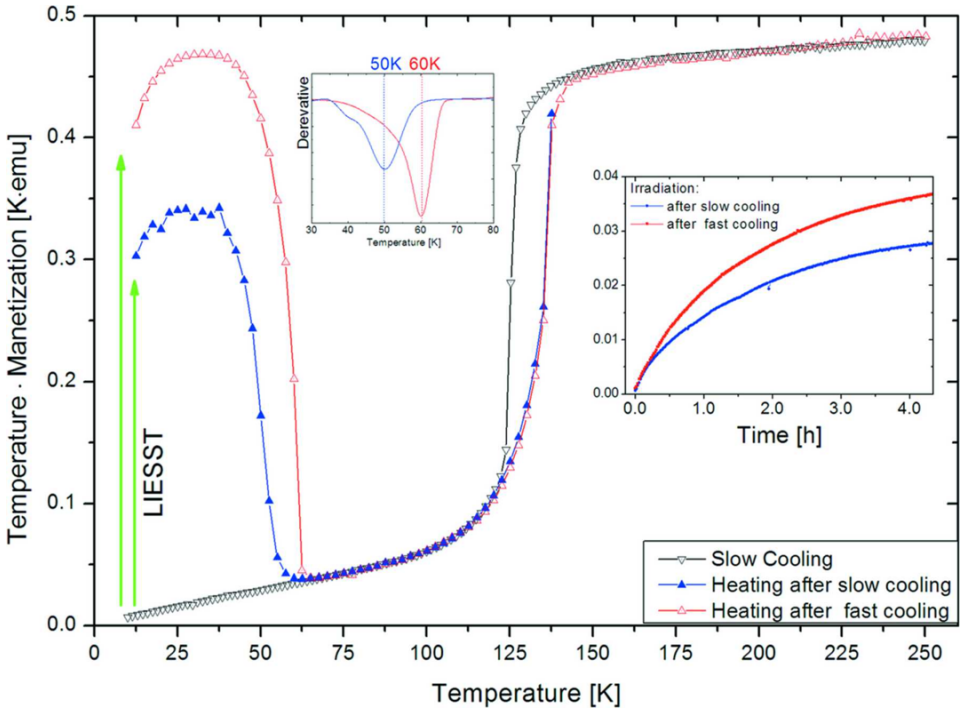

Figure 1.5: The SQUID magnetic measurements of the $[Fe(ptz)_6](BF_4)_2$ single crystal include slow cooling (black) and heating after slow (blue) and fast (red) cooling, as well as the LIESST (green) at 10 K. The inserts illustrate the temperature derivatives of the relaxation curves in the low-temperature range and the time dependence of magnetisation×temperature after irradiation. This figure is taken from Kusz *et al.*[4]

thesis focuses only on the SCO process without a crystallographic phase transition, represented by the red curve in the figure. The supercooled-ordered LS phase was obtained by rapid cooling of a thin single crystal $[Fe(ptz)_6](BF_4)_2$ at a rate of 10 K min^{-1}. The sample in this LS phase was irradiated with green laser light for 240 min at 10 K and then heated to 60 K. The decay of the metastable HS phase back to the LS phase can be observed. This LIESST phenomenon is characterised by the temperature that yields the minimum of the derivative of magnetisation×temperature, namely T_{LIESST} = 60 K. Continuing to warm up to 250 K, $[Fe(ptz)_6](BF_4)_2$ underwent a thermally induced SCO, switching from the LS phase to the HS phase. In the case of rapid cooling, the spin transition occurred abruptly at $T_{1/2}$ = 135 K without hysteresis, that is, $T_{1/2\uparrow} = T_{1/2\downarrow}$ = 135 K.

1.3 Modelling Approaches for Spin Crossover Systems

DFT is the most popular first-principles approach in modelling SCO systems. It has been successful in predicting essential properties such as metal-ligand bond lengths,[50] crystal structures,[51] and molecular vibrations[42] at the single-molecule level. However, the inherent delocalisation error makes DFT struggle to provide reliable ΔH_{HL}.[52] Currently, there is no widely accepted optimal functional for this system. After exhaustive benchmarking, the recommended functionals include B3LYP* (modified with $a_{\mathrm{HF}} = 0.15$),[53,54] M06-L,[51,55] and TPSSh,[51,55,56] but these functionals are typically computationally expensive.

DFT+U is a useful semi-empirical method for treating the strong on-site Coulomb interactions in strongly correlated systems.[57] By incorporating the Hubbard U model with the localised DFT functional, this approach mitigates the over-delocalisation of valence electrons in open *d* orbitals originating from DFT.[58] The primary factor that makes DFT+U appealing for modelling SCO systems, especially in condensed phases, is its significantly lower computational cost than hybrid functionals. Ohlrich and Powell[5] performed DFT+U calculations on ΔH_{HL} of seven iron SCO materials. The errors between the ΔH_{HL} calculated using the Dudarev approach[59] with PBE[60] (Perdew-Burke-Ernzerhof) functional and the experimental measurements are plotted in figure 1.6. The experimental structures provided by Jensen and Cirera[55] were relaxed at the PBE level, maintaining fixed cell shape and volume to obtain the equilibrium structures in both LS and HS states. By adjusting the Hubbard correction value U_{eff}, self-consistent DFT+U calculations were conducted on the equilibrium structures, revealing the dependence of the error on U_{eff}. The study indicated that when $U_{\mathrm{eff}} = 1.6$ eV, the PBE+U method using Dudarev approximation provided a more accurate prediction of ΔH_{HL} compared to TPSSh at a lower cost.[5] In this thesis, we did not directly use the conclusion of $U_{\mathrm{eff}} =$

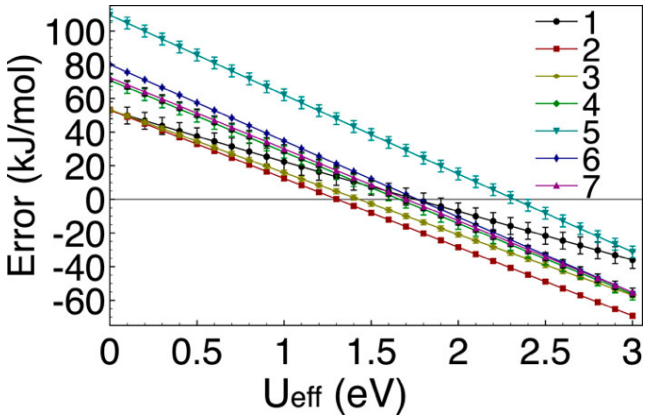

Figure 1.6: At various U_{eff} values, the error between the ΔH_{HL} predicted by PBE+U using the Dudarev approximation and the experimental values. This figure is reprinted from Ohlrich and Powell.[5]

1.6 eV due to the different assumptions in structural optimisation. However, we adopted a similar approach to determine the machine-learned *ab initio* method, which will be elaborated in chapter 3.

Due to the neglect of van der Waals (vdW) interactions or long-range dispersion in semi-local functionals such as PBE,[61] dispersion corrections have been increasingly considered in DFT studies of SCO molecular crystals.[62–64] In the HS state, more *d*-electrons occupy the anti-bonding orbitals, resulting in longer metal-ligand bonds. Consequently, the dispersion contribution to the metal-ligand bonds in the HS state is lower than in the more compact LS state, leading to differences in dispersion interactions between spin states.[65] Dispersion corrections improve the prediction of equilibrium geometries and metal-ligand bond lengths in SCO crystals.[66,67] Dispersion-inclusive DFT methods include Tkatchenko-Scheffler van der Waals[68] (TS-vdW), empirical dispersion corrections[69–72] (DFT-D), exchange-dipole moment[73] (XDM), and many-body dispersion[74,75] (MBD). One of the most widely used and successful corrections in SCO systems is DFT-D3(BJ),[71] which adds the Becke-Johnson[76–78] (BJ) damped atom-pairwise potential to the standard Kohn-Sham DFT, achieving satisfactory accuracy in predicting optimised structures, thermochemistry, and energies.

Even though DFT calculations have given structures and ΔH_{HL} close to the experimental results, simulating the SCO process and accurately predicting $T_{1/2}$ remains challenging. Cirera and Paesani[50]

reported an average error of approximately 58.5 K above experimental values for the $T_{1/2}$ of the [Fe(styrylpyridine)$_4$(NCX)$_2$] (X = S, Se, BH_3, and BPh_3) family when using different exchange-correlation (XC) functionals. This deviation can be attributed to pure DFT calculations being insufficient to describe the SCO phenomenon fully. Firstly, DFT calculations performed at absolute zero cannot appropriately represent the temperature effect on spin-state transitions. Secondly, DFT only provides static geometries and fails to capture the lattice vibrations and thermal expansion in SCO materials.[79] Therefore, introducing molecular dynamics (MD) simulations or QHA can offer a better description of the lattice dynamical properties, thus improving the accuracy of SCO materials modelling.

MD simulations update atomic positions by numerically integrating Newton's equations from a given initial structure, allowing us to understand how the properties of a system evolve over time. Recently, classical MD simulations have been successfully applied to investigate the vibrational properties of various SCO materials.[80-83] In these studies, the force fields (FFs) were parameterised by fitting to DFT data[80,82] or through comparisons with spectroscopic experiments.[81,83] Unlike classical MD simulations, *ab initio* molecular dynamics (AIMD) calculates interatomic forces using DFT at each time step, providing much more accurate predictions. However, due to its high computational cost, only a few studies have used AIMD to simulate SCO systems.[84] As an alternative to MD simulations, the QHA takes into account the contribution of volume-dependent phonons to free energy and also accurately predicts the thermal properties of SCO materials at different temperatures. However, first-principles QHA simulations typically require the phonon spectra of multiple volumes to fit the free energy-volume relationship, which remains expensive computationally.[85,86]

The on-the-fly MLFF has become a highly anticipated method for computing interatomic forces. It learns the statistical relationship between structure and its DFT energy during MD simulations without

requiring any pre-conceived knowledge of chemistry. Once trained, the MLFF can be applied to multiple computational tasks. It overcomes the accuracy limitations of parameterisation and addresses challenges in correctly describing quantum mechanical phenomena in classical MD simulation. Compared with AIMD or first-principles QHA calculations, MLFF has significant advantages in computational efficiency.

However, the critical issues are whether on-the-fly MLFF can accurately model complex SCO systems, achieving DFT-level accuracy in predicting important properties, and whether this approach can significantly accelerate AIMD or QHA calculations to simulate the SCO processes observed in the experiment effectively. If not, what new insights could MLFF provide for the modelling of the SCO lattice?

Chapter 2

Theory

This chapter introduces the theories and relevant backgrounds, including density functional theory and the quasi-harmonic approximation.

2.1 Density Functional Theory

In the mainstream quantum chemistry methods, whether it is the Hartree-Fock (HF) method that treats each electron as being in a mean-field generated by the nucleus and all other electrons, then iteratively solves for a self-consistent numerical solution, the post-HF methods, which include the electron correlations, or the semi-empirical methods that simplify HF to reduce cost, are all require solving the Schrödinger equation to obtain the electronic wavefunctions. This process is mathematically complicated, forcing these methods to have a trade-off between accuracy and system size.

However, DFT opens up a new strategy for dealing with electronic structure problems by calculating the electron density, $\rho(\mathbf{r})$, a physical observable that only depends on spatial coordinates, greatly simplifying the computational complexity. The emergence of DFT has brought revolutionary progress to quantum chemistry.

In this section, we start with the Schrödinger equation, elucidate the fundamental postulates and

core ideas of DFT, and introduce the approximation methods utilised in practical DFT calculations. Finally, we discuss some additional approximations and corrections adopted in this thesis.

2.1.1 The Schrödinger equation and Born-Oppenheimer approximation

In quantum chemistry, a many-particle molecular system in a stationary state is described by the time-independent Schrödinger equation,

$$\hat{H}\Psi = E\Psi \tag{2.1}$$

where the system energy, E, is returned by the Hamiltonian operator, $\hat{H}$. The typical Hamiltonian operator considers the contributions of the kinetic energies of the nuclei and electrons, the attraction between the nuclei and electrons, the repulsion between the electrons, and the repulsion between the nuclei to the total energy of the system,

$$\begin{aligned}\hat{H} &= \hat{T}_n + \hat{T}_e + \hat{V}_{ne} + \hat{V}_{ee} + \hat{V}_{nn} \\ &= -\sum_k \frac{\hbar^2}{2m_k}\nabla_k^2 - \sum_i \frac{\hbar^2}{2m_e}\nabla_i^2 - \sum_i \sum_k \frac{e^2 Z_k}{r_{ik}} + \sum_{i<j} \frac{e^2}{r_{ij}} + \sum_{k<l} \frac{e^2 Z_k Z_l}{r_{kl}}\end{aligned} \tag{2.2}$$

where e is the elementary charge, m is the mass, Z is the atomic number, and r is the distance between particles. In this expression, i and j represent electrons, while k and l represent nuclei. The interaction terms imply that no particle moves independently of other particles, which leads to the inability to separate the variables during the solution of the Schrödinger equation, thus making it difficult to obtain the exact wavefunction, Ψ, of the system. The Born-Oppenheimer approximation decouples the motion of the electrons and the nuclei based on the fact that the electrons move much faster than the nuclei, thus allowing the approximate solution of the electronic wavefunction, Ψ_{el}, for fixed nuclear coordinates. The electronic Schrödinger equation is taken to be

$$\hat{H}_{el}\Psi_{el}(\mathbf{q}_i;\mathbf{q}_k) = E_{el}\Psi_{el}(\mathbf{q}_i;\mathbf{q}_k) \tag{2.3}$$

where the electronic coordinates $\mathbf{q}_i$ are independent variables, and the nuclear coordinates $\mathbf{q}_k$ are parameters. In this case, the kinetic energy term of the nucleus in the original Hamiltonian operator, $\hat{H}$, becomes 0, and the nucleus-nucleus interaction term becomes a constant, resulting in a simplified electron-only Hamiltonian operator, $\hat{H}_{el}$. The electronic energy, E_{el}, defines the potential energy surfaces of the ground and excited states of the system, which help understand most of the chemistry, including molecular geometries, transition states, thermodynamics, and reaction mechanisms.

2.1.2 Hohenberg-Kohn theorems

A uniform electron gas refers to a hypothetical system with a uniform electron density, in which an infinite number of electrons move within an infinite volume with uniformly distributed positive charges. In 1927, Thomas and Fermi[87,88] showed that the energy of a homogeneous electron gas could be calculated without reference to the wavefunction. This idea motivated the real beginning of DFT, when Hohenberg and Kohn proved in their 1964 paper, *Inhomogeneous Electron Gases*,[89] that there exists a unique functional $F[\rho(\mathbf{r})]$ of the electron density in an interacting electron gas, and the ground-state energy can be found at its minimum value.

Two theorems have formed the foundation of the DFT: 1. The Hohenberg-Kohn existence theorem states that the non-degenerate ground-state density determines the external potential, and thus the Hamiltonian operator, and hence the electronic wave function and the electronic energy; 2. The Hohenberg-Kohn variational theorem elaborates that the global minimum of the functional, the ground-state energy, is obtained if and only if the candidate density is the ground-state density.

The Hohenberg-Kohn theorems give an exact description of a many-electron quantum system based on density, allowing direct calculation of the ground-state energy without solving the Schrödinger equation. This results in DFT being more affordable than traditional quantum chemical

methods based on wavefunctions, making it currently the only practical first-principles method available for large and complex systems.

2.1.3 Kohn-Sham DFT

The DFT is exact in theory, but the critical problem is that the exact mathematical expression for the energy density functional, especially concerning the electron-electron interaction term, has yet to be derived. To simplify the problem, Kohn and Sham[90] fictionalised a system of non-interacting electrons whose ground-state electron density is the same as that of the real system of interacting electrons. The advantage of this assumption is that each electron in the system moves independently of the others in a local effective potential, thus representing the many-electron Hamiltonian as a sum of the one-electron operators. At this step, the electronic energy functional can be expressed as

$$\begin{aligned} E[\rho(\mathbf{r})] &= T_s[\rho(\mathbf{r})] + V_{pe}[\rho(\mathbf{r})] + V_{ee}[\rho(\mathbf{r})] + \Delta T[\rho(\mathbf{r})] + \Delta V_{ee}[\rho(\mathbf{r})] \\ &= -\sum_i \frac{\hbar^2}{2m_e}\nabla_i^2 + \int v(\mathbf{r})\rho(\mathbf{r})\,d\mathbf{r} + \frac{1}{2}\int\int \frac{\rho(\mathbf{r})\rho(\mathbf{r'})}{|\mathbf{r}-\mathbf{r'}|}\,d\mathbf{r}\,d\mathbf{r'} \\ &+ E_{\mathrm{xc}}[\rho(\mathbf{r})] \end{aligned} \tag{2.4}$$

where the terms refer, respectively, to the kinetic energy of the non-interacting system, the potential energy of the electrons in the external potential $v(\mathbf{r})$, the self-repulsion of the classical charge distribution, the correction to the kinetic energy due to the electron interactions, and the non-classical correction to all electron-electron repulsion. It should be noted that equation 2.4 does not only apply to the case of electrons moving in the Coulomb potential generated by the point nuclei but to the many-electron system with arbitrary external potential $v(\mathbf{r})$. If the external potential arises by the nucleus, then the second term can be written more specifically as,

$$V_{ne}[\rho(\mathbf{r})] = \sum_k^{\text{nuclei}} \int \frac{Z_k}{|\mathbf{r}-\mathbf{r}_k|}\rho(\mathbf{r})\,d\mathbf{r} \tag{2.5}$$

The last two correction terms in equation 2.4, ΔT and ΔV_{ee}, are combined into E_{xc}, named the exchange-correlation (XC) energy. More precisely, the XC functional contains quantum mechanical exchange and correlation, correction to classical self-interaction of electrons, and kinetic energy differences between the non-interacting and real systems. The energy minimisation by Kohn-Sham DFT involves a pseudoeigenvalue equation,[91]

$$h_i^{\text{KS}} \chi_i = \varepsilon_i \chi_i \tag{2.6}$$

where the eigenfunction χ_i is a single-particle spin-orbital and ε_i is the corresponding orbital energy. The Kohn-Sham operator of one-electron in nuclear potential is

$$h_i^{\text{KS}} = -\frac{\hbar^2}{2m_e}\nabla_i^2 + \sum_k^{\text{nuclei}} \frac{Z_k}{|\mathbf{r}_i - \mathbf{r}_k|} + \int \frac{\rho(\mathbf{r'})}{|\mathbf{r}_i - \mathbf{r'}|} d\mathbf{r'} + V_{xc} \tag{2.7}$$

with

$$V_{\text{xc}} = \frac{\delta E_{\text{xc}}}{\delta \rho} \tag{2.8}$$

Performing Kohn-Sham DFT calculations first requires a trial density matrix ρ and approximate E_{xc}, through which the Slater determinant constructed from a set of orbitals is obtained. Kohn-Sham equations are solved to find the new density matrix, iterating until the difference between the new and the old ρ is less than the desired threshold criterion, outputting the ground state energy. It should be indicated that the method is no longer variational due to the approximation of E_{xc}.

2.1.4 Exchange-correlation functionals

LDA

As the simplest functionals, the local density approximation (LDA) was initially derived from the uniform electron gas model.[91] With slowly varying density, the energy density $\varepsilon_{\text{xc}}^{\text{LDA}}$ at position $\mathbf{r}$

depends only on the electron density ρ at that position, i.e., the local value of the ρ. So, the XC energy of LDA is

$$E_{\mathrm{xc}}^{\mathrm{LDA}} = \int \rho(\mathbf{r}) \varepsilon_{\mathrm{xc}}^{\mathrm{LDA}}[\rho(\mathbf{r})]\, d\mathbf{r} \tag{2.9}$$

The XC energy can be decomposed into exchange and correlation terms,

$$E_{\mathrm{xc}}^{\mathrm{LDA}} = E_{\mathrm{x}}^{\mathrm{LDA}} + E_{\mathrm{c}}^{\mathrm{LDA}} \tag{2.10}$$

where the exchange energy of the uniform electron gas is determined as

$$E_{\mathrm{x}}^{\mathrm{LDA}}[\rho(\mathbf{r})] = -\frac{9\alpha}{8}\left(\frac{3}{\pi}\right)^{1/3} \int \rho^{4/3}(\mathbf{r})\, d\mathbf{r} \tag{2.11}$$

with the constant α = 2/3 for the Slater-Dirac (S) exchange functional.[92] However, there is no exact analytic expression for correlation energy.

GGA

The generalised gradient approximation (GGA) functionals introduce the density gradient to consider the inhomogeneity of electron density in space.[93] Therefore, the XC functionals of GGA depend not merely on the local value of the electron density but also on the extent of the local change of density. The exchange functional is of the form

$$E_{\mathrm{x}}^{\mathrm{GGA}}[\rho(\mathbf{r}), \frac{|\nabla\rho(\mathbf{r})|}{\rho^{4/3}(\mathbf{r})}] = \int \rho^{4/3}(\mathbf{r}) F[\frac{|\nabla\rho(\mathbf{r})|}{\rho^{4/3}(\mathbf{r})}]\, d\mathbf{r} \tag{2.12}$$

where $F[\frac{|\nabla\rho(\mathbf{r})|}{\rho^{4/3}(\mathbf{r})}]$ has different expansions for various exchange functionals. The combination of PBE exchange and PBE correlation forms one of the most famous GGA functionals, the PBE functional,[60] which is also the functional used in this thesis.

Meta-GGA

The meta-generalised gradient approximation (Meta-GGA or mGGA) further considers the second derivative of the electron density and the dependence of kinetic-energy density τ in the XC potential, which is defined as[94]

$$\tau(\mathbf{r}) = \sum_{i}^{\text{occupied}} \frac{1}{2}|\nabla\psi_i(\mathbf{r})|^2 \tag{2.13}$$

So the XC functional of Meta-GGA can be written as

$$E_{\text{xc}}^{\text{mGGA}} = \int \rho^{4/3}(\mathbf{r}) F[\rho(\mathbf{r}), \nabla\rho(\mathbf{r}), \nabla^2\rho(\mathbf{r}), \tau(\mathbf{r}), ...]\, d\mathbf{r} \tag{2.14}$$

Hybrid Functionals

Adding more physical ingredients can systematically improve the XC functionals to a certain extent. However, pure functionals (LDA, GGA, and Meta-GGA) still have difficulties describing, for example, vdW interactions and self-interaction errors. One possible solution is to construct a hybrid functional by the linear mixture of HF exchange with DFT exchange-correlation. This idea was first proposed by Becke,[95] who developed the first hybrid functional, B3PW91, in 1993. The following year, Stephens *et al.* modified B3PW91 by replacing PW91 with LYP to design the widely known B3LYP functional,[96]

$$E_{\text{xc}}^{\text{B3LYP}} = aE_{\text{x}}^{\text{HF}} + (1-a)E_{\text{x}}^{\text{LDA}} + b\Delta E_{\text{x}}^{\text{B}} + (1-c)E_{\text{c}}^{\text{LDA}} + cE_{\text{c}}^{\text{LYP}} \tag{2.15}$$

where a, b, and c are 0.20, 0.72, and 0.81. Because the amount of exact exchange cannot be determined from the first principle, hybrid functionals are semi-empirical and require fitting experimental data to assign coefficients for each component.

2.1.5 DFT+U: adding a Hubbard U term to localised functional

Due to the inability of the approximated XC in pure functionals to completely cancel out the self-interactions in the Hartree term,[97] the spin-state splitting energies are often systematically misestimated. Although hybrid functionals may provide good predictions, the computational cost for SCO systems with hundreds of atoms is extremely high. DFT+U deals with strong on-site Coulomb interactions of localised d and f electrons by adding a Hubbard term to LDA or GGA and is often used for low-cost estimation of ΔH_{HL}.[5] DFT+U was proposed by Anisimov *et al.*[58] and further developed by Dudarev *et al.*[59] The total energy of DFT+U using Dudarev approximation is:[98]

$$E^{\mathrm{DFT+U}} = E^{\mathrm{DFT}} + \frac{U-J}{2}\sum_{\sigma} n_{m,\sigma} - n_{m,\sigma}^2 \tag{2.16}$$

where U is the on-site interaction, J is the exchange interaction, n is the occupation number of atomic orbitals, m is the orbital angular momentum, and σ is the electron spin. The Hubbard correction value is defined as $U_{\mathrm{eff}} = U - J$. The accuracy of DFT+U in predicting enthalpy differences depends on the choice of U_{eff}, which is typically determined empirically by finding a value that reproduces experimental results.

2.2 Lattice Dynamics

Phonons are normal modes in the context of quantum mechanics, used to describe the collective vibrations of atoms in a lattice. For each $\mathbf{k}$ point in the Brillouin zone, which is the symmetric primitive cell centred at the origin of the reciprocal lattice in wave vector space, there are $3M$ phonons with frequencies $\omega_{\mathbf{k},j}$ (where j = 1, 2,..., $3M$), with M representing the number of atoms in the unit cell. Since all calculations in this thesis use only a single $\mathbf{k}$-point to sample the Brillouin zone, the phonon frequencies will be referred to as ω_j in the following discussion. The phonon density of states

$g(\omega)$ describes the number of phonon modes of a particular frequency ω_j within the interval from ω to $\omega + d\omega$, which is defined as[99]

$$g(\omega) = \frac{1}{3M} \sum_{j}^{3M} \delta\left(\omega - \omega_j\right) \tag{2.17}$$

with normalisation of $\int g(\omega)\, d\omega = 1$.

In polyatomic unit cells, phonons are classified as optical and acoustic phonons. In section 1.1, we used the single-molecule model to describe the contributions of intramolecular vibrations, especially metal-ligand vibrations (optical phonons), to vibrational entropy and vibrational enthalpy in SCO processes. However, this model does not account for lattice cooperativity and, therefore, fails to adequately describe the experimentally observed thermal hysteresis[100] and multi-step transitions.[101] This section also discusses low-frequency vibrations (acoustic phonons), primarily induced by non-bonding interactions, which transmit local spin-state changes to neighbouring molecules via long-range elastic forces[82] or "Ising-like" interaction.[102]

2.2.1 Harmonic lattice dynamics

In the harmonic phonon model of lattice dynamics, the vibrational energy of a phonon with frequency ω_j at the energy level n is

$$E_n^{vib} = \hbar\omega_j \left(\frac{1}{2} + n\right) \tag{2.18}$$

where the average number of phonons occupying the mode j is derived by the Bose-Einstein statistics,[103]

$$n = \frac{1}{\exp\left(\frac{\hbar\omega_j}{k_B T} - 1\right)} \tag{2.19}$$

The lowest energy of the phonon mode is called the zero-point vibrational energy,

$$E_0^{vib} = \frac{\hbar\omega_j}{2} \tag{2.20}$$

Under the harmonic approximation, the vibrational energy in the crystal can be regarded as the sum of all phonon modes by,

$$E_{\mathrm{HA}}^{vib}(T) = \sum_{j}^{3M} \left(\frac{\hbar\omega_j}{2} + \frac{\hbar\omega_j}{\exp\left(\frac{\hbar\omega_j}{k_{\mathrm{B}}T} - 1\right)} \right) \tag{2.21}$$

However, this simple model is insufficient to explain the thermal expansion of the crystals, where the equilibrium volume depends on temperature.

2.2.2 Quasi harmonic approximations

Quasi-harmonic approximations (QHA) correct the harmonic model by introducing a dependence of phonon frequencies on volume. Therefore, the vibrational energy of the system in the HS/LS state can be expressed as,

$$E_{\mathrm{HS/LS}}^{vib}(V,T) = \sum_{j}^{3M} \left(\frac{\hbar\omega_{j,\mathrm{HS/LS}}(V)}{2} + \frac{\hbar\omega_{j,\mathrm{HS/LS}}(V)}{\exp\left(\frac{\hbar\omega_{j,\mathrm{HS/LS}}(V)}{k_{\mathrm{B}}T} - 1\right)} \right) \tag{2.22}$$

and the entropy is expressed as,

$$S_{\mathrm{HS/LS}}(V,T) = \frac{\hbar\omega_{j,\mathrm{HS/LS}}(V)}{T\exp\left(\frac{\hbar\omega_{j,\mathrm{HS/LS}}(V)}{k_{\mathrm{B}}T} - 1\right)} - k_{\mathrm{B}}\sum_{j}^{3M} \ln\left[1 - \exp\left(\frac{-\hbar\omega_{j,\mathrm{HS/LS}}(V)}{k_{\mathrm{B}}T}\right)\right] \tag{2.23}$$

Therefore, it is easy to obtain the Helmholtz free energy F in the QHA,[85]

$$\begin{aligned} F_{\mathrm{HS/LS}}(V,T) &= E_{\mathrm{HS/LS}}(V) + E_{\mathrm{HS/LS}}^{vib}(V,T) - TS_{\mathrm{HS/LS}}(V,T) \\ &= \left[E_{\mathrm{HS/LS}}(V) + \sum_{j}^{3M} \frac{\hbar\omega_{j,\mathrm{HS/LS}}(V)}{2}\right] + k_{\mathrm{B}}T\sum_{j}^{3M} \ln\left[1 - \exp\left(\frac{-\hbar\omega_{j,\mathrm{HS/LS}}(V)}{k_{\mathrm{B}}T}\right)\right] \end{aligned} \tag{2.24}$$

where $E_{\mathrm{HS/LS}}$ represents the electronic energy in the HS/LS state, and the second term is the zero-point motion energy F^{ZP}. The sum of the electronic and zero-point motion terms in brackets represents the energy at 0 K. The last term is the thermal excitation energy, which changes with temperature. At a fixed temperature, the equilibrium volume V_{eq} can be obtained by minimising $F(V,T)$. Then, the thermal expansion coefficient is defined as,

$$\alpha_V(T) = \frac{1}{V_{\mathrm{eq}}(T)}\left(\frac{\partial V_{\mathrm{eq}}(T)}{\partial T}\right)_{\mathrm{P}} \tag{2.25}$$

Chapter 3

Method

This chapter presents the software used for dataset generation, post-processing, and analysis in this thesis. Then, the details of MLFF training and the DFT calculations to validate MLFF performance are described. Finally, we illustrate how MLFFs are employed for QHA predictions.

3.1 Software

VASP

All DFT calculations were performed using the Vienna *Ab initio* Simulation Package[104] (VASP) version 6.4.2 with projector augmented wave[105] (PAW) pseudopotentials, including the determination of the machine-learned *ab initio* method and the generation of the reference dataset. VASP was also used to run AIMD simulations to train MLFFs and sample the training configurations on the fly.

Phonopy

Phonopy[106,107] is an open-source package that allows the VASP interface to post-process phonon calculations. Phonopy 24.7.1 was used to calculate the phonon density of states (pDoS) and perform MLFF-based QHA calculations.

VESTA

Visualisation for Electronic and Structural Analysis[108] (VESTA) software was used to inspect and visualise the crystal structure and extract structural information such as lattice parameters and bond lengths.

ASE

Atomic Simulation Environment[109] (ASE) is a Python package that automates VASP calculations and extracts forces and energies from the outputs. ASE 3.23.0b1 was used with Python 3.11 to support MLFF functionality in VASP. It was integrated with the built-in MD modules for conducting MLFF-driven MD simulations.

3.2 Choice of DFT Method

The accuracy and robustness of MLFFs are fundamentally determined by the reference *ab initio* method. Consequently, conducting test calculations prior to MLFF training is crucial to ensure that the chosen DFT method can reproduce experimental properties, especially ΔH_{HL}. As discussed in chapter 1, test calculations were performed with VASP, using the PBE functional and adopting D3 correction with BJ damping to account for vdW interactions. A Hubbard U potential term was added to the Fe(II) ions to correct the over-delocalisation of strongly correlated *d* electrons. This theoretical method is hereafter referred to as PBE-D3(BJ)+U. To optimise the U_{eff} value of DFT+U, an approach similar to that described by Ohlrich and Powell[5] was used. Spin polarisation was not considered for the LS state. For the HS state, the calculations were restricted to S=2 by setting the difference in the number of electrons in the up and down spin components and specifying the initial magnetic

moments of the Fe atoms. A plane-wave cutoff energy of 500 eV was used, and the convergence criterion for electron energy minimisation (ELM) was set to 1.0×10^{-6} eV. A stopping criterion for ionic optimisation minimisation (IOM) was also set so that the optimisation of the ionic positions would stop when the maximum force acting on the atoms was less than 0.01 eV/Å. Only the Γ centre was sampled in the Brillouin zone. The use of symmetry was switched off. Full relaxations with conjugate gradient algorithm were performed for both LS and HS states by gradually adjusting U_{eff}, with the starting geometries provided in appendix A.2, to investigate the impact of U_{eff} on ΔH_{HL}. The optimal U_{eff} was obtained at the minimum absolute error of ΔH_{HL}, which is calculated from

$$\text{Absolute Error} = |\text{Calculated Value} - \text{Experimental Value}| \tag{3.1}$$

and the PBE-D3(BJ)+U method with the optimal U_{eff} was chosen for subsequent DFT calculation and MLFF training. More details of the relaxation calculation settings are given in appendix A.6.1.

3.3 Reference Data

To test the performance of the developed MLFFs, *ab initio* reference data containing the relaxed lattice parameters, average Fe-N bond lengths, ΔH_{HL}, and pDoS were calculated. The lattice parameters and bond lengths for both spin states were collected from the relaxations performed using PBE-D3(BJ)+U with the optimal U_{eff} in test calculations. Keeping other settings unchanged, self-consistent calculations were performed on the optimised geometries of the LS and HS states by reading the predicted wavefunctions. Then, the reference ΔH_{HL} was calculated from their total energies. The Hessian matrices were calculated using the finite differences approach for the optimised geometries to obtain the phonon frequencies, with each ion having a positive and negative displacement of 0.015 Å in each direction. Input details for VASP phonon calculations are available in appendix A.6.3.

Phonopy was used to extract the outputs from VASP phonon calculations and generate the force constants. The pDoS for each spin state was then calculated by sampling at the Γ centre on the mesh with a Gaussian smearing width of 0.5 eV.

3.4 Training Data

The built-in MLFF feature in VASP allows the sampling and assembling of training datasets during MD simulations. MD simulations of the $[Fe(ptz)_6](BF_4)_2$ unit cell in both LS and HS states were conducted within the NpT ensemble, which is a constant pressure and constant temperature ensemble, using the Parrinello-Rahman algorithm. The simulations began with DFT relaxed geometries and employed PBE-D3(BJ)+U as the reference method to train the corresponding MLFFs on the fly. In these simulations, the friction coefficients for lattice and atomic degrees of freedom were set to 10 ps^{-1}. A time step of 2 fs was selected, and the mass of the hydrogen atom was increased to 4 amu to enhance simulation stability. The system temperature was regulated using the Langevin thermostat, initially equilibrating at 300 K, then setting to 100 K for further training.

The MLFF is constructed from a basis set that relies on a local reference configuration, including atoms and their surrounding neighbourhoods and is dynamically expanded during the MD simulations.[110,111] In MLFF training, the maximum number of local reference configurations for each species was set to 3000. Once this limit was reached, VASP continued the calculation and selected some configurations from old and new samplings to discard, ensuring the number of local reference configurations was maintained at 3000. Four prior Bayesian error estimations in forces (BEEF) were stored in memory to update the learning threshold (CTIFOR), which determines the frequency of *ab initio* calculations. Additionally, two configurations were temporarily stored as candidates for training

Table 3.1: Datasets used in MLFF training.

Spin states	Temperature (K)	Number of configurations at each temperature	Total number of configurations
LS	300	208	393
	100	185	
HS	300	176	347
	100	171	

data. For the 300 K training, the CTIFOR was increased to 1.35 times the original value to reduce the sampling frequency, whereas the default CTIFOR was applied for the 100 K training. A continuation run was performed if the number of configurations collected during one run was insufficient. In continuation runs at the same temperature, the initial CTIFOR was set to the final CTIFOR from the previous run to skip unnecessary sampling. Details of the parameter settings for MLFF training are provided in appendix A.6.4. Table 3.1 summarises the training datasets for MLFFs of LS and HS states.

The FF parameters were readjusted after sufficient configurations had been collected. Since the accuracy of the total energy was more critical than forces and stresses in the production runs, the scaling of the fitted potential energy was increased to 10 times the default. Standard three-body descriptors were sparsified to 50% to improve computational efficiency. Relative to the DFT reference values, the fitting accuracy of the refitted MLFFs for predicting total energy and forces was evaluated using the root mean square errors (RMSEs), which are expressed as

$$\text{RMSE of energies} = \sqrt{\frac{1}{m}\sum_{i=1}^{m}(E_{\text{MLFF},i} - E_{\text{DFT},i})^2} \tag{3.2}$$

$$\text{RMSE of forces} = \sqrt{\frac{1}{mM}\sum_{i=1}^{mM}\|\mathbf{F}_{\text{MLFF},i} - \mathbf{F}_{\text{DFT},i}\|^2} \tag{3.3}$$

where m is the total number of configurations in training datasets. Each configuration has an MLFF-predicted energy, E_{MLFF}, and a DFT-calculated reference energy, E_{DFT}. In the unit cell of $[Fe(ptz)_6](BF_4)_2$ studied in this thesis, there are $M = 321$ atoms. Therefore, the number of forces on

atoms is $m \times M$, with each force having three components: x, y, and z. Similarly, the error between the force predicted by the MLFF, $\mathbf{F}_{\mathrm{MLFF},i}$, and the force calculated by the DFT, $\mathbf{F}_{\mathrm{DFT},i}$, was determined for configuration i. With the other settings aligned with DFT calculations, the MLFFs were then used to benchmark relaxation, single-point energy, and phonon predictions for assessing accuracy.

3.5 Quasi-Harmonic Approximation Based on Machine Learning Force Fields

The MLFF-based QHA calculations for both spin states were carried out using the Phonopy package. The MLFF pre-optimised unit cells were scaled by factors of 0.99, 0.995, 1.005, 1.025, and 1.03 to introduce isotropic lattice variations. Subsequently, the five structures were relaxed using MLFFs with variable cell shapes and ionic positions while fixing the cell volumes. The electronic energy at each volume was obtained. The phonon frequencies at each volume were then calculated using the finite displacement approach[112] with MLFFs. According to the Birch-Murnaghan isothermal equation of state,[113,114] 30 Helmholtz free energy-volume curves were fitted at 10 K intervals over the temperature range from 0 to 290 K. By minimising the volume at each temperature, the variations of equilibrium volume and the thermal expansion coefficient with temperature were determined.

Chapter 4

Results and Discussion

This chapter provides the results of the study, divided into four sections. First, the *ab initio* reference method for MLFF training will be determined by fitting the experimental enthalpy difference. Next, the MLFF training process and the final errors will be summarised. A series of benchmarks will be conducted to evaluate the performance of MLFFs. Finally, MLFFs will be used to perform QHA calculations to obtain the thermal expansion properties of the SCO lattice.

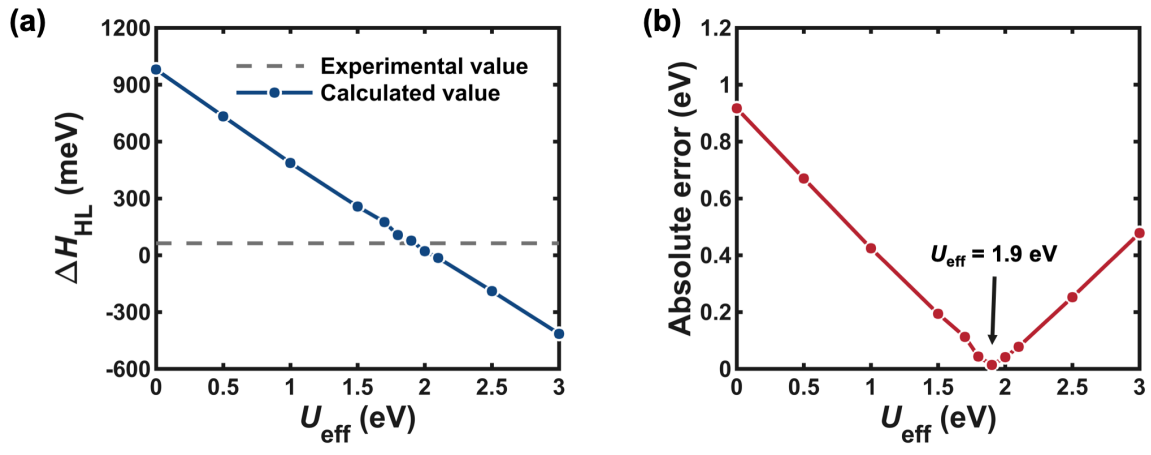

Figure 4.1: (a) U_{eff}-dependence of the enthalpy difference ΔH_{HL}. The unit cells of $[Fe(ptz)_6](BF_4)_2$ in LS and HS states were fully relaxed using the PBE-D3(BJ)+U method with different U_{eff} values. The calculated ΔH_{HL} at each U_{eff} was obtained from self-consistent calculations on the optimised structures using the same functional. The experimental ΔH_{HL} is 63.2 meV; (b) The absolute error between the calculated and experimental values of ΔH_{HL} under different U_{eff} values. The optimal U_{eff} of 1.9 eV was obtained at the minimum absolute error.

4.1 Overview of Reference *Ab Initio* Method

To determine the Hubbard correction value U_{eff} in the reference method PBE-D3(BJ)+U for MLFF training, seven U_{eff} values were initially tested in the range from 0 (disabling DFT+U) to 3.0 eV, with intervals of 0.5 eV. For each U_{eff}, the enthalpy difference ΔH_{HL} was calculated based on the electronic energy difference between the relaxed geometries of the HS and LS states. As U_{eff} increased, the calculated ΔH_{HL} decreased from 980.4 meV at 0 eV to -414.8 meV at 3.0 eV. The experimental ΔH_{HL} (63.2 meV)[49] is less than the calculated ΔH_{HL} at U_{eff} = 1.5 eV and greater than that at U_{eff} = 2.0 eV, and it is closer to the latter. Therefore, four additional U_{eff} values (1.7, 1.8, 1.9 and 2.1 eV) were tested. The calculated ΔH_{HL} for a total of 11 U_{eff} values are plotted in figure 4.1 (a), and the absolute errors of the calculated values compared to the experimental values are also shown in figure 4.1 (b). When the interval for testing U_{eff} values is 0.5 eV, the relationship between the calculated ΔH_{HL} and U_{eff} is roughly linear. However, some noise is observed when the interval is reduced to 0.1 eV, resulting in deviations from linearity. By comparing the absolute errors at each U_{eff}, it is concluded that the optimal U_{eff} value is obtained at U_{eff} = 1.9 eV, with a calculated ΔH_{HL} of 77.0 meV, which is only 13.8 meV greater than the experimental value. Although it is feasible to test more values by further reducing the interval of U_{eff} values to obtain more accurate calculated ΔH_{HL}, this would consume unnecessary computational resources. In contrast, the calculated ΔH_{HL} at U_{eff} = 1.9 eV has reached a satisfactory level.

The optimal U_{eff} is slightly larger than the U_{eff} of 1.6 eV suggested by Ohlrich and Powell.[5] This may be attributed to two factors. First, including dispersion correction results in a larger spin-state splitting energy, as the dispersion contributions differ between the HS and LS states. Second, the unit cells were fully relaxed rather than relaxing only the ionic positions, resulting in different cell

volumes for the HS and LS states, which better represent the actual situations of SCO systems.

4.2 Parameterisation of Machine-learned Force Fields

The unit cells of $[Fe(ptz)_6](BF_4)_2$ in the LS and HS states, relaxed using the PBE-D3(BJ)+U functional with U_{eff} = 1.9 eV at 0 K, are recorded in appendix A.3. Using these structures as starting points, MD simulations were run at 300 K, followed by 100 K, with 8000 timesteps for the LS system and 14000 timesteps for the HS system. During this simulation, the changes in temperature and energies of the LS and HS systems are shown in figure 4.2 (a) and (c), respectively. Figure 4.2 (b) and (d) describe how the MLFFs are sampled during the MD calculation.

At each time step, the MLFFs predicted energies, forces, and stresses and estimated their actual errors and Bayesian errors. When the BEEF exceeded a specific CTIFOR, set at the start of training and dynamically adjusted based on the average BEEF from the previous timesteps, the current FFs were considered insufficiently accurate. In such cases, a DFT step was enforced to calculate the energies, forces, and stresses for the current timestep, and the reference configuration was added to the training dataset. The MLFFs were built by interpolating existing data. When the BEEF was below the CTIFOR, the MD simulations propagated using the MLFF predictions. During 4000–5000 timesteps, the instances where BEEF exceeded CTIFOR significantly decreased, indicating that the MLFFs became more accurate and the sampling frequency was reduced. When enough training data had been collected at 300 K, learning continued at 100 K until the dataset sampling was complete. The MD simulations predicted by the MLFFs have significantly accelerated compared to the AIMD simulations during the initial steps. The trained FFs were re-parameterised by sparsifying the standard three-body descriptors, and the final MLFFs for benchmarking and production runs were developed.

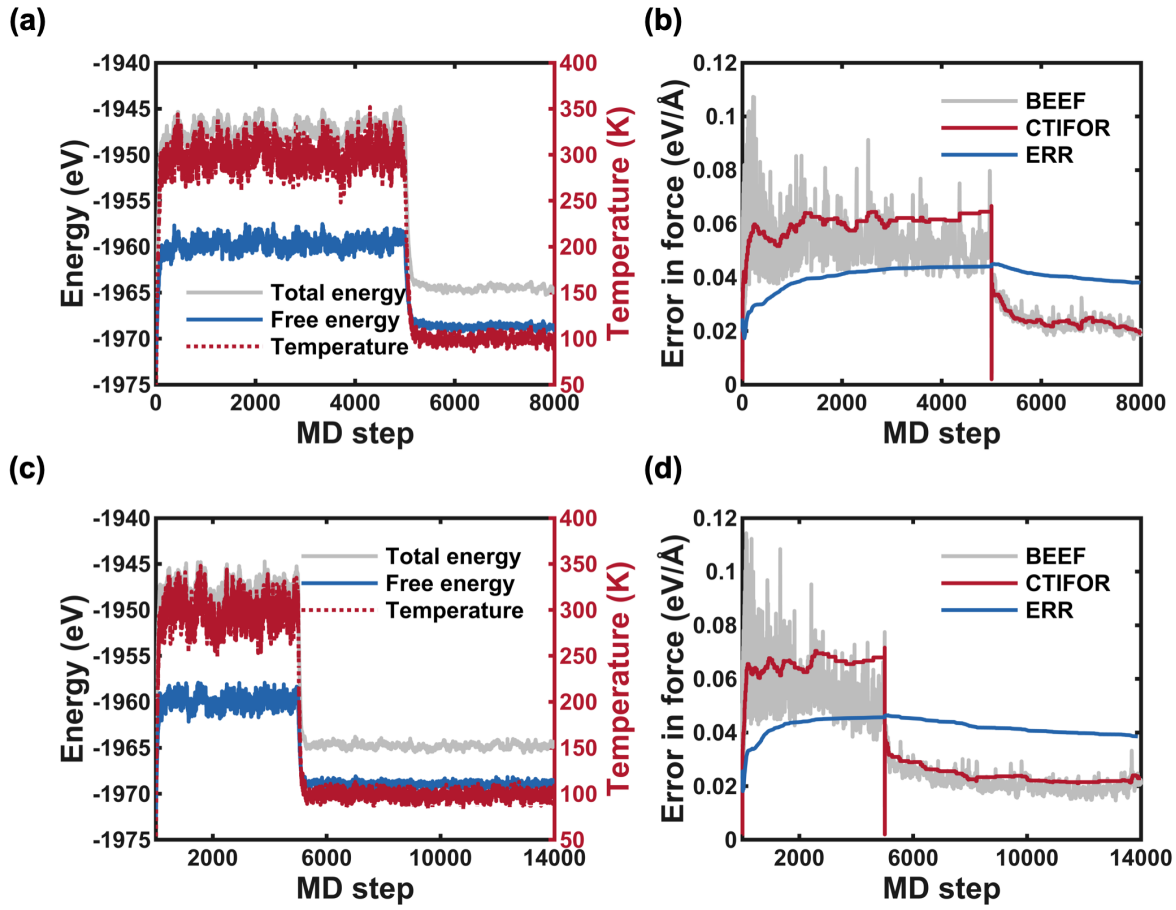

Figure 4.2: (a) Fluctuations in total energy, free energy, and temperature in the LS state system during 8000 timesteps of MD simulations. For the first 5000 MD steps, the temperature was controlled at 300 K. In the subsequent 3000 steps, the system temperature was set to 100 K for further training to capture more configurations within the SCO temperature range. (b) Evolution of the real errors in forces (ERR), Bayesian error estimations in forces (BEEF), and learning threshold (CTIFOR) during the training of the LS state MLFF; (c) Changes in total energy, free energy, and temperature in the HS state system over 14000 MD steps. The first 5000 steps were performed at 300 K, followed by 9000 steps at 100 K to sample a comparable number of configurations to the LS state; (d) Evolution of ERR, BEEF, and CTIFOR in forces during HS state MLFF training.

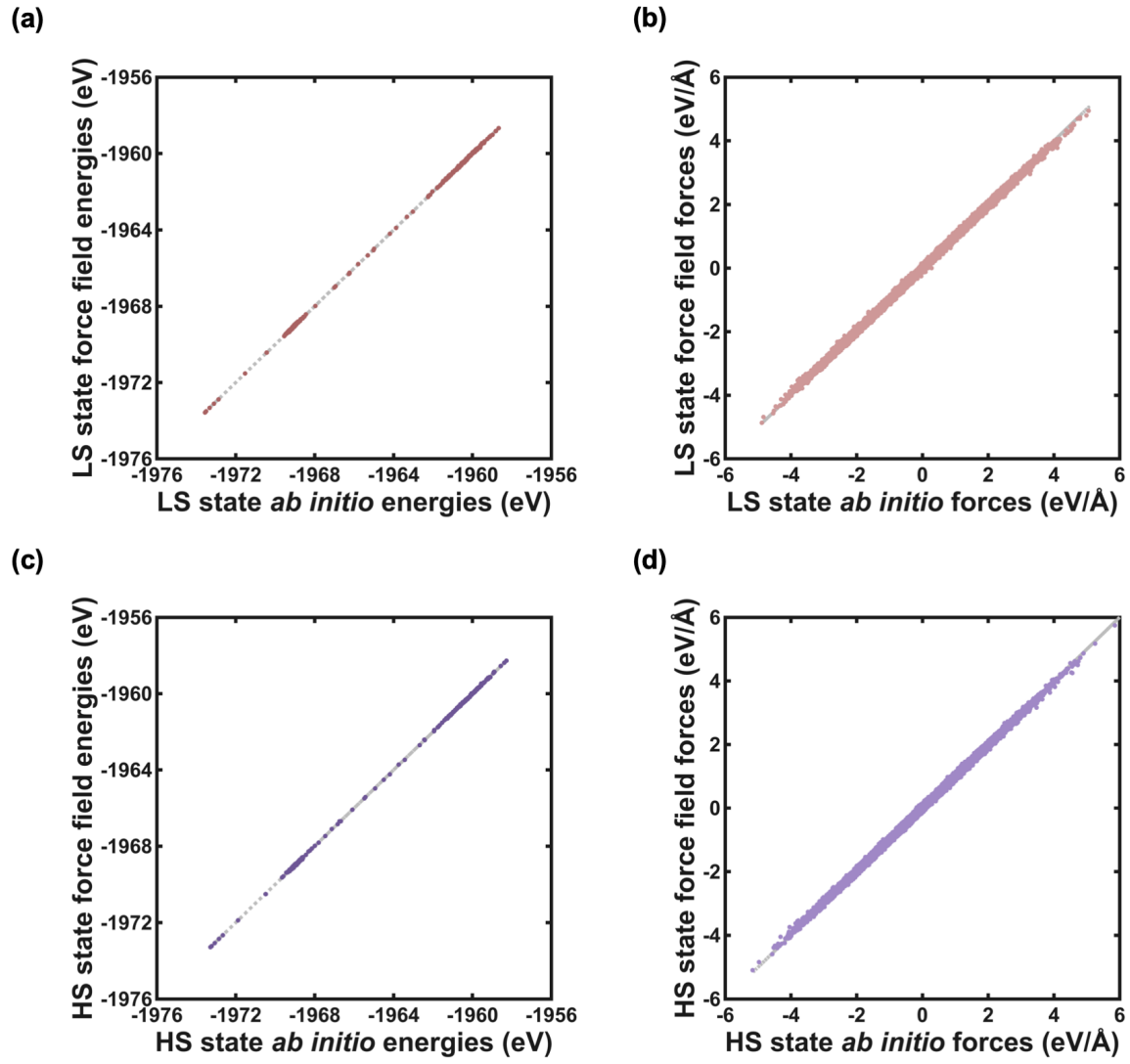

Figure 4.3: Regression results comparing the force field data with the *ab initio* data in the final refitting step for (a) total energies of the LS state, (b) forces on atoms in the LS state, (c) total energies of the HS state and (d) forces on atoms in the HS state. The diagonal grey line represents a perfect fit, indicating that the MLFF and *ab initio* data are identical. The closer the data points are to this line, the better the fit.

4.3 Benchmarking: Prediction of Energies and Forces

In this thesis, all DFT calculations have converged, so it is assumed that geometry optimisations and self-consistent calculations have reached global minima. These DFT results are believed to be accurate and can be used as references to benchmark MLFFs across multiple properties. Once the MLFFs are developed, the priority is to benchmark whether MLFFs accurately describe the force

Table 4.1: Final root mean square errors (RMSEs) of MLFFs.

Spin states	RMSE of forces (meV/Å)	RMSE of total energy (meV)
LS	26.61	23.56
HS	27.24	24.96

and total energy. The forces and total energy of 393 configurations in the LS training dataset were predicted using the LS MLFF and the PBE-D3(BJ)+U functional, with the comparison results shown in figure 4.3 (a) and (b). Similarly, the results for 347 configurations in the HS training dataset are plotted in figure 4.3 (c) and (d). It can be observed that almost all data points are distributed along the perfectly fitted grey diagonal lines, suggesting that both MLFFs demonstrate good performance in predicting total energy and forces. For both the LS and HS cases, the maximum deviation in total energy is less than 100 meV, and the maximum deviation in atomic forces is less than 300 meV/Å. Based on these results, the final fitting errors for total energy and forces are listed in table 4.1. These results were compared with previous similar work in which Wieser and Zojer developed MLFFs using VASP for five metal-organic frameworks, yielding an RMSE of 160–290 meV for total energy and an RMSE of 80–95 meV/Å for forces in the final training step.[115] It has shown that the MLFFs developed in this thesis have achieved satisfactory accuracy in predicting energy and forces.

4.4 Benchmarking: Crystallography and Enthalpy Differences

The ability of MLFF to predict the equilibrium geometry for each spin state was evaluated. Full relaxation was performed using PBE-D3(BJ)+U and MLFF on the same starting structures. The cell parameters, volumes, and average metal-ligand bond lengths of the relaxed geometries are compared in table 4.2. The MLFFs provided lattice constants that are almost identical to those from DFT, except for the c parameter, which is slightly larger by ~ 0.1 Å. The prediction of the unit cell volume was

Table 4.2: Crystallographic and energy information of $[Fe(ptz)_6](BF_4)_2$ obtained by experiments[7] and calculations.

	Experimental		**DFT**		**MLFF**	
	LS	**HS**	**LS**	**HS**	**LS**	**HS**
Chemical formula	$C_{24}H_{48}B_2F_8N_{24}Fe$					
M_W	902.33					
Z	3	3	3	3	3	3
a (Å)	10.70	10.88	10.66	10.89	10.62	10.88
b (Å)	10.70	10.88	10.66	10.89	10.62	10.88
c (Å)	31.90	31.48	31.68	30.82	31.78	30.95
α (°)	90	90	90	90	90	90
β (°)	90	90	90	90	90	90
γ (°)	120	120	120	120	120	120
V (Å^3)	3163.5	3227.8	3117.9	3163.0	3107.2	3172.1
ΔV_{HL} (Å^3)	64.3		45.1		64.9	
$\overline{d}_{Fe\text{-}N}$ (Å)	1.99	2.18	1.98	2.19	1.98	2.19
$\Delta\overline{d}_{Fe\text{-}N}$ (Å)	0.19		0.21		0.21	
Energy (eV)			-1973.6	-1973.4	-1973.6	-1973.3
ΔH_{HL} (meV)	63.2		77.0		80.2	

also successful, with an error of only $\sim 0.3\%$. The MLFF also accurately reproduced the DFT results for the average F-N bond lengths and the change in average F-N bond lengths from the LS to HS state. This indicates that MLFFs have a strong ability to determine the equilibrium geometry, benefiting from their accuracy in predicting atomic forces.

Compared with the experimental results in table 4.2, the main discrepancy in the lattice constants still appears in the c parameter, especially for the HS state, where both calculated values are ~ 0.5 Å smaller than the experimental values. There are evident errors in the predicted volumes, particularly for the HS state, where the error from DFT is as high as 64.8 Å^3. The computational results tend to give smaller volumes. One possible reason is that the calculations were performed at 0 K, while experiments at higher temperatures involve thermal expansion, resulting in larger volumes. However, the experimental structures used were measured at 10 K, so thermal expansion is not expected to be that significant. Another possible explanation is that the vdW correction applied in the calculations may have overly contracted the crystal volumes. This could also explain why the calculation provides

smaller metal-ligand bond lengths for the LS state but larger metal bond lengths for the HS state. The difference in the effect of dispersion correction on the metal-ligand bond lengths between spin states has been discussed in section 1.3.

Interestingly, for all structural properties, the MLFF predictions are closer to the experimental results than the DFT predictions, especially the volume difference between the HS and LS states. Whether this indicates that MLFFs can offer more accurate equilibrium geometry predictions than DFT is worth further investigation. Moreover, MLFFs have the potential to capture thermal expansion via QHA, while modelling the thermal expansion coefficients remains a significant challenge for DFT.[116]

It should be noted that a particular feature of this system is that the ΔH_{HL} is small relative to other similar materials. For example, the ΔH_{HL} of the six Fe(II) SCO materials studied by Jensen and Cirera range from 160 to 320 meV.[55] This small ΔH_{HL} can result in numerically insignificant errors becoming significant in relative terms. However, in this case, the MLFF prediction of the ΔH_{HL} compared to the reference data remains impressive, being only 3.2 meV higher than the DFT result, recalling that the difference between the DFT and the experimental ΔH_{HL} is 13.8 meV.

4.5 Benchmarking: Phonons

The vibrational properties of the SCO lattices are determined by phonons, with the phonon density of states (pDoS) showing the number of phonon modes at various frequencies in the crystal. The predictions of pDoS from DFT and MLFF are compared, as shown in figure 4.4. It can be seen that the MLFFs reproduced the full frequency range pDoS calculated by the DFT well, except for the higher predictions around the frequency of 92 THz. Since low-frequency phonons transmit

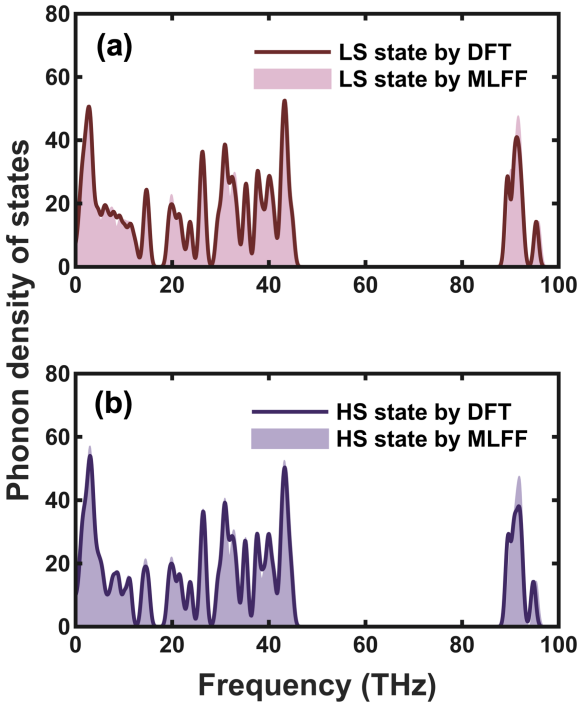

Figure 4.4: The comparison of phonon density of states by DFT calculations (lines) and MLFF predictions (shaded areas) for (a) LS states and (b) HS states.

elastic interactions within the lattice and dominate cooperativity in SCO,[117] only the low-frequency vibrational range of 1–10 THz is the focus. The MLFF pDoS show only minor deviations from the DFT data in the low-frequency region. Additionally, the distinct shapes of the pDoS curve make it easy to distinguish between the LS and HS states.

In summary, after on-the-fly learning from DFT, the MLFFs are capable of independently predicting SCO-related properties, including equilibrium geometries, enthalpy differences, and phonons, without relying on additional *ab initio* calculations, while achieving the same level of accuracy as DFT. However, MLFF significantly outperformed DFT in computational efficiency. Table A.1 provides the time for computing different job types with DFT and MLFF. Except for the similar time taken for self-consistent calculations of equilibrium geometries, MLFF accelerated the relaxations and phonon calculations by several orders of magnitude. Most notably, when calculating phonons for the HS state using 96 CPUs, MLFF took only 10 minutes compared to 6 days and 11 hours with DFT.

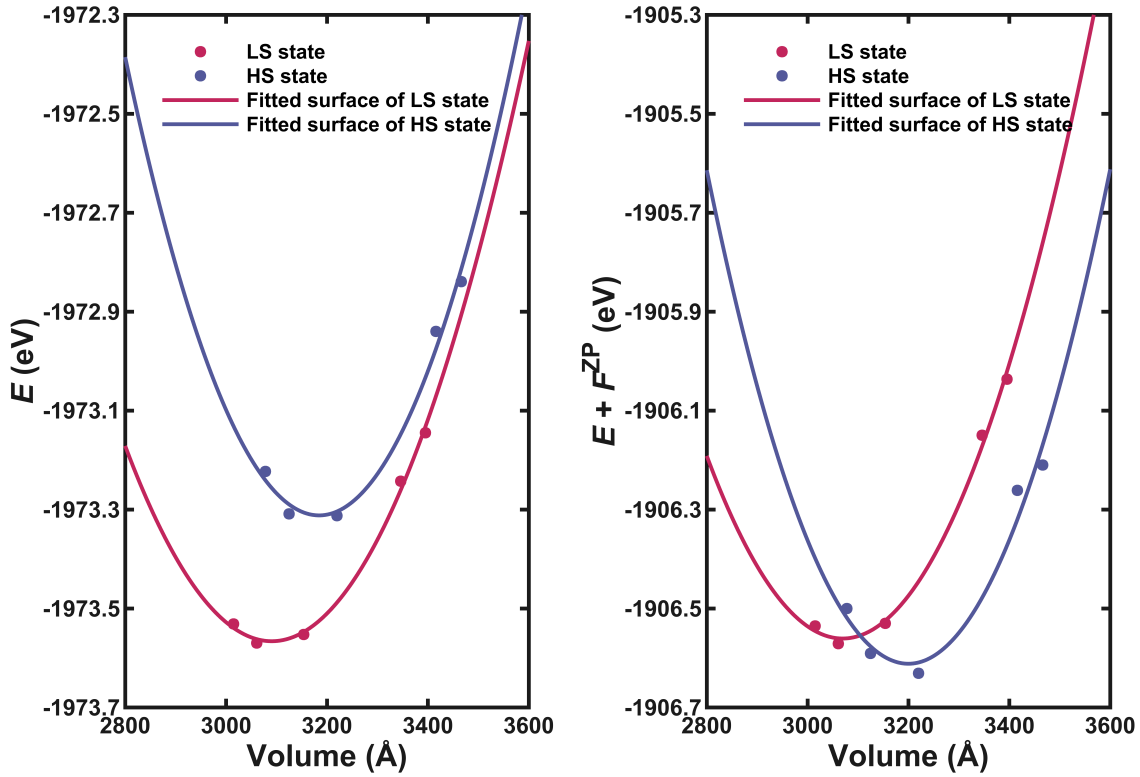

Figure 4.5: (a) The electronic energy surfaces $E(V)$ of the LS and HS states constructed by quadratic fitting of data points; (b) The Helmholtz free energy surfaces $F(V)$ at 0 K, which also represent the surfaces of electronic energy E plus zero-point motion energy F^{ZP}.

4.6 Force Field-Predicted Quasi-Harmonic Approximation Calculations

The relationship between electronic energy and volume was derived from volume-fixed relaxations using MLFFs. The electronic energy surfaces for both LS and HS states were obtained by quadratic fitting of five volume points. As shown in figure 4.5 (a), the electronic energy of the HS state at the minimum volume on the fitted surface is 84.8 meV higher than that of the LS state, consistent with the ΔH_{HL} calculated from the optimised unit cells. According to QHA, the phonon frequencies at different volumes were computed using MLFF. The variation of Helmholtz free energy with volume at 0 K was obtained, plotted in figure 4.5 (b). The 0 K Helmholtz free energy surfaces of LS and

HS states were also constructed through quadratic fitting of data points. The equilibrium volumes were changed after considering the temperature-independent zero-point motion. Compared to the minimum volume of the electronic energy surface, the minimum volume of the Helmholtz free energy surface for the LS state decreased by 21.1 $Å^3$, while for the HS state, it increased by 15.4 $Å^3$. This indicates that considering zero-point motions causes a slight change in the lattice parameters, known as zero-point lattice expansion. A more significant effect of zero-point motion is that it dramatically changes the energy difference between HS and LS states. The zero-point motion energy of the LS state is 101.8 meV higher than that of the HS state, even exceeding the electronic energy difference. This alters the ground state from LS to HS, which would imply that thermally induced SCO cannot occur.

This zero-point renormalisation is often neglected in DFT calculations of ΔH_{HL}, primarily to avoid the high computational costs associated with phonon calculations.[5,55] Our results indicate that zero-point effects play a crucial role in accurately calculating the ΔH_{HL}, and oversimplification may lead to subsequent studies being based on incorrect conclusions. In recent years, some studies have started to focus on zero-point corrections,[118] for example, highlighting that zero-point renormalisation must be taken into account in non-diabatic effects to obtain accurate electronic band gaps in semiconductors and insulators.[119,120] This aspect has rarely been mentioned in the current studies of SCO materials. If the zero-point effect is considered from the beginning, we would expect to get a optimal U_{eff} value greater than 1.9 eV. In fact, some literatures have indicated that, for Fe(II) complexes, the U_{eff} value for obtaining the correct spin-state splitting energy should be much larger than 1.9 eV.[121–123]

The Helmholtz free energy surfaces at different temperatures are shown in figure 4.6. It can be observed that, even at 290 K, the fitting surfaces for the HS state still accurately describe each volume point. In contrast, the LS state data points increasingly deviate from the quadratic fitting surfaces as

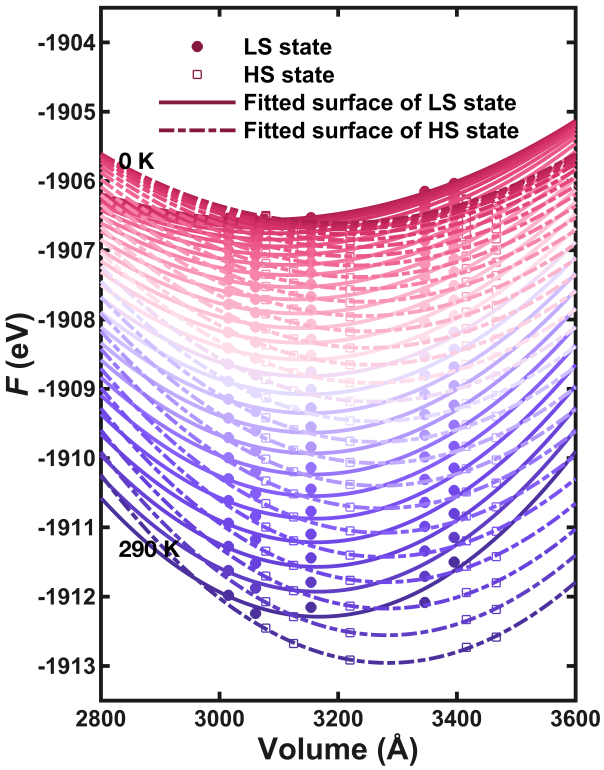

Figure 4.6: The Helmholtz free energy F of the LS and HS states versus volume at temperatures from 0 K to 290 K in 10 K intervals. The Helmholtz free energy surfaces of the LS state (solid lines) and HS state (dotted lines) were obtained by quadratic fitting of the plus-sign and circle data points, respectively. The data points were generated by QHA calculations based on MLFFs.

the temperature rises, indicating stronger anharmonicity in the LS state. The Helmholtz free energy surfaces of both LS and HS states gradually stabilise with temperature, and this stabilisation is more significant for the HS state since entropy favours the HS state. At 290 K, the Helmholtz free energy surface of the LS state decreased by 5.7 eV compared to 0 K, while the HS state decreased by 6.3 eV. Suppose the Helmholtz free energy of the LS state is lower than that of the HS state at absolute zero. In that case, the difference in entropy effects will lead to the minimum volume of the HS state surface having the same energy as the minimum volume of the LS state surface at a specific temperature, which should be the thermal transition temperature $T_{1/2}$. Unfortunately, with our method, the Helmholtz free energy surface of the HS state is always lower than that of the LS state. The variation of the minimum volume on the Helmholtz free energy surface with temperature is also

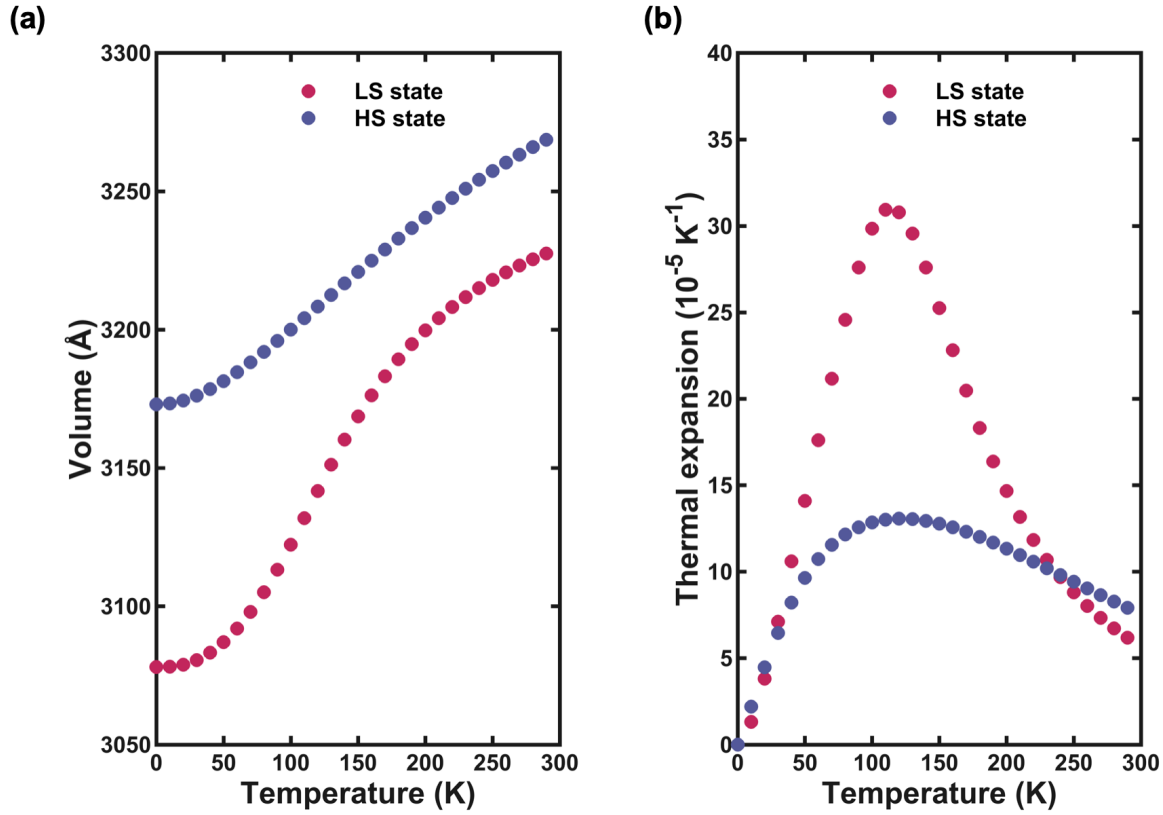

Figure 4.7: (a) Equilibrium volume V_{eq} of $[Fe(ptz)_6](BF_4)_2$ unit cell as a function of temperature in LS and HS states; (b) Variation of the thermal expansion coefficient α_V with the temperature predicted by the MLFFs.

observed, which is more clearly illustrated in figure 4.7 (a). It shows that the equilibrium volume increases with temperature for both the LS and HS states, known as the thermal expansion effect. The thermal expansion coefficient date α_V, reflecting the rate of volume change with temperature, is shown in figure 4.7 (b). During temperature increases, the thermal expansion of the LS state is more significant than that of the HS state, which reduces the relative stability of the LS state and promotes the SCO to the HS state.

The limitation of the strategy described here lies in the underlying DFT reference, which incorrectly estimated the spin-state splitting energy at 0 K due to neglecting zero-point effects, rather than any limitation of the MLFF itself. If a theoretical method that correctly describes the ΔH_{HL} of the system is chosen to train the MLFFs, the machine-learned potentials developed under this

strategy could be capable of predicting $T_{1/2}$ of $[Fe(ptz)_6](BF_4)_2$ through QHA calculations and have the potential to be further applied to other SCO systems. Overall, the results for MLFFs are promising. In addition, a possible ML-driven MD simulation scheme will be proposed in section 5.1.

Chapter 5

Conclusion

In this thesis, two machine learning force fields for the low-spin and high-spin states of the spin-crossover lattice $[Fe(ptz)_6](BF_4)_2$ were developed. The force fields were trained through on-the-fly learning from molecular dynamics simulations, using PBE-D3(BJ)+U with U_{eff} = 1.9 eV as the reference method. Benchmark tests were performed on spin-crossover-related properties, including energies, forces, optimised geometries, the enthalpy difference between spin states, and the phonon density of states. The machine learning force fields achieved the same accuracy as the DFT with higher computational efficiency, notably accelerating the phonon calculations by three orders of magnitude. Quasi-harmonic approximation calculations based on machine-learned force fields provided reliable predictions of thermal expansion effects, which have significant implications for understanding lattice dynamics in spin-crossover system. Using DFT, these calculations would be time-consuming. Furthermore, it was found that the zero-point effects are crucial in estimating the enthalpy difference, even exceeding the electronic contribution. Therefore, future DFT+U calculations should consider the zero-point renormalisation to obtain an accurate enthalpy difference. An reliable underlying DFT method combined with the machine learning force fields development strategy offers a promising pathway for efficient and accurate modelling of solid-state spin-crossover materials.

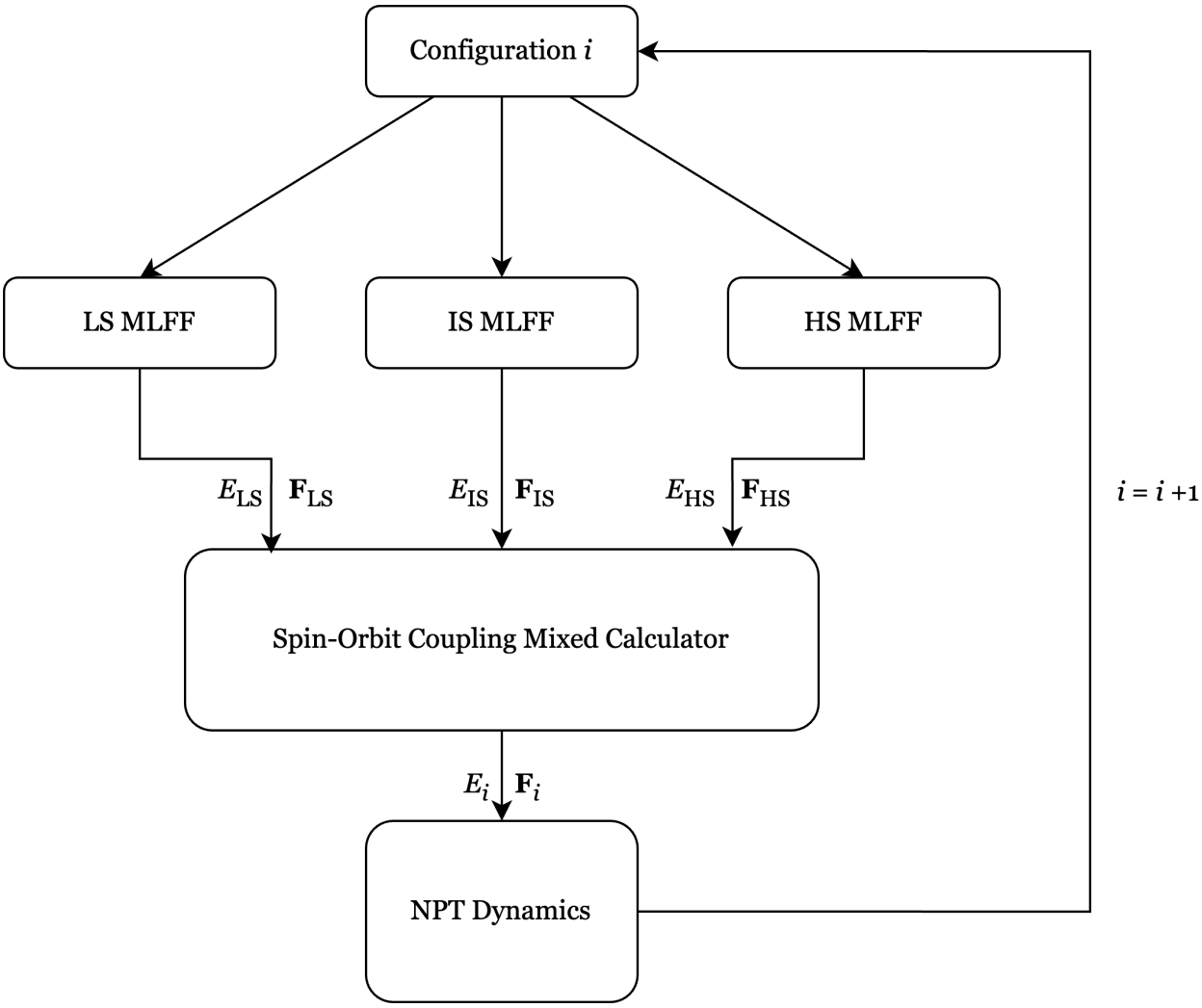

Figure 5.1: Flowchart of molecular dynamics simulations driven by machine learned force fields.

5.1 Future Work

5.1.1 Machine Learning-Driven Molecular Dynamics Simulations

Compared to QHA, MD can directly simulate the effects of temperature on lattice vibrations and structure to capture spin crossover. Therefore, integrating MLFF with MD simulations would be a more ideal approach. In this section, we have preliminarily developed a scheme that uses our MLFFs to drive MD simulations, as shown in figure 5.1. To allow the lattice system to change its spin states, we introduced an intermediate spin state (S = 1 and 2S + 1 = 3) and trained the IS MLFF for it. Introducing spin-orbit coupling (SCO) into the electronic Hamiltonian enables mixing between states

with a total spin angular momentum difference of ± 1.[124]

In this scheme, we provide the initial configuration and timestep, with the SOC mixed calculator integrating the outputs of each MLFF to calculate forces and energies for MD simulations. The working principle is as follows: for configuration i, the ASE interface VASP initiates MLFFs for self-consistent calculations, resulting in LS state energy and force denoted as E_{LS} and $\mathbf{F}_{\mathrm{LS}}$, IS state energy and force denoted as E_{IS} and $\mathbf{F}_{\mathrm{IS}}$, and HS state energy and force denoted as E_{HS} and $\mathbf{F}_{\mathrm{HS}}$. The spin-orbit interaction Hamiltonian in bases of $|\mathrm{LS}\rangle$, $|\mathrm{IS}\rangle$, and $|\mathrm{HS}\rangle$ can be expressed as[10]

$$\begin{aligned}\hat{H}_{\mathrm{SO}} = {} & E_{\mathrm{LS}} |\mathrm{LS}\rangle \langle \mathrm{LS}| + E_{\mathrm{IS}} |\mathrm{IS}\rangle \langle \mathrm{IS}| + E_{\mathrm{HS}} |\mathrm{HS}\rangle \langle \mathrm{HS}| \\ & + \zeta \left(\sqrt{6}\ |\mathrm{LS}\rangle \langle \mathrm{IS}| + \sqrt{3}\ |\mathrm{HS}\rangle \langle \mathrm{IS}| - \sqrt{6}\ |\mathrm{IS}\rangle \langle \mathrm{LS}| - \sqrt{3}\ |\mathrm{IS}\rangle \langle \mathrm{HS}| \right)\end{aligned} \tag{5.1}$$

where the SOC constant ζ should be calculated from first principles or MLFF. We diagonalise the Hamiltonian 5.1 to obtain the eigenvalues $\tilde{E}_{\mathrm{LS}}$, $\tilde{E}_{\mathrm{IS}}$ and $\tilde{E}_{\mathrm{HS}}$, along with the eigenvectors $|\tilde{\mathrm{LS}}\rangle$, $|\tilde{\mathrm{IS}}\rangle$, and $|\tilde{\mathrm{HS}}\rangle$. Then, the mixed force and energy are calculated by

$$\mathbf{F}_i = \langle \tilde{\mathrm{LS}} | \tilde{\mathrm{LS}} \rangle \cdot \mathbf{F}_{\mathrm{LS}} + \langle \tilde{\mathrm{IS}} | \tilde{\mathrm{IS}} \rangle \cdot \mathbf{F}_{\mathrm{IS}} + \langle \tilde{\mathrm{HS}} | \tilde{\mathrm{HS}} \rangle \cdot \mathbf{F}_{\mathrm{HS}} \tag{5.2}$$

$$E_i = \langle \tilde{\mathrm{LS}} | \tilde{\mathrm{LS}} \rangle \cdot E_{\mathrm{LS}} + \langle \tilde{\mathrm{IS}} | \tilde{\mathrm{IS}} \rangle \cdot E_{\mathrm{IS}} + \langle \tilde{\mathrm{HS}} | \tilde{\mathrm{HS}} \rangle \cdot E_{\mathrm{HS}} \tag{5.3}$$

Given the force and timestep, we can predict the configuration for the next MD step, configuration $i+1$, using NPT dynamics,[125–127] which combines Nosé-Hoover[128–130] and Parrinello-Rahman[131–133] dynamics to create the NPT ensemble.

A possible ML-driven MD simulation approach uses a timestep of 2 fs. The LS state relaxed structure from MLFF is simulated at 50 K for 20 ps to reach equilibrium. Then, the temperature is increased from 50 K to 250 K in increments of 10 K, running for 20 ps at each temperature (an example Python script for this process is provided in appendix A.7). Subsequently, the system is cooled from 250 K to 50 K at 10 K intervals. During the MD simulations, system information such as

temperature, potential energy, kinetic energy, and total energy is collected at 200 fs intervals, and structural information of the configurations, including lattice parameters, volume, and Fe-N bond lengths, is also recorded. The volume and the metal-ligand bond lengths are used as observables to monitor the spin states of the system over time and predict the thermal transition temperature $T_{1/2}$.

However, a current technical issue is that if a VASP calculator on ASE is used to perform self-consistent calculations for three MLFFs at each MD step, there will be only a slight improvement in efficiency. For a non-equilibrium configuration in the MD trajectory, DFT takes about half an hour to calculate the energy and force for one spin state, whereas MLFF takes around 2 minutes. Since the three force fields are not computed in parallel on ASE, the time required for each MD step is approximately 7 minutes. The previously described MD simulation approach involves 535000 MD steps, meaning it would take more than seven years to complete MLFF-based MD simulations for a unit cell under this scheme. From appendix A.1, it can be seen that MLFFs take only 8-10 minutes for expensive phonon calculations. But for cheaper self-consistent calculations of equilibrium geometries, MLFF sometimes takes longer than DFT because initialising MLFF in VASP takes nearly 2 minutes. Once initialisation is complete, MLFFs can carry out rapid predictions. When MLFF is used in VASP to conduct MD simulations for a single spin state, each MD step takes only a few seconds, but it would be difficult to simulate the SCO effect without using SOC. Future research will aim to solve this technical problem, such as improving computational efficiency by avoiding restarting VASP at each MD step. Once this issue can be resolved, achieving high-accuracy MD simulations that capture the underlying quantum effects over supercells and long timescales will be possible.

Bibliography

[1] Vallone, S. P.; Tantillo, A. N.; dos Santos, A. M.; Molaison, J. J.; Kulmaczewski, R.; Chapoy, A.; Ahmadi, P.; Halcrow, M. A.; Sandeman, K. G. *Advanced Materials* **2019**, *31*, 1807334.

[2] Tan, H.; Nadeem, M.; Powell, B. J. Unpublished work.

[3] Shelest, V. V.; Khristov, A. V.; Levchenko, G. G. *Low Temperature Physics* **2016**, *42*, 505–512.

[4] Kusz, J.; Zubko, M.; Neder, R. B.; Gütlich, P. *Acta Crystallographica Section B* **2012**, *68*, 40–56.

[5] Ohlrich, M.; Powell, B. J. *The Journal of Chemical Physics* **2020**, *153*, 104107.

[6] Tuchagues, J.-P.; Bousseksou, A.; Molnár, G.; McGarvey, J. J.; Varret, F. *Spin Crossover in Transition Metal Compounds III*; Springer Berlin Heidelberg: Berlin, Heidelberg, 2004; pp 84–103.

[7] Kusz, J.; Spiering, H.; Gütlich, P. *Journal of Applied Crystallography* **2004**, *37*, 589–595.

[8] Jeftić, J.; Hauser, A. *The Journal of Physical Chemistry B* **1997**, *101*, 10262–10270.

[9] Cambi, L.; Szegö, L. *Berichte der deutschen chemischen Gesellschaft (A and B Series)* **1931**, *64*, 2591–2598.

[10] Nadeem, M.; Cruddas, J.; Ruzzi, G.; Powell, B. J. *Journal of the American Chemical Society* **2022**, *144*, 9138–9148.

[11] Hauser, A. *Spin Crossover in Transition Metal Compounds II*; Springer Berlin Heidelberg: Berlin, Heidelberg, 2004; pp 155–198.

[12] Gütlich, P.; Ksenofontov, V.; Gaspar, A. B. *Coordination Chemistry Reviews* **2005**, *249*, 1811–1829.

[13] Negre, N.; Goiran, M.; Bousseksou, A.; Haasnoot, J.; Boukheddaden, K.; Askenazy, S.; Varret, F. *Synthetic Metals* **2000**, *115*, 289–292.

[14] Carlin, R. L.; van Duyneveldt, A. J. *Magnetic Properties of Transition Metal Compounds*; Springer Berlin Heidelberg: Berlin, Heidelberg, 1977.

[15] Gaspar, A. B.; Molnár, G.; Rotaru, A.; Shepherd, H. J. *Comptes Rendus Chimie* **2018**, *21*, 1095–1120.

[16] Collet, E.; Guionneau, P. *Comptes Rendus Chimie* **2018**, *21*, 1133–1151.

[17] Faulmann, C.; Jacob, K.; Dorbes, S.; Lampert, S.; Malfant, I.; Doublet, M.-L.; Valade, L.; Real, J. A. *Inorganic Chemistry* **2007**, *46*, 8548–8559.

[18] Rotaru, A.; Gural'skiy, I. A.; Molnár, G.; Salmon, L.; Demont, P.; Bousseksou, A. *Chem. Commun.* **2012**, *48*, 4163–4165.

[19] Shakirova, O. G.; Os'kina, I. A.; Korotaev, E. V.; Petrov, S. A.; Kuratieva, N. V.; Tikhonov, A. Y.; Lavrenova, L. G. *International Journal of Molecular Sciences* **2023**, *24*, 9853.

[20] Pillet, S. *Journal of Applied Physics* **2021**, *129*, 181101.

[21] Kulshreshtha, S.; Iyer, R. *Chemical Physics Letters* **1987**, *134*, 239–244.

[22] Kulshreshtha, S.; Sasikala, R.; König, E. *Chemical Physics Letters* **1986**, *123*, 215–217.

[23] O'Connor, C. J. *Molecule-Based Magnetic Materials*; American Chemical Society, 1996; Chapter 4, pp 44–66.

[24] Zhang, J. L.; Zhong, J. Q.; Lin, J. D.; Hu, W. P.; Wu, K.; Xu, G. Q.; Wee, A. T. S.; Chen, W. *Chem. Soc. Rev.* **2015**, *44*, 2998–3022.

[25] Ekanayaka, T. K.; Hao, G.; Mosey, A.; Dale, A. S.; Jiang, X.; Yost, A. J.; Sapkota, K. R.; Wang, G. T.; Zhang, J.; N'Diaye, A. T.; Marshall, A.; Cheng, R.; Naeemi, A.; Xu, X.; Dowben, P. A. *Magnetochemistry* **2021**, *7*, 37.

[26] Bartual-Murgui, C.; Akou, A.; Thibault, C.; Molnár, G.; Vieu, C.; Salmon, L.; Bousseksou, A. *J. Mater. Chem. C* **2015**, *3*, 1277–1285.

[27] Linares, J.; Codjovi, E.; Garcia, Y. *Sensors* **2012**, *12*, 4479–4492.

[28] Kahn, O.; Kröber, J.; Jay, C. *Advanced Materials* **1992**, *4*, 718–728.

[29] Shepherd, H. J.; Gural'skiy, I. A.; Quintero, C. M.; Tricard, S.; Salmon, L.; Molnár, G.; Bousseksou, A. *Nature Communications* **2013**, *4*, 2607.

[30] Kahn, O.; Martinez, C. J. *Science* **1998**, *279*, 44–48.

[31] Atmani, C.; El Hajj, F.; Benmansour, S.; Marchivie, M.; Triki, S.; Conan, F.; Patinec, V.; Handel, H.; Dupouy, G.; Gómez-García, C. J. *Coordination Chemistry Reviews* **2010**, *254*, 1559–1569.

[32] Janet, J. P.; Kulik, H. J. *The Journal of Physical Chemistry A* **2017**, *121*, 8939–8954.

[33] Janet, J. P.; Chan, L.; Kulik, H. J. *The Journal of Physical Chemistry Letters* **2018**, *9*, 1064–1071.

[34] Nandy, A.; Duan, C.; Taylor, M. G.; Liu, F.; Steeves, A. H.; Kulik, H. J. *Chemical Reviews* **2021**, *121*, 9927–10000.

[35] Pauling, L. *Journal of Chemical Education* **1962**, *39*, 461.

[36] Bethe, H. *Annalen der Physik* **1929**, *395*, 133–208.

[37] Sarmah, A.; Hobza, P. *Nanoscale Adv.* **2020**, *2*, 2907–2913.

[38] Delgado, T.; Enachescu, C.; Tissot, A.; Hauser, A.; Guénée, L.; Besnard, C. *J. Mater. Chem. C* **2018**, *6*, 12698–12706.

[39] Bousseksou, A.; McGarvey, J. J.; Varret, F.; Real, J. A.; Tuchagues, J.-P.; Dennis, A. C.; Boillot, M. L. *Chemical Physics Letters* **2000**, *318*, 409–416.

[40] Sorai, M.; Seki, S. *Journal of Physics and Chemistry of Solids* **1974**, *35*, 555–570.

[41] Nicolazzi, W.; Bousseksou, A. *Comptes Rendus Chimie* **2018**, *21*, 1060–1074.

[42] Wu, J.; Sousa, C.; de Graaf, C. *Magnetochemistry* **2019**, *5*, 49.

[43] Nakamoto, T.; Tan, Z.-C.; Sorai, M. *Inorganic Chemistry* **2001**, *40*, 3805–3809.

[44] Gütlich, P.; Gaspar, A. B.; Garcia, Y. *Beilstein Journal of Organic Chemistry* **2013**, *9*, 342–391.

[45] Létard, J.-F.; Capes, L.; Chastanet, G.; Moliner, N.; Létard, S.; Real, J.-A.; Kahn, O. *Chemical Physics Letters* **1999**, *313*, 115–120.

[46] Decurtins, S.; Gütlich, P.; Köhler, C.; Spiering, H.; Hauser, A. *Chemical Physics Letters* **1984**, *105*, 1–4.

[47] Hauser, A. *Chemical Physics Letters* **1986**, *124*, 543–548.

[48] Allen, F. H. *Acta Crystallographica Section B* **2002**, *58*, 380–388.

[49] Hauser, A.; Guetlich, P.; Spiering, H. *Inorganic Chemistry* **1986**, *25*, 4245–4248.

[50] Cirera, J.; Paesani, F. *Inorganic Chemistry* **2012**, *51*, 8194–8201.

[51] Vennelakanti, V.; Taylor, M. G.; Nandy, A.; Duan, C.; Kulik, H. J. *The Journal of Chemical Physics* **2023**, *159*, 024120.

[52] Romero, S.; Baruah, T.; Zope, R. R. *The Journal of Chemical Physics* **2023**, *158*, 054305.

[53] Reiher, M.; Salomon, O.; Artur Hess, B. *Theoretical Chemistry Accounts* **2001**, *107*, 48–55.

[54] Reiher, M. *Inorganic Chemistry* **2002**, *41*, 6928–6935.

[55] Jensen, K. P.; Cirera, J. *The Journal of Physical Chemistry A* **2009**, *113*, 10033–10039.

[56] Cirera, J.; Via-Nadal, M.; Ruiz, E. *Inorganic Chemistry* **2018**, *57*, 14097–14105.

[57] Himmetoglu, B.; Floris, A.; de Gironcoli, S.; Cococcioni, M. *International Journal of Quantum Chemistry* **2014**, *114*, 14–49.

[58] Anisimov, V. I.; Zaanen, J.; Andersen, O. K. *Phys. Rev. B* **1991**, *44*, 943–954.

[59] Dudarev, S. L.; Botton, G. A.; Savrasov, S. Y.; Humphreys, C. J.; Sutton, A. P. *Phys. Rev. B* **1998**, *57*, 1505–1509.

[60] Perdew, J. P.; Burke, K.; Ernzerhof, M. *Phys. Rev. Lett.* **1996**, *77*, 3865–3868.

[61] Reilly, A. M.; Tkatchenko, A. *The Journal of Chemical Physics* **2013**, *139*, 024705.

[62] Miyawaki, A.; Mochida, T.; Sakurai, T.; Ohta, H.; Takahashi, K. *Inorganic Chemistry* **2020**, *59*, 12295–12303.

[63] Navarro, L.; Rodriguez, F.; Cirera, J. *Dalton Trans.* **2021**, *50*, 8704–8710.

[64] Arias-Olivares, D.; de Armas, R. S.; Calzado, C. *Materials Today Chemistry* **2023**, *30*, 101489.

[65] Mejía-Rodríguez, D.; Albavera-Mata, A.; Fonseca, E.; Chen, D.-T.; Cheng, H.-P.; Hennig, R. G.; Trickey, S. *Computational Materials Science* **2022**, *206*, 111161.

[66] Roy Chowdhury, S.; Nguyen, N.; Vlaisavljevich, B. *The Journal of Physical Chemistry A* **2023**, *127*, 3072–3081.

[67] Kepp, K. P. *Inorganic Chemistry* **2016**, *55*, 2717–2727.

[68] Tkatchenko, A.; Scheffler, M. *Phys. Rev. Lett.* **2009**, *102*, 073005.

[69] Grimme, S. *Journal of Computational Chemistry* **2006**, *27*, 1787–1799.

[70] Grimme, S.; Antony, J.; Ehrlich, S.; Krieg, H. *The Journal of Chemical Physics* **2010**, *132*, 154104.

[71] Grimme, S.; Ehrlich, S.; Goerigk, L. *Journal of Computational Chemistry* **2011**, *32*, 1456–1465.

[72] Caldeweyher, E.; Ehlert, S.; Hansen, A.; Neugebauer, H.; Spicher, S.; Bannwarth, C.; Grimme, S. *The Journal of Chemical Physics* **2019**, *150*, 154122.

[73] Becke, A. D.; Johnson, E. R. *The Journal of Chemical Physics* **2007**, *127*, 154108.

[74] Tkatchenko, A.; DiStasio, R. A.; Car, R.; Scheffler, M. *Phys. Rev. Lett.* **2012**, *108*, 236402.

[75] Ambrosetti, A.; Reilly, A. M.; DiStasio, J., Robert A.; Tkatchenko, A. *The Journal of Chemical Physics* **2014**, *140*, 18A508.

[76] Johnson, E. R.; Becke, A. D. *The Journal of Chemical Physics* **2005**, *123*, 024101.

[77] Becke, A. D.; Johnson, E. R. *The Journal of Chemical Physics* **2005**, *123*, 154101.

[78] Johnson, E. R.; Becke, A. D. *The Journal of Chemical Physics* **2006**, *124*, 174104.

[79] Enachescu, C.; Nicolazzi, W. *Comptes Rendus Chimie* **2018**, *21*, 1179–1195.

[80] Meyer, R.; Mücksch, C.; Wolny, J. A.; Schünemann, V.; Urbassek, H. M. *Chemical Physics Letters* **2019**, *733*, 136666.

[81] Mi, S.; Fahs, A.; Molnár, G.; Nicolazzi, W.; Bousseksou, A. *Chemical Physics Letters* **2023**, *811*, 140232.

[82] Herz, J.; Meyer, R.; Wolny, J. A.; Schünemann, V.; Urbassek, H. M. *Applied Physics A* **2023**, *129*, 345.

[83] Mi, S.; Molnár, G.; Ridier, K.; Nicolazzi, W.; Bousseksou, A. *Phys. Rev. B* **2024**, *109*, 054103.

[84] Tarafder, K.; Kanungo, S.; Oppeneer, P. M.; Saha-Dasgupta, T. *Phys. Rev. Lett.* **2012**, *109*, 077203.

[85] Carrier, P.; Wentzcovitch, R.; Tsuchiya, J. *Phys. Rev. B* **2007**, *76*, 064116.

[86] Huang, L.-F.; Lu, X.-Z.; Tennessen, E.; Rondinelli, J. M. *Computational Materials Science* **2016**, *120*, 84–93.

[87] Thomas, L. H. *Mathematical Proceedings of the Cambridge Philosophical Society* **1927**, *23*, 542–548.

[88] Fermi, E. *Rend. Accad. Naz. Lincei* **1927**, *6*, 32.

[89] Hohenberg, P.; Kohn, W. *Physical Review* **1964**, *136*, B864–B871.

[90] Kohn, W.; Sham, L. J. *Physical Review* **1965**, *137*, A1697–A1705.

[91] Kohn, W.; Sham, L. J. *Physical Review* **1965**, *140*, A1133–A1138.

[92] Dirac, P. A. M. *Mathematical Proceedings of the Cambridge Philosophical Society* **1930**, *26*, 376–385.

[93] Perdew, J. P.; Yue, W. *Phys. Rev. B* **1986**, *33*, 8800–8802.

[94] Becke, A. D. *The Journal of Chemical Physics* **1988**, *88*, 1053–1062.

[95] Becke, A. D. *The Journal of Chemical Physics* **1993**, *98*, 5648–5652.

[96] Stephens, P. J.; Devlin, F. J.; Chabalowski, C. F.; Frisch, M. J. *The Journal of Physical Chemistry* **1994**, *98*, 11623–11627.

[97] Tolba, S. A.; Gameel, K. M.; Ali, B. A.; Almossalami, H. A.; Allam, N. K. In *Density Functional Calculations*; Yang, G., Ed.; IntechOpen: Rijeka, 2018; Chapter 1.

[98] Yu, M.; Yang, S.; Wu, C.; Marom, N. *npj Computational Materials* **2020**, *6*, 180.

[99] Ashcroft, N.; Mermin, N. *Solid State Physics*; HRW international editions; Holt, Rinehart and Winston, 1976.

[100] Brooker, S. *Chem. Soc. Rev.* **2015**, *44*, 2880–2892.

[101] Murphy, M. J.; Zenere, K. A.; Ragon, F.; Southon, P. D.; Kepert, C. J.; Neville, S. M. *Journal of the American Chemical Society* **2017**, *139*, 1330–1335.

[102] Nishino, M.; Singh, Y.; Boukheddaden, K.; Miyashita, S. *Journal of Applied Physics* **2021**, *130*, 141102.

[103] Parlinski, K. In *Encyclopedia of Condensed Matter Physics*; Bassani, F., Liedl, G. L., Wyder, P., Eds.; Elsevier: Oxford, 2005; pp 98–102.

[104] Kresse, G.; Furthmüller, J. *Phys. Rev. B* **1996**, *54*, 11169–11186.

[105] Blöchl, P. E. *Phys. Rev. B* **1994**, *50*, 17953–17979.

[106] Togo, A.; Chaput, L.; Tadano, T.; Tanaka, I. *J. Phys. Condens. Matter* **2023**, *35*, 353001.

[107] Togo, A. *J. Phys. Soc. Jpn.* **2023**, *92*, 012001.

[108] Momma, K.; Izumi, F. *Journal of Applied Crystallography* **2011**, *44*, 1272–1276.

[109] Larsen, A. H. et al. *Journal of Physics: Condensed Matter* **2017**, *29*, 273002.

[110] Liu, P.; Verdi, C.; Karsai, F.; Kresse, G. *Phys. Rev. Mater.* **2021**, *5*, 053804.

[111] Verdi, C.; Karsai, F.; Liu, P.; Jinnouchi, R.; Kresse, G. *npj Computational Materials* **2021**, *7*, 156.

[112] Parlinski, K.; Li, Z. Q.; Kawazoe, Y. *Phys. Rev. Lett.* **1997**, *78*, 4063–4066.

[113] Murnaghan, F. D. *American Journal of Mathematics* **1937**, *59*, 235–260.

[114] Birch, F. *Phys. Rev.* **1947**, *71*, 809–824.

[115] Wieser, S.; Zojer, E. *npj Computational Materials* **2024**, *10*, 18.

[116] Kamencek, T.; Schrode, B.; Resel, R.; Ricco, R.; Zojer, E. *Advanced Theory and Simulations* **2022**, *5*, 2200031.

[117] Spiering, H. *Spin Crossover in Transition Metal Compounds III*; Springer Berlin Heidelberg: Berlin, Heidelberg, 2004; pp 171–195.

[118] Engel, M.; Miranda, H.; Chaput, L.; Togo, A.; Verdi, C.; Marsman, M.; Kresse, G. *Phys. Rev. B* **2022**, *106*, 094316.

[119] Miglio, A.; Brousseau-Couture, V.; Godbout, E.; Antonius, G.; Chan, Y.-H.; Louie, S. G.; Côté, M.; Giantomassi, M.; Gonze, X. *npj Computational Materials* **2020**, *6*, 167.

[120] Brousseau-Couture, V.; Godbout, E.; Côté, M.; Gonze, X. *Phys. Rev. B* **2022**, *106*, 085137.

[121] Lebègue, S.; Pillet, S.; Ángyán, J. G. *Phys. Rev. B* **2008**, *78*, 024433.

[122] Bučko, T.; Hafner, J.; Lebègue, S.; Ángyán, J. G. *Phys. Chem. Chem. Phys.* **2012**, *14*, 5389–5396.

[123] Chen, J.; Millis, A. J.; Marianetti, C. A. *Phys. Rev. B* **2015**, *91*, 241111.

[124] Yang, B.; Gagliardi, L.; Truhlar, D. G. *Phys. Chem. Chem. Phys.* **2018**, *20*, 4129–4136.

[125] Holian, B. L.; De Groot, A. J.; Hoover, W. G.; Hoover, C. G. *Phys. Rev. A* **1990**, *41*, 4552–4553.

[126] Simone Melchionna, G. C.; Holian, B. L. *Molecular Physics* **1993**, *78*, 533–544.

[127] Melchionna, S. *Phys. Rev. E* **2000**, *61*, 6165–6170.

[128] Nosé, S. *The Journal of Chemical Physics* **1984**, *81*, 511–519.

[129] Hoover, W. G. *Phys. Rev. A* **1985**, *31*, 1695–1697.

[130] Evans, D. J.; Holian, B. L. *The Journal of Chemical Physics* **1985**, *83*, 4069–4074.

[131] Parrinello, M.; Rahman, A. *Phys. Rev. Lett.* **1980**, *45*, 1196–1199.

[132] Parrinello, M.; Rahman, A. *Journal of Applied Physics* **1981**, *52*, 7182–7190.

[133] Parrinello, M.; Rahman, A. *The Journal of Chemical Physics* **1982**, *76*, 2662–2666.

Appendix A

Appendix

A.1 Time Information

Table A.1: Computational time and the number of CPUs used for various job types.

Job types	Total time (s)		CPUs	
	LS	HS	LS	HS
DFT full relaxation	14880	25198	96	96
DFT self-consistent calculation	61	151	96	96
DFT phonon	1911158	559171	28	96
MLFF train	845853	1652491	28	28
MLFF refit	9213	8473	96	96
MLFF full relaxation	119	107	96	96
MLFF self-consistent calculation	106	104	96	96
MLFF phonon	532	607	96	96

In table A.1, self-consistent calculations refer to a self-consistent calculation of the relaxed geometry to obtain more accurate energy, which typically converges quickly. For the self-consistent calculations of non-equilibrium geometries, the chosen DFT method usually takes more than half an hour, whereas the MLFF takes about 2 minutes. The training of the MLFF and the DFT phonon calculation for the LS state was carried out on the SMP Getafix cluster, as these jobs have long runtimes. On Getafix, there is no limitation on wall time, and 28 CPUs were requested for a single job. The calculations for the remaining job types were performed on the UQ Bunya supercomputer, requesting 96 CPUs.

A.2 Starting Geometries in POSCAR Format

LS State

The initial structure of the LS state was obtained from experiment.[7]

```
C24 H48  N24 Fe, 2(B F4)
1.0
       10.7010002136         0.0000000000         0.0000000000
       -5.3505001068         9.2673380309         0.0000000000
        0.0000000000         0.0000000000        31.8999996185
   Fe    N    C    H    F    B
    3   72   72  144   24    6
Direct
     0.000000000          0.000000000          0.000000000
     0.666666687          0.333333343          0.333333343
     0.333333343          0.666666687          0.666666687
     0.047370002          0.876450002          0.035620000
     0.952629983          0.123549998          0.964380026
     0.123549998          0.170919999          0.035620000
     0.876450002          0.829079986          0.964380026
     0.829079986          0.952629983          0.035620000
     0.170919999          0.047370002          0.964380026
     0.714036644          0.209783331          0.368953347
     0.619296670          0.456883341          0.297713339
     0.790216684          0.504253328          0.368953347
     0.543116689          0.162413329          0.297713339
     0.495746672          0.285963327          0.368953347
     0.837586641          0.380703330          0.297713339
     0.380703330          0.543116689          0.702286661
     0.285963327          0.790216684          0.631046653
     0.456883341          0.837586641          0.702286661
     0.209783331          0.495746672          0.631046653
     0.162413329          0.619296670          0.702286661
     0.504253328          0.714036644          0.631046653
     0.165150002          0.929380000          0.061530001
     0.834850013          0.070620000          0.938470006
     0.070620000          0.235770002          0.061530001
     0.929380000          0.764230013          0.938470006
     0.764230013          0.834850013          0.061530001
     0.235770002          0.165150002          0.938470006
     0.831816673          0.262713343          0.394863337
     0.501516640          0.403953344          0.271803319
     0.737286687          0.569103360          0.394863337
     0.596046686          0.097563334          0.271803319
```

```
0.430896670     0.168183327     0.394863337
0.902436674     0.498483330     0.271803319
0.498483330     0.596046686     0.728196681
0.168183327     0.737286687     0.605136693
0.403953344     0.902436674     0.728196681
0.262713343     0.430896670     0.605136693
0.097563334     0.501516640     0.728196681
0.569103360     0.831816673     0.605136693
0.169430003     0.823099971     0.079779997
0.830569983     0.176899999     0.920220017
0.176899999     0.346329987     0.079779997
0.823099971     0.653670013     0.920220017
0.653670013     0.830569983     0.079779997
0.346329987     0.169430003     0.920220017
0.836096644     0.156433329     0.413113326
0.497236669     0.510233343     0.253553331
0.843566656     0.679663360     0.413113326
0.489766657     0.987003326     0.253553331
0.320336670     0.163903326     0.413113326
0.012996669     0.502763331     0.253553331
0.502763331     0.489766657     0.746446669
0.163903326     0.843566656     0.586886644
0.510233343     0.012996669     0.746446669
0.156433329     0.320336670     0.586886644
0.987003326     0.497236669     0.746446669
0.679663360     0.836096644     0.586886644
0.054030001     0.700690031     0.066129997
0.945969999     0.299309999     0.933870018
0.299309999     0.353340000     0.066129997
0.700690031     0.646659970     0.933870018
0.646659970     0.945969999     0.066129997
0.353340000     0.054030001     0.933870018
0.720696688     0.034023333     0.399463326
0.612636685     0.632643342     0.267203331
0.965976655     0.686673343     0.399463326
0.367356658     0.979993343     0.267203331
0.313326657     0.279303342     0.399463326
0.020006666     0.387363344     0.267203331
0.387363344     0.367356658     0.732796669
0.279303342     0.965976655     0.600536644
0.632643342     0.020006666     0.732796669
0.034023333     0.313326657     0.600536644
0.979993343     0.612636685     0.732796669
0.686673343     0.720696688     0.600536644
0.980599999     0.734099984     0.039349999
```

```
0.019400001     0.265899986     0.960650027
0.265899986     0.246499985     0.039349999
0.734099984     0.753499985     0.960650027
0.753499985     0.019400001     0.039349999
0.246499985     0.980599999     0.960650027
0.647266686     0.067433350     0.372683346
0.686066687     0.599233329     0.293983340
0.932566643     0.579833329     0.372683346
0.400766671     0.086833350     0.293983340
0.420166671     0.352733344     0.372683346
0.913166642     0.313933343     0.293983340
0.313933343     0.400766671     0.706016660
0.352733344     0.932566643     0.627316654
0.599233329     0.913166642     0.706016660
0.067433350     0.420166671     0.627316654
0.086833350     0.686066687     0.706016660
0.579833329     0.647266686     0.627316654
0.890900016     0.547199965     0.143299997
0.109099999     0.452800006     0.856700003
0.452800006     0.343699992     0.143299997
0.547199965     0.656300008     0.856700003
0.656300008     0.109099999     0.143299997
0.343699992     0.890900016     0.856700003
0.557566643     0.880533338     0.476633340
0.775766671     0.786133349     0.190033332
0.119466670     0.677033365     0.476633340
0.213866666     0.989633322     0.190033332
0.322966665     0.442433327     0.476633340
0.010366674     0.224233329     0.190033332
0.224233329     0.213866666     0.809966683
0.442433327     0.119466670     0.523366690
0.786133349     0.010366674     0.809966683
0.880533338     0.322966665     0.523366690
0.989633322     0.775766671     0.809966683
0.677033365     0.557566643     0.523366690
0.031399999     0.557500005     0.078029998
0.968599975     0.442499995     0.921970010
0.442499995     0.473899990     0.078029998
0.557500005     0.526099980     0.921970010
0.526099980     0.968599975     0.078029998
0.473899990     0.031399999     0.921970010
0.698066652     0.890833318     0.411363333
0.635266662     0.775833309     0.255303323
0.109166659     0.807233334     0.411363333
0.224166676     0.859433353     0.255303323
```

```
0.192766666     0.301933348     0.411363333
0.140566662     0.364733338     0.255303323
0.364733338     0.224166676     0.744696677
0.301933348     0.109166659     0.588636696
0.775833309     0.140566662     0.744696677
0.890833318     0.192766666     0.588636696
0.859433353     0.635266662     0.744696677
0.807233334     0.698066652     0.588636696
0.015799999     0.534200013     0.125300005
0.984200001     0.465799987     0.874700010
0.465799987     0.481599987     0.125300005
0.534200013     0.518400013     0.874700010
0.518400013     0.984200001     0.125300005
0.481599987     0.015799999     0.874700010
0.682466686     0.867533326     0.458633333
0.650866687     0.799133301     0.208033323
0.132466659     0.814933300     0.458633333
0.200866684     0.851733327     0.208033323
0.185066685     0.317533344     0.458633333
0.148266658     0.349133343     0.208033323
0.349133343     0.200866684     0.791966677
0.317533344     0.132466659     0.541366637
0.799133301     0.148266658     0.791966677
0.867533326     0.185066685     0.541366637
0.851733327     0.650866687     0.791966677
0.814933300     0.682466686     0.541366637
0.896000028     0.664000034     0.025500000
0.104000002     0.335999995     0.974500000
0.335999995     0.231999993     0.025500000
0.664000034     0.768000007     0.974500000
0.768000007     0.104000002     0.025500000
0.231999993     0.896000028     0.974500000
0.562666655     0.997333348     0.358833343
0.770666659     0.669333339     0.307833344
0.002666662     0.565333307     0.358833343
0.330666661     0.101333342     0.307833344
0.434666663     0.437333345     0.358833343
0.898666680     0.229333326     0.307833344
0.229333326     0.330666661     0.692166686
0.437333345     0.002666662     0.641166687
0.669333339     0.898666680     0.692166686
0.997333348     0.434666663     0.641166687
0.101333342     0.770666659     0.692166686
0.565333307     0.562666655     0.641166687
0.879000008     0.519999981     0.173600003
```

```
0.120999999     0.479999989     0.826399982
0.479999989     0.358999997     0.173600003
0.519999981     0.641000032     0.826399982
0.641000032     0.120999999     0.173600003
0.358999997     0.879000008     0.826399982
0.545666695     0.853333354     0.506933331
0.787666678     0.813333333     0.159733325
0.146666661     0.692333341     0.506933331
0.186666682     0.974333346     0.159733325
0.307666689     0.454333335     0.506933331
0.025666656     0.212333336     0.159733325
0.212333336     0.186666682     0.840266645
0.454333335     0.146666661     0.493066669
0.813333333     0.025666656     0.840266645
0.853333354     0.307666689     0.493066669
0.974333346     0.787666678     0.840266645
0.692333341     0.545666695     0.493066669
0.795000017     0.476000011     0.129099995
0.204999998     0.523999989     0.870900035
0.523999989     0.319000006     0.129099995
0.476000011     0.680999994     0.870900035
0.680999994     0.204999998     0.129099995
0.319000006     0.795000017     0.870900035
0.461666673     0.809333324     0.462433338
0.871666670     0.857333302     0.204233333
0.190666661     0.652333319     0.462433338
0.142666683     0.014333342     0.204233333
0.347666681     0.538333356     0.462433338
0.985666633     0.128333330     0.204233333
0.128333330     0.142666683     0.795766652
0.538333356     0.190666661     0.537566662
0.857333302     0.985666633     0.795766652
0.809333324     0.347666681     0.537566662
0.014333342     0.871666670     0.795766652
0.652333319     0.461666673     0.537566662
0.904999971     0.646000028     0.139400005
0.094999999     0.354000002     0.860599995
0.354000002     0.259000003     0.139400005
0.646000028     0.740999997     0.860599995
0.740999997     0.094999999     0.139400005
0.259000003     0.904999971     0.860599995
0.571666658     0.979333341     0.472733349
0.761666656     0.687333345     0.193933323
0.020666668     0.592333317     0.472733349
0.312666655     0.074333332     0.193933323
```

```
0.407666653     0.428333342     0.472733349
0.925666690     0.238333330     0.193933323
0.238333330     0.312666655     0.806066692
0.428333342     0.020666668     0.527266681
0.687333345     0.925666690     0.806066692
0.979333341     0.407666653     0.527266681
0.074333332     0.761666656     0.806066692
0.592333317     0.571666658     0.527266681
0.940999985     0.481999993     0.063400000
0.059000000     0.518000007     0.936599970
0.518000007     0.458999991     0.063400000
0.481999993     0.541000009     0.936599970
0.541000009     0.059000000     0.063400000
0.458999991     0.940999985     0.936599970
0.607666671     0.815333307     0.396733344
0.725666642     0.851333320     0.269933343
0.184666678     0.792333364     0.396733344
0.148666665     0.874333322     0.269933343
0.207666665     0.392333329     0.396733344
0.125666678     0.274333328     0.269933343
0.274333328     0.148666665     0.730066657
0.392333329     0.184666678     0.603266656
0.851333320     0.125666678     0.730066657
0.815333307     0.207666665     0.603266656
0.874333322     0.725666642     0.730066657
0.792333364     0.607666671     0.603266656
0.115000002     0.550000012     0.067199998
0.884999990     0.449999988     0.932799995
0.449999988     0.564999998     0.067199998
0.550000012     0.435000002     0.932799995
0.435000002     0.884999990     0.067199998
0.564999998     0.115000002     0.932799995
0.781666696     0.883333325     0.400533319
0.551666677     0.783333302     0.266133338
0.116666652     0.898333311     0.400533319
0.216666684     0.768333316     0.266133338
0.101666674     0.218333334     0.400533319
0.231666654     0.448333323     0.266133338
0.448333323     0.216666684     0.733866692
0.218333334     0.116666652     0.599466681
0.783333302     0.231666654     0.733866692
0.883333325     0.101666674     0.599466681
0.768333316     0.551666677     0.733866692
0.898333311     0.781666696     0.599466681
0.004000000     0.440999985     0.129500002
```

```
0.995999992     0.559000015     0.870499969
0.559000015     0.563000023     0.129500002
0.440999985     0.436999977     0.870499969
0.436999977     0.995999992     0.129500002
0.563000023     0.004000000     0.870499969
0.670666695     0.774333298     0.462833345
0.662666678     0.892333329     0.203833327
0.225666687     0.896333337     0.462833345
0.107666649     0.770333290     0.203833327
0.103666648     0.329333335     0.462833345
0.229666680     0.337333322     0.203833327
0.337333322     0.107666649     0.796166658
0.329333335     0.225666687     0.537166655
0.892333329     0.229666680     0.796166658
0.774333298     0.103666648     0.537166655
0.770333290     0.662666678     0.796166658
0.896333337     0.670666695     0.537166655
0.104000002     0.601000011     0.138899997
0.896000028     0.398999989     0.861100018
0.398999989     0.503000021     0.138899997
0.601000011     0.497000009     0.861100018
0.497000009     0.896000028     0.138899997
0.503000021     0.104000002     0.861100018
0.770666659     0.934333324     0.472233325
0.562666655     0.732333302     0.194433331
0.065666653     0.836333334     0.472233325
0.267666668     0.830333352     0.194433331
0.163666680     0.229333326     0.472233325
0.169666663     0.437333345     0.194433331
0.437333345     0.267666668     0.805566669
0.229333326     0.065666653     0.527766645
0.732333302     0.169666663     0.805566669
0.934333324     0.163666680     0.527766645
0.830333352     0.562666655     0.805566669
0.836333334     0.770666659     0.527766645
0.962260008     0.862349987     0.331699997
0.037740000     0.137649998     0.668300033
0.137649998     0.099909998     0.331699997
0.862349987     0.900089979     0.668300033
0.900089979     0.037740000     0.331699997
0.099909998     0.962260008     0.668300033
0.628926694     0.195683330     0.665033340
0.704406679     0.470983326     0.001633336
0.804316640     0.433243334     0.665033340
0.529016674     0.233423337     0.001633336
```

```
     0.566756666          0.371073335          0.665033340
     0.766576648          0.295593321          0.001633336
     0.295593321          0.529016674          0.998366654
     0.371073335          0.804316640          0.334966660
     0.470983326          0.766576648          0.998366654
     0.195683330          0.566756666          0.334966660
     0.233423337          0.704406679          0.998366654
     0.433243334          0.628926694          0.334966660
     0.000000000          0.000000000          0.273259997
     0.000000000          0.000000000          0.726740003
     0.666666687          0.333333343          0.606593311
     0.666666687          0.333333343          0.060073335
     0.333333343          0.666666687          0.939926684
     0.333333343          0.666666687          0.393406659
     0.000000000          0.000000000          0.317160010
     0.000000000          0.000000000          0.682839990
     0.666666687          0.333333343          0.650493324
     0.666666687          0.333333343          0.016173324
     0.333333343          0.666666687          0.983826697
     0.333333343          0.666666687          0.349506646
```

HS State

The initial structure of the HS state was obtained from the FF relaxation.

```
C24 H48  N24 Fe, 2(B F4)
1.0
    10.8659898963704631    0.0000000034218521   -0.0000000000000000
    -5.4329949511983813    9.4102232858666142   -0.0000000000000000
    -0.0000000000000000    0.0000000000000000   30.9257781786954098
   Fe    N    C    H    F    B
    3   72   72  144   24    6
Direct
  0.0000000000000000  0.0000000000000000 -0.0000000000000000
  0.6666666870000029  0.3333333429999996  0.3333333429999996
  0.3333333429999996  0.6666666870000029  0.6666666870000029
  0.0441956425279266  0.8606689326800708  0.0406486190847511
  0.9558043354720710  0.1393310523199315  0.9593513659152442
  0.1393310523199386  0.1835267018478552  0.0406486190847511
  0.8606689326800637  0.8164733281521405  0.9593513659152442
  0.8164733281521405  0.9558043354720710  0.0406486190847511
  0.1835267018478552  0.0441956425279266  0.9593513659152442
  0.7108622915279269  0.1940022756800704  0.3739819470847530
  0.6224710214720702  0.4726643803199332  0.2926847089152437
  0.8059976943199413  0.5168600448478616  0.3739819470847530
```

```
0.5273356196800595  0.1498066411521444  0.2926847089152437
0.4831399841521439  0.2891376784720710  0.3739819470847530
0.8501933588478553  0.3775289785279294  0.2926847089152437
0.3775289785279294  0.5273356196800666  0.7073152610847537
0.2891376784720710  0.8059976943199342  0.6260180529152470
0.4726643803199403  0.8501933588478553  0.7073152610847537
0.1940022756800633  0.4831399841521439  0.6260180529152470
0.1498066411521444  0.6224710214720702  0.7073152610847537
0.5168600448478616  0.7108622915279269  0.6260180529152470
0.1603233736545728  0.9096007640359953  0.0668537955631491
0.8396766113454224  0.0903992069639985  0.9331461814368524
0.0903992069639985  0.2507225796185748  0.0668537955631491
0.9096007640359953  0.7492774343814276  0.9331461814368524
0.7492774343814275  0.8396766113454224  0.0668537955631491
0.2507225796185749  0.1603233736545728  0.9331461814368524
0.8269900156545755  0.2429341220359998  0.4001871315631443
0.5063432983454252  0.4237325499640050  0.2664795254368490
0.7570658629640026  0.5840559386185745  0.4001871315631443
0.5762674500359946  0.0826107553814242  0.2664795254368490
0.4159440913814267  0.1730099553454257  0.4001871315631443
0.9173892516185789  0.4936567016545745  0.2664795254368490
0.4936567016545745  0.5762674500359946  0.7335204455631456
0.1730099553454257  0.7570658629640026  0.5998128684368552
0.4237325499640050  0.9173892516185788  0.7335204455631456
0.2429341220359998  0.4159440913814267  0.5998128684368552
0.0826107553814242  0.5063432983454252  0.7335204455631456
0.5840559386185746  0.8269900156545755  0.5998128684368552
0.1642876290572367  0.8032717974625696  0.0845712785675004
0.8357123849427579  0.1967281875374328  0.9154287364324976
0.1967281875374328  0.3610158175946734  0.0845712785675004
0.8032717974625695  0.6389841824053343  0.9154287364324976
0.6389841824053272  0.8357123849427579  0.0845712785675004
0.3610158175946734  0.1642876290572437  0.9154287364324976
0.8309543010572413  0.1366051404625692  0.4179046065675023
0.5023790119427558  0.5300615165374312  0.2487620504324982
0.8633948295374284  0.6943491305946700  0.4179046065675023
0.4699384834625688  0.9723174964053350  0.2487620504324982
0.3056508394053270  0.1690456989427582  0.4179046065675023
0.0276824835946779  0.4976209580572422  0.2487620504324982
0.4976209580572422  0.4699384834625688  0.7512379495675017
0.1690456989427653  0.8633948295374283  0.5820953634325026
0.5300615165374313  0.0276824835946779  0.7512379495675017
0.1366051404625692  0.3056508394053270  0.5820953634325026
0.9723174964053279  0.5023790119427558  0.7512379495675017
0.6943491305946700  0.8309543010572413  0.5820953634325026
```

0.0498548056508781 0.6832970387058455 0.0698893983621209
0.9501451753491236 0.3167029612941613 0.9301105866378818
0.3167029612941613 0.3665577559450277 0.0698893983621209
0.6832970387058384 0.6334422150549738 0.9301105866378818
0.6334422150549738 0.9501451753491236 0.0698893983621209
0.3665577559450278 0.0498548056508781 0.9301105866378818
0.7165214516508743 0.0166303727058411 0.4032227263621225
0.6168118623491264 0.6500362742941659 0.2634439306378779
0.9833696472941609 0.6998910989450270 0.4032227263621225
0.3499636957058391 0.9667755880549688 0.2634439306378779
0.3001089010549726 0.2834785183491236 0.4032227263621225
0.0332244329450298 0.3831881376508732 0.2634439306378779
0.3831881376508732 0.3499636957058391 0.7365560393621196
0.2834785183491236 0.9833696472941538 0.5967772736378776
0.6500362742941659 0.0332244329450298 0.7365560393621196
0.0166303727058411 0.3001089010549727 0.5967772736378776
0.9667755880549688 0.6168118623491264 0.7365560393621196
0.6998910989450270 0.7165214516508743 0.5967772736378776
0.9763600634468408 0.7194902228681329 0.0431011723631443
0.0236399495531571 0.2805097771318673 0.9568988386368599
0.2805097771318744 0.2568698405787218 0.0431011723631443
0.7194902228681258 0.7431301594212781 0.9568988386368599
0.7431301594212852 0.0236399495531429 0.0431011723631443
0.2568698405787147 0.9763600634468550 0.9568988386368599
0.6430266904468458 0.0528235548681279 0.3764345043631392
0.6903066235531550 0.6138430911318679 0.2902321526368612
0.9471764641318771 0.5902031545787226 0.3764345043631392
0.3861568788681224 0.0764635024212778 0.2902321526368612
0.4097968454212845 0.3569732795531448 0.3764345043631392
0.9235364675787198 0.3096933764468591 0.2902321526368612
0.3096933764468449 0.3861568788681294 0.7097678473631394
0.3569732795531590 0.9471764641318700 0.6235654656368578
0.6138430911318750 0.9235364675787269 0.7097678473631394
0.0528235548681209 0.4097968454212774 0.6235654656368578
0.0764635024212849 0.6903066235531408 0.7097678473631394
0.5902031545787155 0.6430266904468600 0.6235654656368578
0.8729768888543629 0.5318711667936731 0.1462546585794310
0.1270231341456351 0.4681288332063278 0.8537453554205703
0.4681288332063278 0.3411056920606882 0.1462546585794310
0.5318711667936730 0.6588942779393093 0.8537453554205703
0.6588942779393164 0.1270231341456280 0.1462546585794310
0.3411056920606881 0.8729768888543700 0.8537453554205703
0.5396435158543608 0.8652044807936738 0.4795879875794296
0.7936897981456400 0.8014621462063241 0.1870786694205709
0.1347955052063255 0.6744390350606878 0.4795879875794296

```
0.1985378387936707  0.9922276509393114  0.1870786694205709
0.3255609649393122  0.4603564551456262  0.4795879875794296
0.0077723660606935  0.2063102018543675  0.1870786694205709
0.2063102018543604  0.1985378387936707  0.8129213305794289
0.4603564551456333  0.1347955052063255  0.5204119824205682
0.8014621462063242  0.0077723660606935  0.8129213305794289
0.8652044807936738  0.3255609649393122  0.5204119824205682
0.9922276509393185  0.7936897981456329  0.8129213305794289
0.6744390350606807  0.5396435158543679  0.5204119824205682
0.0243770805248755  0.5421714463750806  0.0819658033787486
0.9756229164751350  0.4578285236249245  0.9180342116212487
0.4578285236249317  0.4822056071497969  0.0819658033787486
0.5421714463750735  0.5177944218502019  0.9180342116212487
0.5177944218501948  0.9756229164751279  0.0819658033787486
0.4822056071498040  0.0243770805248755  0.9180342116212487
0.6910437705248679  0.8755048193750756  0.4152991313787508
0.6422896024751342  0.7911618666249236  0.2513675246212460
0.1244951876249291  0.8155389511497931  0.4152991313787508
0.2088381483750735  0.8511277358502026  0.2513675246212460
0.1844610638501978  0.3089562594751276  0.4152991313787508
0.1488722641498041  0.3577104275248753  0.2513675246212460
0.3577104275248753  0.2088381483750806  0.7486324753787542
0.3089562594751276  0.1244951876249220  0.5847008386212466
0.7911618666249307  0.1488722641497970  0.7486324753787542
0.8755048193750685  0.1844610638502049  0.5847008386212466
0.8511277358501955  0.6422896024751271  0.7486324753787542
0.8155389511498002  0.6910437705248750  0.5847008386212466
0.9951777754209233  0.5128616447305199  0.1302386873748627
0.0048222145790760  0.4871383552694806  0.8697613126251300
0.4871383552694877  0.4823161406903900  0.1302386873748627
0.5128616447305128  0.5176838593096098  0.8697613126251300
0.5176838593095956  0.0048222145790760  0.1302386873748627
0.4823161406904042  0.9951777754209233  0.8697613126251300
0.6618444124209221  0.8461949587305206  0.4635720303748694
0.6714889005790751  0.8204716682694773  0.2030946406251322
0.1538050272694853  0.8156494546903910  0.4635720303748694
0.1795283167305180  0.8510172323096048  0.2030946406251322
0.1843505303095901  0.3381555575790754  0.4635720303748694
0.1489827976904047  0.3285110994209249  0.2030946406251322
0.3285110994209249  0.1795283167305251  0.7969053743748729
0.3381555575790754  0.1538050272694781  0.5364279986251292
0.8204716682694844  0.1489827976903905  0.7969053743748729
0.8461949587305135  0.1843505303096043  0.5364279986251292
0.8510172323095906  0.6714889005790751  0.7969053743748729
0.8156494546904052  0.6618444124209221  0.5364279986251292
```

0.8788344817210020 0.6443350086446464 0.0267329864417147
0.1211655112790010 0.3556649613553506 0.9732670065582885
0.3556649613553436 0.2344994430763457 0.0267329864417147
0.6443350086446535 0.7655005269236523 0.9732670065582885
0.7655005269236452 0.1211655112790152 0.0267329864417147
0.2344994430763528 0.8788344817209878 0.9732670065582885
0.5455011677210012 0.9776683816446485 0.3600663064417089
0.7878322052790009 0.6889983043553507 0.3066003495582879
0.0223316283553449 0.5678327860763448 0.3600663064417089
0.3110016956446568 0.0988338859236528 0.3066003495582879
0.4321672139236475 0.4544988322790131 0.3600663064417089
0.9011660990763490 0.2121678247209873 0.3066003495582879
0.2121678247210015 0.3110016956446426 0.6933996794417108
0.4544988322789989 0.0223316283553521 0.6399336935582913
0.6889983043553436 0.9011660990763419 0.6933996794417108
0.9776683816446556 0.4321672139236546 0.6399336935582913
0.0988338859236457 0.7878322052790151 0.6933996794417108
0.5678327860763519 0.5455011677209870 0.6399336935582913
0.8514766519060547 0.5044646093085980 0.1806492377104132
0.1485233480939453 0.4955354206913966 0.8193507922895821
0.4955354206913966 0.3470120725974518 0.1806492377104132
0.5044646093085980 0.6529878974025385 0.8193507922895821
0.6529878974025385 0.1485233480939453 0.1806492377104132
0.3470120725974518 0.8514766519060476 0.8193507922895821
0.5181433389060505 0.8377979233085988 0.5139825807104129
0.8151900340939445 0.8288687636913969 0.1526840912895853
0.1622020916913987 0.6803454155974586 0.5139825807104129
0.1711312513086009 0.9863212704025406 0.1526840912895853
0.3196545844025486 0.4818566910939447 0.5139825807104129
0.0136787385974494 0.1848099809060531 0.1526840912895853
0.1848099809060531 0.1711312513086009 0.8473158937104172
0.4818566910939447 0.1622020916913987 0.4860174192895871
0.8288687636913969 0.0136787385974494 0.8473158937104172
0.8377979233085988 0.3196545844025486 0.4860174192895871
0.9863212704025406 0.8151900340939516 0.8473158937104172
0.6803454155974586 0.5181433389060434 0.4860174192895871
0.7753403310469736 0.4649029107366970 0.1279385015692365
0.2246596839530241 0.5350970892633036 0.8720615284307653
0.5350970892633036 0.3104374203102773 0.1279385015692365
0.4649029107366970 0.6895625796897310 0.8720615284307653
0.6895625796897239 0.2246596839530312 0.1279385015692365
0.3104374203102844 0.7753403310469665 0.8720615284307653
0.4420069870469707 0.7982362237366936 0.4612718445692362
0.8913263559530292 0.8684304032633043 0.2053948264307654
0.2017637612633085 0.6437707333102732 0.4612718445692362

```
0.1315695817366911  0.0228959286897304  0.2053948264307654
0.3562292666897114  0.5579930419530356  0.4612718445692362
0.9771040473102811  0.1086736510469678  0.2053948264307654
0.1086736510469749  0.1315695817366911  0.7946051585692375
0.5579930419530285  0.2017637612633085  0.5387281554307632
0.8684304032633043  0.9771040473102740  0.7946051585692375
0.7982362237366936  0.3562292666897185  0.5387281554307632
0.0228959286897233  0.8913263559530363  0.7946051585692375
0.6437707333102803  0.4420069870469636  0.5387281554307632
0.8978569029976388  0.6425746844448683  0.1425629386452545
0.1021431190023632  0.3574252855551369  0.8574370463547476
0.3574252855551440  0.2552821595527833  0.1425629386452545
0.6425746844448612  0.7447178404472162  0.8574370463547476
0.7447178404472091  0.1021431190023560  0.1425629386452545
0.2552821595527904  0.8978569029976459  0.8574370463547476
0.5645235299976367  0.9759080574448704  0.4758962676452526
0.7688097840023641  0.6907586295551325  0.1907703893547474
0.0240919525551378  0.5886154725527880  0.4758962676452526
0.3092413704448598  0.0780511694472149  0.1907703893547474
0.4113844974472100  0.4354764400023538  0.4758962676452526
0.9219488455527901  0.2311902159976429  0.1907703893547474
0.2311902159976358  0.3092413704448669  0.8092295806452503
0.4354764400023610  0.0240919525551307  0.5241037323547468
0.6907586295551396  0.9219488455527830  0.8092295806452503
0.9759080574448633  0.4113844974472171  0.5241037323547468
0.0780511694472078  0.7688097840023570  0.8092295806452503
0.5886154725527951  0.5645235299976438  0.5241037323547468
0.9332293279254289  0.4661489848224361  0.0626391647015438
0.0667706790745682  0.5338510151775570  0.9373608202984585
0.5338510151775570  0.4670803431029782  0.0626391647015438
0.4661489848224432  0.5329196568970216  0.9373608202984585
0.5329196568970145  0.0667706790745753  0.0626391647015438
0.4670803431029853  0.9332293279254218  0.9373608202984585
0.5998960149254318  0.7994822978224402  0.3959724937015426
0.7334373580745703  0.8671843291775577  0.2706941632984578
0.2005176871775546  0.8004136571029792  0.3959724937015426
0.1328156558224451  0.8662529698970187  0.2706941632984578
0.1995863278970161  0.4001040150745779  0.3959724937015426
0.1337470001029859  0.2665626419254225  0.2706941632984578
0.2665626419254296  0.1328156558224451  0.7293058067015465
0.4001040150745708  0.2005176871775546  0.6040275062984577
0.8671843291775577  0.1337470001029788  0.7293058067015465
0.7994822978224402  0.1995863278970232  0.6040275062984577
0.8662529698970116  0.7334373580745774  0.7293058067015465
0.8004136571029863  0.5998960149254247  0.6040275062984577
```

0.1179336726098182 0.5359983998863287 0.0719918168608506
0.8820663563901804 0.4640016291136700 0.9280082061391478
0.4640016291136629 0.5819353027234917 0.0719918168608506
0.5359983998863358 0.4180646972765081 0.9280082061391478
0.4180646972765152 0.8820663563901733 0.0719918168608506
0.5819353027234846 0.1179336726098253 0.9280082061391478
0.7846003296098188 0.8693317138863295 0.4053251378608485
0.5487329833901783 0.7973349731136734 0.2613415191391519
0.1306683011136681 0.9152686157234888 0.4053251378608485
0.2026650418863315 0.7513980112765091 0.2613415191391519
0.0847313612765129 0.2153996553901695 0.4053251378608485
0.2486019737234862 0.4512670166098287 0.2613415191391519
0.4512670166098215 0.2026650418863244 0.7386584808608480
0.2153996553901766 0.1306683011136752 0.5946748331391528
0.7973349731136663 0.2486019737234934 0.7386584808608480
0.8693317138863366 0.0847313612765057 0.5946748331391528
0.7513980112765162 0.5487329833901712 0.7386584808608480
0.9152686157234817 0.7846003296098260 0.5946748331391528
0.9717496706961752 0.4031116848463420 0.1353071491313214
0.0282503293038246 0.5968883151536581 0.8646928368686776
0.5968883151536439 0.5686379858498343 0.1353071491313214
0.4031116848463562 0.4313620141501666 0.8646928368686776
0.4313620141501738 0.0282503293038317 0.1353071491313214
0.5686379858498272 0.9717496706961681 0.8646928368686776
0.6384163566961745 0.7364449978463461 0.4686404771313233
0.6949170163038205 0.9302216291536589 0.1980261798686771
0.2635549871536418 0.9019712988498314 0.4686404771313233
0.0697783488463605 0.7646953271501629 0.1980261798686771
0.0980286781501709 0.3615836733038281 0.4686404771313233
0.2353046578498246 0.3050830136961676 0.1980261798686771
0.3050830136961747 0.0697783488463463 0.8019737901313203
0.3615836733038211 0.2635549871536561 0.5313595228686768
0.9302216291536447 0.2353046578498318 0.8019737901313203
0.7364449978463603 0.0980286781501638 0.5313595228686768
0.7646953271501700 0.6949170163038276 0.8019737901313203
0.9019712988498243 0.6384163566961674 0.5313595228686768
0.0926247892288359 0.5814621343107682 0.1485818671297459
0.9073752177711618 0.4185378656892318 0.8514181328702547
0.4185378656892390 0.5111626469180884 0.1485818671297459
0.5814621343107611 0.4888373530819112 0.8514181328702547
0.4888373530819183 0.9073752177711474 0.1485818671297459
0.5111626469180812 0.0926247892288502 0.8514181328702547
0.7592914682288374 0.9147954483107690 0.4819152101297458
0.5740419047711647 0.7518711786892289 0.1847514618702525
0.0852045296892362 0.8444959609180892 0.4819152101297458

```
 0.2481288063107592  0.8221706660819158  0.1847514618702525
 0.1555040090819228  0.2407085467711453  0.4819152101297458
 0.1778293189180791  0.4259581252288530  0.1847514618702525
 0.4259581252288387  0.2481288063107663  0.8152485531297445
 0.2407085467711596  0.0852045296892291  0.5180848198702505
 0.7518711786892360  0.1778293189180862  0.8152485531297445
 0.9147954483107619  0.1555040090819157  0.5180848198702505
 0.8221706660819230  0.5740419047711502  0.8152485531297445
 0.8444959609180820  0.7592914682288519  0.5180848198702505
 0.9667650603933594  0.8634915252436559  0.3318476441546671
 0.0332349516066418  0.1365085047563403  0.6681523258453375
 0.1365085047563403  0.1032735501497020  0.3318476441546671
 0.8634915252436559  0.8967264648502954  0.6681523258453375
 0.8967264648502954  0.0332349516066418  0.3318476441546671
 0.1032735501497020  0.9667650603933594  0.6681523258453375
 0.6334316863933608  0.1968248232436616  0.6651809871546668
 0.6999016266066364  0.4698418477563403  0.0014856988453323
 0.8031751617563399  0.4366068781497042  0.6651809871546668
 0.5301581522436609  0.2300597788502965  0.0014856988453323
 0.5633930918502933  0.3665682836066369  0.6651809871546668
 0.7699402211497038  0.3000983733933635  0.0014856988453323
 0.3000983733933635  0.5301581522436609  0.9985143111546684
 0.3665682836066369  0.8031751617563399  0.3348190128453333
 0.4698418477563403  0.7699402211497038  0.9985143111546684
 0.1968248232436616  0.5633930918502933  0.3348190128453333
 0.2300597788502965  0.6999016266066364  0.9985143111546684
 0.4366068781497041  0.6334316863933608  0.3348190128453333
 0.0000000000000000  0.0000000000000000  0.2709610154871244
-0.0000000000000000  0.0000000000000000  0.7290389845128752
 0.6666666870000029  0.3333333429999996  0.6042943284871291
 0.6666666870000029  0.3333333429999996  0.0623723165128778
 0.3333333429999996  0.6666666870000029  0.9376277014871240
 0.3333333429999996  0.6666666870000029  0.3957056415128760
-0.0000000000000000 -0.0000000000000000  0.3167463260461285
 0.0000000000000000  0.0000000000000000  0.6832536449538728
 0.6666666870000029  0.3333333429999996  0.6500796690461280
 0.6666666870000029  0.3333333429999996  0.0165870079538740
 0.3333333429999996  0.6666666870000029  0.9834129820461252
 0.3333333429999996  0.6666666870000029  0.3499203309538719
```

A.3 Relaxed Geometries in POSCAR Format

All optimised structures were obtained by full relaxations that allow changes in cell volume, shape, and ionic position under the PBE-D3(BJ)+U level with U_{eff} = 1.9 eV.

LS State

```
C24 H48  N24 Fe, 2(B F4)
1.0
    10.6611394107522823    0.0005231828606030    0.0009402986145547
    -5.3301169456883288    9.2326596258656792   -0.0003459812237778
     0.0028284748738364    0.0004466219562126   31.6755394006301465
   Fe    N    C    H    F    B
    3   72   72  144   24    6
Direct
  0.0000627563533499  0.0000067922687326 -0.0000088813839743
  0.6666129471192020  0.3334090149027027  0.3333360482962796
  0.3334320231245312  0.6666431453117636  0.6666643905904084
  0.0475744507935358  0.8770602302303204  0.0359311663768188
  0.9525335995240058  0.1229066809410889  0.9640474030055708
  0.1230041819603364  0.1704133476041037  0.0359314534167447
  0.8770782502707437  0.8295920143226804  0.9640580563661560
  0.8296429610639332  0.9525544418630560  0.0359468856391166
  0.1705023756647452  0.0475136123492776  0.9640347029924484
  0.7141474450055242  0.2104816392323486  0.3692856952303420
  0.6190811213548916  0.4562806730462145  0.2973867106704723
  0.7895463206439891  0.5038659282701999  0.3692737802205371
  0.5436687825095542  0.1629616294629926  0.2974027417627326
  0.4961900592346203  0.2859172561010769  0.3692842317740811
  0.8370763406457258  0.3809235059333836  0.2973823586248590
  0.3809239556703654  0.5437216337786486  0.7026110400794903
  0.2859305734250698  0.7895582830867610  0.6307086425403036
  0.4563451383693908  0.8370570251530828  0.7026021033176375
  0.2104675992853774  0.4961889021284043  0.6307317597184765
  0.1629923456345161  0.6192094861250859  0.7026161358394531
  0.5038895775707753  0.7141138962446038  0.6307227170025622
  0.1666449293117048  0.9300448160436894  0.0613921867350456
  0.8334700759179666  0.0699100409568882  0.9385828130126839
  0.0700130716445018  0.2365110033275604  0.0613993495304619
  0.9300577011776697  0.7634777617406566  0.9385944718425362
  0.7635554896546447  0.8334664154846195  0.0614086315900175
  0.2365986745667174  0.1666088688115406  0.9385742910777217
  0.8332289857090918  0.2634546598089231  0.3947424763907699
  0.5000866911284513  0.4032923676098996  0.2718933596430367
```

```
0.7365695241144163  0.5698883338900677  0.3947785241261531
0.5966694195107476  0.0968558351944880  0.2719434199615125
0.4301402665965789  0.1668785313741848  0.3947664146651276
0.9031717215730479  0.4999787262745033  0.2719060629927991
0.4999862448611360  0.5966976081143196  0.7280753550334648
0.1668650078345681  0.7365646574811637  0.6052452656024495
0.4033527432841200  0.9031529086075446  0.7280700518479671
0.2634375234211629  0.4300892945374954  0.6052573109295901
0.0969457190178892  0.5001729319554281  0.7280993660223786
0.5699882576799927  0.8331758108036594  0.6052507142202289
0.1709708976967171  0.8235850801956475  0.0799219013455003
0.8291186819448202  0.1763662482924744  0.9200606886995945
0.1764609616193146  0.3472766842845478  0.0799294287686763
0.8236037355195881  0.6527094541421761  0.9200657766414242
0.6527643315070296  0.8291296661640707  0.0799433110868489
0.3473852969850225  0.1709365786253166  0.9200383162715485
0.8375717961917752  0.1569853437565093  0.4132598449902306
0.4957810719575830  0.5097590056112370  0.2533605031563278
0.8430349061419944  0.6806520723986368  0.4133068887385120
0.4902267850455669  0.9860693027618616  0.2534175257310356
0.3193890200770691  0.1625928721314831  0.4133125234999311
0.0139675810056399  0.5042877270277322  0.2533829119482056
0.5043087757732805  0.4902289378094161  0.7466004330536858
0.1625042211106262  0.8430220631284975  0.5867267560057681
0.5098021536019233  0.0139167282491564  0.7466006966120655
0.1569725871518179  0.3193170540060588  0.5867320232477077
0.9861662077487318  0.4958551260056613  0.7466350648225226
0.6807279457229612  0.8374362326491268  0.5867047367280340
0.0540631453305863  0.6999009812485355  0.0666310620692570
0.9459972346084407  0.3000563807632062  0.9333621193342330
0.3001436013522260  0.3540354817537769  0.0666316281823244
0.6999257157915675  0.6459732540251448  0.9333600648485393
0.6459831875679256  0.9460483377928951  0.0666541777931502
0.3541532827939854  0.0540077653662995  0.9333249746795031
0.7206633697352277  0.0333044621851900  0.3999650937412899
0.6126188567539403  0.6334452324926922  0.2666825356037202
0.9667151639626976  0.6874785962094125  0.3999705615169819
0.3665385408705282  0.9793129820503019  0.2667093949555647
0.3125944566474235  0.2794923813161207  0.4000112035703887
0.0207453059552945  0.3873854238515208  0.2666939044638649
0.3874111957262307  0.3665502208509300  0.7333025124990380
0.2793811788806621  0.9667130746644159  0.6000290440065736
0.6334843791533185  0.0206735442822103  0.7333036437964082
0.0332970269919216  0.3125618663703406  0.6000390924041394
0.9793486517582732  0.6127357472488383  0.7333259099005764
```

```
 0.6874660515802914  0.7204953450874633  0.5999959936031569
-0.0216477502016124  0.7332034994231266  0.0397663713726432
 0.0217245888248965  0.2667645740927768  0.9602219772656292
 0.2668520803538212  0.2450113438796077  0.0397638935665563
 0.7332209874096404  0.7550001671418212  0.9602234100191429
 0.7550033355321584  0.0217864949622903  0.0397853458207474
 0.2451303773560133 -0.0217200822115110  0.9601928897140012
 0.6449351670120200  0.0666204743921044  0.3731112032323862
 0.6882709277435407  0.6001366137105089  0.2935694347176784
 0.9334058001200106  0.5785260754300404  0.3730772691708388
 0.3998122611865145  0.0883425455084348  0.2935693126142830
 0.4215668391958403  0.3551574301828881  0.3731211671601424
 0.9117151172842605  0.3116930928903551  0.2935627296230314
 0.3117035309171549  0.3998648540709029  0.7064390991715743
 0.3551182299113360  0.9334202177880120  0.6268854170673773
 0.6001928677041828  0.9116579815565884  0.7064336352061172
 0.0666095578340670  0.4215750773594455  0.6269103439322500
 0.0883365698760927  0.6884261501064567  0.7064447217609318
 0.5784820599819350  0.6448438341838223  0.6268818121340641
 0.8889589310521163  0.5446530410734576  0.1447139255276297
 0.1110490858169237  0.4553498859424098  0.8552874059599705
 0.4553302671262687  0.3442991988067762  0.1447221519023476
 0.5446693538895553  0.6556972940316828  0.8552811541944958
 0.6557175544695694  0.1110372046842595  0.1447560132568210
 0.3442700160135412  0.8889598135302338  0.8552237364393399
 0.5556316421026143  0.8779950489187404  0.4780503649886803
 0.7777260265052763  0.7886737105989745  0.1886064562800369
 0.1220100698381134  0.6776288334485193  0.4780426756558629
 0.2113320305364804  0.9890189878341117  0.1886187064727687
 0.3224326039336368  0.4443649487249323  0.4781679025921796
 0.0109723658543369  0.2222901109821268  0.1886132440239678
 0.2222957555978364  0.2113269991598873  0.8113850649001882
 0.4443825637239214  0.1220165231686445  0.5219542195766405
 0.7886652207782215  0.0109568814078446  0.8113892704938305
 0.8779933912417535  0.3223582895963601  0.5219568580531174
 0.9890524819988801  0.7777156237286613  0.8114070357845542
 0.6775579235573830  0.5556068912134455  0.5218366615871960
 0.0308847078622262  0.5571781853779961  0.0786943415085776
 0.9691406368847425  0.4427797867581022  0.9213164434580497
 0.4428317819720464  0.4735953505919626  0.0786901057282728
 0.5572202796305743  0.5264231148424443  0.9213114378342859
 0.5264387658962308  0.9692265968110663  0.0787223898379773
 0.4736657284328885  0.0307931537938737  0.9212454412209488
 0.6975101175956812  0.8905747814270211  0.4120121396126557
 0.6358059635219317  0.7761774414322397  0.2546192354381837
```

```
 0.1094515648290862  0.8069956887984038  0.4120240203563784
 0.2238489058755061  0.8597538766744599  0.2546583278361101
 0.1931011818043306  0.3027299356188005  0.4121052058473610
 0.1402812245656681  0.3641690200186604  0.2546356623611267
 0.3642269934315214  0.2238261031444121  0.7453674092927509
 0.3024910343920750  0.1094259579199100  0.5879865984298855
 0.7761724352614900  0.1402420056808719  0.7453591451480656
 0.8905707662932766  0.1930262795488129  0.5879869085367855
 0.8597730166745690  0.6358829590426118  0.7453821459858259
 0.8069216091611878  0.6972072827344996  0.5878952834859009
 0.0141529666187251  0.5320356044119331  0.1261851952618331
-0.0141439843227298  0.4679553491693406  0.8738259427815418
 0.4679584523418542  0.4820942029924459  0.1261815548767255
 0.5320539404824285  0.5179137594960255  0.8738248309215255
 0.5179302828683228 -0.0141022641316457  0.1262123658472301
 0.4820936962412153  0.0140888450463163  0.8737516079175769
 0.6808211057535669  0.8653996818547917  0.4595044178612654
 0.6525392344624961  0.8013155407956553  0.2071281506382428
 0.1346246829940962  0.8154329089258850  0.4595119039611041
 0.1987062911493333  0.8512334841686664  0.2071679981378149
 0.1846313914574782  0.3192965500813714  0.4596016474369233
 0.1487620305158466  0.3474656689786627  0.2071451212604798
 0.3474832904042106  0.1986958777697627  0.7928587358644541
 0.3191853771094719  0.1346060034003222  0.5404957813785016
 0.8012915118098909  0.1487529324786691  0.7928502850171317
 0.8653936955179115  0.1845773916586795  0.5404975456767818
 0.8512601706707760  0.6525650905018171  0.7928713991060210
 0.8153697377235182  0.6806658249173811  0.5403975095863487
 0.8785282587500172  0.6542682600628409  0.0245892547287121
 0.1215356210059111  0.3457053312145870  0.9754039909172720
 0.3457991084262068  0.2240951543359262  0.0245910165427309
 0.6542935206182855  0.7759372386390757  0.9753972560281726
 0.7759345239485667  0.1216581741035405  0.0246221023470351
 0.2242170194711886  0.8784191779977542  0.9753603594452809
 0.5450829271154201  0.9876931549339019  0.3579449955292363
 0.7880557125155628  0.6790797003662952  0.3087626412764617
 0.0123398183055501  0.5576478606606344  0.3578811559829302
 0.3208676661122882  0.1092616545996275  0.3087402613592496
 0.4424520074494008  0.4549807442385009  0.3579354290177189
 0.8908033469838680  0.2118562923900629  0.3087443896581480
 0.2118684717967440  0.3209347859618423  0.6912654332291949
 0.4549526212316145  0.0123554789296750  0.6420593213888139
 0.6791328609052535  0.8907361389141565  0.6912590991870445
 0.9876858018556259  0.4424901307319152  0.6420961673015437
 0.1092310868783048  0.7882584656799859  0.6912625634221669
```

0.5575436874137050 0.5449846164943835 0.6420560151694431
0.8765433159363670 0.5193083802650041 0.1785730076923202
0.1234709820818330 0.4807205772953080 0.8214311156312167
0.4806282212208784 0.3572519887749168 0.1785829877667612
0.5193614799944024 0.6427352369536699 0.8214210354693123
0.6427436403195536 0.1233966989739079 0.1786159748677452
0.3571925313128979 0.8765553020806786 0.8213637075843129
0.5432446154095448 0.8526313388461491 0.5119080891739971
0.7901569133576540 0.8140111136512911 0.1547471586745536
0.1473516994285788 0.6905826918544355 0.5119009311179289
0.1860285209852767 0.9760484913431683 0.1547588466482835
0.3094583618877295 0.4566885156159273 0.5120283743394033
0.0239463077006371 0.2099022809901188 0.1547544351149849
0.2098841032873124 0.1860009604737793 0.8452450278061097
0.4568118184875239 0.1474033280345648 0.4880985053888247
0.8139647295011059 0.0239029966479402 0.8452498154368728
0.8526512537442816 0.3093898944055483 0.4880994949031781
0.9760938962187714 0.7901064575791684 0.8452662844373574
0.6905147807680768 0.5432846265183534 0.4879749804913594
0.7865737938955984 0.4705966462895538 0.1288759604559074
0.2134373645367257 0.5293779311302601 0.8711295611579771
0.5294210019365237 0.3159549172006138 0.1288981782319211
0.4705937893253470 0.6840513030756504 0.8711087726872255
0.6841015829183577 0.2134676352993399 0.1289286245497309
0.3159069670300533 0.7865467621181140 0.8710597664829737
0.4532370744621583 0.8039458327187911 0.4622159618576389
0.8801134615161165 0.8627186357962418 0.2044455896716650
0.1960788561998978 0.6492799355108247 0.4622070883834790
0.1372666260566549 0.0173898611053292 0.2044444558617835
0.3508425659109728 0.5468183482330886 0.4623485600261334
0.9826234336843838 0.1198826074011052 0.2044479810110464
0.1199062482298827 0.1372609055824668 0.7955503233428303
0.5467689627908380 0.1960401196936633 0.5377987296834685
0.8627559096780971 0.9826167765142481 0.7955633946484688
0.8039413239150981 0.3507185957906960 0.5377964820689393
0.0174328451636766 0.8801328515529525 0.7955723528183962
0.6491725098229242 0.4531533069916267 0.5376527725598700
0.9070308160868147 0.6549599475297263 0.1410469798992685
0.0929650222973325 0.3450334241187356 0.8589459290553692
0.3450393132410137 0.2520619612948890 0.1410549710885301
0.6549680445709883 0.7479294069020740 0.8589433912039445
0.7479335632841627 0.0929324522464009 0.1410868122204015
0.2520702720308630 0.9070803482281272 0.8589063290061617
0.5737050373747445 0.9883059122149105 0.4743940238958056
0.7596352232473386 0.6783597701723860 0.1922743323406055

```
0.0117144175097768  0.5853894806597439  0.4743846969530353
0.3216364949165768  0.0812396613825166  0.1922837187101906
0.4146179239919044  0.4262248029781883  0.4744811593402767
0.9187433191352021  0.2403737605774355  0.1922773904815893
0.2403699129781422  0.3216331041092033  0.8077134103103627
0.4263020240140177  0.0117009965252261  0.5256085715549615
0.6783743307546146  0.9187206158964579  0.8077202485083226
0.9882979135970805  0.4145846432982158  0.5256150936389996
0.0812627870140457  0.7596021980185269  0.8077410397755355
0.5853712390684532  0.5737373354668180  0.5255330518681525
0.9332220603995003  0.4777583136400082  0.0619458825259924
0.0667934669299491  0.5221944685545120  0.9380668420605647
0.5222881158572097  0.4553110075628722  0.0619663717775116
0.4777942691610437  0.5447154377742055  0.9380500906923082
0.5447434741246999  0.0669461231088432  0.0619882048647076
0.4553833980908688  0.9330818561839332  0.9379815953131455
0.5998365183824139  0.8111524180476790  0.3952694555611711
0.7334892236713096  0.8555887932966746  0.2713603455750901
0.1888463095892679  0.7886916047701821  0.3952725523692070
0.1444094017268150  0.8780469530556976  0.2713905153136210
0.2114534087943427  0.4005116701723191  0.3953974671443464
0.1219845183629466  0.2664681549798925  0.2713798234657911
0.2665622726222459  0.1444002109813615  0.7286212813439763
0.4001413808212388  0.1888596454348199  0.6047367026267011
0.8556278320140441  0.1219516219356990  0.7286374491578289
0.8111607289687998  0.2112982870474215  0.6047404172818925
0.8780367599946376  0.7335779067827337  0.7286413278102193
0.7885441167849474  0.5994067600409940  0.6045978864575013
0.1229901154807234  0.5494649295462481  0.0664909501781133
0.8770185824101794  0.4504416254629505  0.9335290646656905
0.4505625024323642  0.5733941583795565  0.0664673032119795
0.5495211699629822  0.4266353740908010  0.9335300104423150
0.4266520937489891  0.8771626168320906  0.0665037122773956
0.5734905192645108  0.1228579198859557  0.9334466662640750
0.7896232145440640  0.8828939550754049  0.3997987453356641
0.5437168291588576  0.7839032120601509  0.2668277120882737
0.1171883459555744  0.9068199079482792  0.3998218316403738
0.2161290661456180  0.7599654024283218  0.2668856030337982
0.0932785523630131  0.2107236004312927  0.3998801946316141
0.2400883028526701  0.4562495698981537  0.2668411613526222
0.4563374995441740  0.2161113403004469  0.7331706610968383
0.2103520501406599  0.1170568121656783  0.6001999092929504
0.7838987444799663  0.2400292858635408  0.7331288257002055
0.8828775987947710  0.0932198352698517  0.6001871135972738
0.7600035785735549  0.5437797297978257  0.7331698744271536
```

```
  0.9067663528530326  0.7891878429639035  0.6001204680227503
 -0.0018459223117150  0.4230956348433929  0.1313806014238566
  0.0018780526780757  0.5769100190707647  0.8686427156275279
  0.5769048550402543  0.5750113410834954  0.1313708125085236
  0.4231180965154113  0.4249779966267504  0.8686412761854461
  0.4250088779749509  0.0019367558972930  0.1313990763640221
  0.5749832651281114 -0.0019970358727418  0.8685539841560548
  0.6648129544920012  0.7564492046738656  0.4646864902617108
  0.6685765654035798  0.9102701318680974  0.2019331766350983
  0.2435767160903748  0.9083441464134688  0.4646971520501498
  0.0897576373453604  0.7583067858100347  0.2019869597895900
  0.0917242229687907  0.3353456115977176  0.4648081897160623
  0.2416853098434821  0.3314302069145515  0.2019546679728869
  0.3314737069720187  0.0897542211600359  0.7980594369357208
  0.3351921374613635  0.2435549453915287  0.5353129814823294
  0.9102353666742243  0.2416739122572819  0.7980398681085837
  0.7564537158408227  0.0916414834335066  0.5353155599880650
  0.7583372265451306  0.6686007144835824  0.7980597508452010
  0.9082711329050928  0.6646113261807404  0.5351815733847722
  0.1165232283346682  0.6080772226904062  0.1418643634103111
  0.8834851349305703  0.3919411647670016  0.8581441225977761
  0.3919317848543102  0.5084706332588242  0.1418608172947229
  0.6080886198772490  0.4915464144095221  0.8581442052625669
  0.4915447165036947  0.8834959859529097  0.1418895755492843
  0.5085067664795393  0.1164942502880833  0.8580726703780968
  0.7832017736419868  0.9414100937781891  0.4751835040308729
  0.5501705310642407  0.7252949755369408  0.1914457133990829
  0.0586161131306900  0.8418024202290597  0.4752059377935900
  0.2747253209072049  0.8248339680991645  0.1914947765271354
  0.1582089811127782  0.2168404716754355  0.4752511854455041
  0.1751285877236024  0.4498507330184508  0.1914618281398230
  0.4498513655256778  0.2747292599723891  0.8085408294117439
  0.2168117277986930  0.0585844935434114  0.5248166384690797
  0.7252579614856439  0.1751269408980726  0.8085259599570043
  0.9414109123775946  0.1582047256181859  0.5248083224224975
  0.8248894039807638  0.5501734334335311  0.8085523160951532
  0.8417903874436009  0.7831303856789037  0.5247550653794500
  0.9667234975697961  0.8614399966373477  0.3301458987937528
  0.0324021956235788  0.1383965796435269  0.6698554555699552
  0.1379131115402734  0.1056993369333297  0.3302187307771651
  0.8616819868188640  0.8940467023833344  0.6698326824300628
  0.8936698788122575  0.0328200216472111  0.3299996448593648
  0.1060095785468733  0.9675999010648293  0.6698428581315626
  0.6339085027866364  0.1944610609361511  0.6634511804224553
  0.6990413959080045  0.4717148435695587  0.0031892433985056
```

```
  0.8049138216208673  0.4387782038313878  0.6635928165393040
  0.5283097612988027  0.2273282939746260  0.0031933016588110
  0.5606970577599366  0.3655956414059315  0.6634795524155558
  0.7726700027099468  0.3009611180179570  0.0031842917613137
  0.3001606998565917  0.5279139776567234  0.9967978859812490
  0.3658508577545073  0.8055365488803691  0.3365883338336308
  0.4711240595212444  0.7723175010282577  0.9968756651907047
  0.1946276320133730  0.5612247681870208  0.3365368269016161
  0.2267348132431847  0.6989254664278747  0.9966570917719764
  0.4390272032937769  0.6344425009439972  0.3364536895946631
  0.0000135917430058  0.0000034266214368  0.2704534794991478
 -0.0000142918167349 -0.0000031777012475  0.7295462429836602
  0.6669179107717512  0.3333162789026832  0.6038327038782426
  0.6666527095665220  0.3333307119736550  0.0628797291148143
  0.3333472937712220  0.6666678114889792  0.9371199289041765
  0.3333170777082417  0.6666671677021196  0.3962127672427204
 -0.0004260330750282 -0.0000133292136260  0.3151583589046458
  0.0000156057941745  0.0000064745789244  0.6848265029593417
  0.6666063041838226  0.3330355075013794  0.6485388205143431
  0.6666642000892142  0.3333345421273436  0.0181660641909383
  0.3328541877614755  0.6664467793988474  0.9818195777747433
  0.3332000480173996  0.6669594635921707  0.3514995196645767
```

HS State

```
C24 H48  N24 Fe, 2(B F4)
1.0
    10.8852554838067697   -0.0023464248514590    0.0028554022340893
    -5.4446601704346600    9.4284608493062763   -0.0002043799829878
     0.0082403999942024    0.0040150396005067   30.8229431077831570
   Fe    N    C    H    F    B
    3   72   72  144   24    6
Direct
  0.0000248435066920  0.0000136902459192 -0.0000062536908130
  0.6666445816887029  0.3333153961437521  0.3333348568592389
  0.3333270001507730  0.6666577108518348  0.6666636970719018
  0.0451543225228171  0.8611382107545086  0.0401725322438623
  0.9548585574332005  0.1388808642517553  0.9598234011329807
  0.1405046190343490  0.1838087576175912  0.0397527362682197
  0.8595105713411073  0.8162143933090932  0.9602417406991473
  0.8156616120331741  0.9541624669609422  0.0400147040334811
  0.1843979095304401  0.0459050558338491  0.9599785870259731
  0.7118266247335037  0.1944516522852092  0.3735042260759370
  0.6215148421151192  0.4721913251935929  0.2931581222429165
  0.8071396576541850  0.5170916960200170  0.3730979420109986
  0.5261639995897885  0.1495218703459117  0.2935773318696684
```

0.4822597226235255 0.2874016187005711 0.3733507058817749
0.8510424791474165 0.3792460029298060 0.2933153585480927
0.3782569616621544 0.5281118774614664 0.7069453651201332
0.2884029422400977 0.8052114816930594 0.6263817015149116
0.4712229568103173 0.8494689146834745 0.7074106811945499
0.1954105097193666 0.4838421768199956 0.6259238584898127
0.1510372836008975 0.6229039848188133 0.7073240607007771
0.5156192786316758 0.7104000699146846 0.6260055683668168
0.1614326174473189 0.9108650637076038 0.0662924613050782
0.8385637684499480 0.0891481000960978 0.9337107049838718
0.0899372615193432 0.2504748644083021 0.0655063791995322
0.9099949195735821 0.7494799039395696 0.9344840020601216
0.7480911346726752 0.8375705141666283 0.0660041862569275
0.2519729328474701 0.1625155500466017 0.9339972169470780
0.8281307579804739 0.2441794698939544 0.3996128856433687
0.5052391122819367 0.4224671065129583 0.2670370523719414
0.7566743432113756 0.5838553590030593 0.3988504956446542
0.5767271247241069 0.0828561085015063 0.2678218234047559
0.4146844860865501 0.1707982150387033 0.3993352646095000
0.9185700840281117 0.4958028820923719 0.2673091169299911
0.4959830390245228 0.5774544810119209 0.7324333489070137
0.1706748101436386 0.7558711807129808 0.6008947413893577
0.4221136993922106 0.9179126559031386 0.7329315377000440
0.2445261818633845 0.4154001321268476 0.6004052009530463
0.0835012197485704 0.5057740402133579 0.7330934852180785
0.5831430489641078 0.8275245347265191 0.6002335796112808
0.1664015761041224 0.8051959967783093 0.0841047700977136
0.8335755328967085 0.1948137444063097 0.9159038948404253
0.1950362430713991 0.3607115708178425 0.0835733776591083
0.8048448668424496 0.6392902034090311 0.9164160743758233
0.6383023693553519 0.8337268056632807 0.0839264049951122
0.3617953027841395 0.1663996758553246 0.9160852212085354
0.8331106097311831 0.1385114039265224 0.4174212595925166
0.5002729766936527 0.5281387178672295 0.2492255735182932
0.8618363016105681 0.6940438776572796 0.4169146026115342
0.4716248620652317 0.9726178028476935 0.2497567313129075
0.3048748755137372 0.1669311028334406 0.4172510534278874
0.0283659458410883 0.4996552920488713 0.2493888764974685
0.5005029316645159 0.4717925320419365 0.7503006347367753
0.1661529673794123 0.8615345986470969 0.5830290210349393
0.5281255853757516 0.0285310412253221 0.7505623954607881
0.1385186313093148 0.3047750485842774 0.5827758058151947
0.9725211122136317 0.5004326454772453 0.7506686422856845
0.6941311975094214 0.8328785545212983 0.5826602724767094
0.0523781078976191 0.6851599694805283 0.0696494770087428

```
0.9475982288234693  0.3148527339396772  0.9303557755953606
0.3156332139044680  0.3668381806809261  0.0695033158092178
0.6842937860930658  0.6332682769379340  0.9304892334656019
0.6334357128687360  0.9486747097988616  0.0695779703790246
0.3666791314213301  0.0514597134498154  0.9304326384151155
0.7190736750292049  0.0184747044490132  0.4029748972856368
0.6142939116884275  0.6481730022234202  0.2636826740973617
0.9823779029342136  0.7000367800559446  0.4028443677159057
0.3510305943873893  0.9664905277914185  0.2638299475065721
0.2999978768170372  0.2818741792493331  0.4029032799374486
0.0332838704945012  0.3847517593177039  0.2637552767129157
0.3850706120798216  0.3517704932660018  0.7363239293760184
0.2815861272613272  0.9815553426080189  0.5970060556454461
0.6478830391378789  0.0330272975744339  0.7364351470017605
0.0187590868459996  0.3002745291973785  0.5969022009224311
0.9670443555168403  0.6151011721196430  0.7363789006724495
0.6996258751748485  0.7182235535391995  0.5969541029150999
0.9782707265589337  0.7202726559305782  0.0427385361104047
0.0217231355137499  0.2797453143742087  0.9572616561511250
0.2813245335912594  0.2575074827928288  0.0427370378405515
0.7186884853111475  0.7426096502628267  0.9572573736180412
0.7429093532341904  0.0223094367338055  0.0427307833276260
0.2571878328186801  0.9777938619180172  0.9572709392787988
0.6449468476018845  0.0535862346896458  0.3760702252943223
0.6883975927787973  0.6130565533523983  0.2905942880393121
0.9479629460447774  0.5906753483901906  0.3760829450452720
0.3853422277764395  0.0758233813515130  0.2905960518346294
0.4094834065040374  0.3555251764501382  0.3760608986882638
0.9238346922482260  0.3111380846460379  0.2906142969941535
0.3101942353088517  0.3872613111694499  0.7099114691638908
0.3564646392535599  0.9460610658040186  0.6234158242655932
0.6121467340072273  0.9223540159699852  0.7101001695005333
0.0544869131038553  0.4109526412569187  0.6232344450155934
0.0772217543104016  0.6899793579598712  0.7098809541362068
0.5894510598135317  0.6433392915602862  0.6234521531984404
0.8778640142731219  0.5346304988751410  0.1469001365787773
0.1221407394992779  0.4653645552908815  0.8531217297713294
0.4654907801447622  0.3433272285691629  0.1469045179864789
0.5344315390958064  0.6565454584026750  0.8530049205157157
0.6565274210972012  0.1221396532862942  0.1470775828390823
0.3433988096804992  0.8778078635325273  0.8529953467930700
0.5445114644072226  0.8679608095080746  0.4802030819691007
0.7887977360123979  0.7987018742527366  0.1864299014606124
0.1322319981952413  0.6767872056091084  0.4803303228485107
0.2011842943113776  0.9900123916080894  0.1864320870701849
```

0.3232603898525520 0.4555093997518719 0.4803434510107588
0.0100994438298733 0.2112210357271140 0.1862719639761441
0.2111686348077684 0.2010954721528854 0.8136672225325889
0.4554935613103069 0.1322349634664253 0.5196649344688536
0.7988686870905704 0.0101073960486754 0.8136873024459749
0.8677908361518206 0.3232204040599771 0.5196499079147813
0.9898618169102140 0.7889453460232342 0.8136710656105265
0.6767968050279460 0.5443845382623995 0.5196663124668743
0.0275356833122656 0.5446911917934264 0.0819578386688280
0.9724285797828964 0.4553146254792770 0.9180411295230656
0.4557187851441326 0.4829464758009144 0.0819546789263518
0.5441500657141107 0.5172293761600139 0.9180475647835129
0.5180010819048237 0.9739136245269013 0.0819068751470171
0.4821243180259757 0.0262414413309220 0.9180999990010572
0.6942331714250507 0.8780085724259821 0.4152909905672018
0.6391303549469555 0.7886415202871617 0.2513757418952343
0.1225303641648371 0.8160721977990000 0.4152825192133014
0.2109439268378166 0.8503827637479452 0.2513781974284500
0.1845488994472367 0.3070981721703007 0.4152335044238784
0.1487373759919126 0.3595312768678515 0.2514274862825034
0.3603213459080493 0.2113275416593169 0.7486102391938281
0.3063390041180069 0.1220004109641177 0.5847218160343761
0.7885552282332321 0.1487486016776894 0.7486223208240289
0.8780961123718389 0.1845563769960507 0.5847103858919737
0.8510636271497845 0.6395540835939036 0.7486281113423874
0.8156140473991118 0.6937828703087526 0.5847046675980202
0.0000277938689199 0.5166571718635422 0.1305180068015369
-0.0000317018892856 0.4833421269543915 0.8694818334893727
0.4833540462734096 0.4833719845857832 0.1305216956790151
0.5166436085681072 0.5166260244240326 0.8694764980155414
0.5166696480386388 0.0000261086139678 0.1305179771164356
0.4833266139228563 0.9999683656018523 0.8694881104945799
0.6666960637811657 0.8499892390526175 0.4638511459644716
0.6666372745020954 0.8166764050043573 0.2028150015754462
0.1500227169301340 0.8167074173100985 0.4638570924373971
0.1833152269708870 0.8499627539775352 0.2028120600280222
0.1833396879809183 0.3333645936264235 0.4638447228855119
0.1499945182931686 0.3333055855687025 0.2028193162831301
0.3333578557729562 0.1833315448956209 0.7971858721203975
0.3333093892685751 0.1500034531949923 0.5361467873748395
0.8166842224301754 0.1500156677655252 0.7971838723977832
0.8499811074911647 0.1833140237240113 0.5361493520598367
0.8499946932467115 0.6666698531979628 0.7971897906265025
0.8166706067815334 0.6666610249829125 0.5361437289627574
0.8809438466389894 0.6444743799528544 0.0264816146149722

```
0.1190655302693688  0.3555447952240927  0.9735111486275556
0.3575181541668738  0.2357723737859971  0.0268068466919069
0.6425394685767986  0.7643961787997368  0.9731924339973110
0.7655686119419687  0.1201167156621404  0.0265427479394782
0.2345244526402661  0.8799743532407914  0.9734504580661724
0.5475940209418890  0.9777923147321795  0.3598257850823386
0.7857270496642745  0.6888553235536453  0.3068503938294015
0.0241013090271844  0.5688722326369238  0.3601485647370083
0.3091495747469367  0.0975534200107969  0.3065286683818180
0.4321481794533753  0.4533424662599555  0.3598796052884168
0.9012001832079415  0.2133484555201152  0.3068082174711385
0.2116977834475627  0.3117856351448020  0.6941195337356899
0.4549611823881356  0.0215408182063964  0.6392080857426269
0.6874513593439824  0.8992155417342234  0.6942332897624452
0.9791778215240345  0.4340876421211768  0.6390997620621987
0.0995030100598764  0.7878376908739522  0.6937992223593376
0.5671819126314241  0.5454886342802754  0.6395362498655824
0.8579622276786819  0.5084304531247095  0.1815028391147173
0.1421642216965400  0.4916237299778305  0.8185279991601567
0.4913953736826806  0.3496973055579624  0.1815238118859629
0.5085845223723227  0.6500076442882972  0.8183751841674219
0.6497834098924267  0.1414264334645416  0.1817018353711961
0.3499307540984956  0.8582874869299086  0.8183822154525423
0.5244782724738593  0.8417099571946509  0.5147973275862012
0.8086848963975235  0.8248900090900445  0.1518260874797799
0.1580747839682273  0.6833251810515781  0.5149606406108643
0.1752820958067295  0.9836583929665147  0.1518129088014553
0.3167023432910917  0.4749550992748089  0.5149636624725965
0.0168201165078205  0.1919176235551944  0.1516469562735266
0.1914555478916940  0.1748761752761049  0.8482733728497195
0.4752055561200960  0.1584550270000413  0.4850595531526149
0.8251025204339859  0.0167621273934536  0.8482862328405528
0.8415519258993331  0.3165692882467594  0.4850518812122693
0.9831035996161370  0.8085430279802148  0.8482688396491267
0.6835448575469747  0.5247810575370543  0.4850682579037134
0.7799186390994511  0.4664011680471887  0.1289280042806766
0.2200275682131172  0.5335336402645575  0.8711297823445902
0.5340689388269425  0.3139101049855882  0.1289881726118683
0.4657976090562894  0.6860202629181490  0.8708630086102606
0.6861797768752751  0.2202868757025263  0.1292259234085497
0.3138230244141278  0.7797760204415768  0.8709088398188888
0.4466331836495888  0.7997805153011175  0.4621928656004340
0.8867515185866179  0.8669402768032411  0.2043974777665657
0.2008628528081547  0.6473076738356653  0.4624738300153847
0.1326043139598276  0.0194231036408710  0.2043509227733536
```

0.3528891830883945 0.5535883251858590 0.4624549056323277
0.9803984915081715 0.1130649621851490 0.2041248879474417
0.1131542884485335 0.1327691158567888 0.7957377777570550
0.5535099473845427 0.2005554827505552 0.5375947376880903
0.8671646039282002 0.9803923580964485 0.7957385762440783
0.7995016635848604 0.3529358602651090 0.5376022174474401
0.0195274516256623 0.8869231210566536 0.7957186591407461
0.6471350665296873 0.4464092692256556 0.5376193888424685
0.9014233239325503 0.6445830393767795 0.1429034814011787
0.0985382343065409 0.3553952367325783 0.8571142304352645
0.3556307079526184 0.2567069981383018 0.1428458146264320
0.6442750890090982 0.7432216540502276 0.8570491754352727
0.7432127259142972 0.0989938069384209 0.1430650349915060
0.2567406871642722 0.9009825069699930 0.8570285954051718
0.5681052106704484 0.9779244136289030 0.4762062145108506
0.7652448053707909 0.6887519734845571 0.1904296385227516
0.0223883693765523 0.5901161998278256 0.4762842653997070
0.3110441541042470 0.0766317212395246 0.1904939596462930
0.4099035678591590 0.4323050171223555 0.4763198099569318
0.9234606357037463 0.2344364493922910 0.1902821561192015
0.2345288638470897 0.3109953124458241 0.8096993460452068
0.4321281651841901 0.0223324790600786 0.5236313320796046
0.6889253003416215 0.9235334899101988 0.8097540652723499
0.9777388221813365 0.4097973064720649 0.5235809152748752
0.0765355924100441 0.7657464033324906 0.8097395544534440
0.5901263480723322 0.5675869165454122 0.5235995225805844
0.9359896434681313 0.4681709900201378 0.0628993831570845
0.0639553730356419 0.5318451370569092 0.9371035435379846
0.5327746293408926 0.4686253378424518 0.0629268048667623
0.4671362144307417 0.5317359415978613 0.9370315942762470
0.5339086864566515 0.0661713987267514 0.0630709264691284
0.4663519838028187 0.9340974243978483 0.9369701794439002
0.6026989449007500 0.8014802777719939 0.3962306300116406
0.7306780272257047 0.8651631687900072 0.2704336689128758
0.1995404780338662 0.8015431515502494 0.3963046105185036
0.1338882889399720 0.8647056817523133 0.2704053760502806
0.2003497053475098 0.3992555766320694 0.3963652799044438
0.1328904948405525 0.2673357432245297 0.2702858887458312
0.2685560957885929 0.1347593575095330 0.7296387473375094
0.3981034917702656 0.1985663353099286 0.6036945856120283
0.8649437437401265 0.1333313588698646 0.7296113677795323
0.8016955965033857 0.1999501633009979 0.6037228642946855
0.8660834849203333 0.7311153495050314 0.7295795269093430
0.8006041777617013 0.6022251929274006 0.6037533074710263
0.1206509319364645 0.5384493793640494 0.0716939155039493

```
0.8792969794192539  0.4615385512942588  0.9282976894919743
0.4613638406134979  0.5820125891500358  0.0717140150386814
0.5383662959304364  0.4181418173801302  0.9283397239345992
0.4186139930084382  0.8813359213499955  0.0713849565177497
0.5815117579679625  0.1189147067023427  0.9285755978035148
0.7873589038439696  0.8717768316035354  0.4050323651773084
0.5460147556003968  0.7948806210714112  0.2616400561120460
0.1283269378019293  0.9151585198625882  0.4049805074134841
0.2052970109289576  0.7513160185150228  0.2616185836221100
0.0851628352646567  0.2144356063805184  0.4047551065171749
0.2481252132464328  0.4521601559039113  0.2619217632701685
0.4533562803025202  0.2051460127432785  0.7382150447032758
0.2133043684115623  0.1281827072071415  0.5951157696320643
0.7948154088418870  0.2479392717785771  0.7381859010895658
0.8718413730161028  0.0853628944235121  0.5951404035885932
0.7519071461709464  0.5463442830073114  0.7382999403745248
0.9147685323681977  0.7869988059182197  0.5950308475489980
0.9777882943620781  0.4076389187909443  0.1358574492369342
0.0222133582855891  0.5923635915815524  0.8641375968498289
0.5922837349778146  0.5703283037944263  0.1359142561296490
0.4077406979843068  0.4296051049974655  0.8640818609926487
0.4295920702674539  0.0218163577519476  0.1358828658333499
0.5703779090323251  0.9781409948932469  0.8641201039066354
0.6444583974996618  0.7409727268999066  0.4691989587968498
0.6888753536542457  0.9256943344969869  0.1974746942199101
0.2589237364524053  0.9037312899310798  0.4692517522860405
0.0743832261899864  0.7630082156550183  0.1974166726468806
0.0962860741528748  0.3551866599956961  0.4692149826726565
0.2370384434900161  0.3114667943116101  0.1974526125705355
0.3113358829757215  0.0743751285621956  0.8024962611547299
0.3553346410142084  0.2589582407302197  0.5308372920574985
0.9257156314072053  0.2369768442233154  0.8024231231222263
0.7409535547866856  0.0963531262171095  0.5309045695740311
0.7629368341267726  0.6885570370387299  0.8024551544095466
0.9037252191399612  0.6447725080676696  0.5308746018641600
0.0978029053881921  0.5863784650468812  0.1485116566925667
0.9022162229060059  0.4136175864772806  0.8514794927138336
0.4133784832038252  0.5111818922232969  0.1484882200583728
0.5866931057635622  0.4887883907494121  0.8515646339610079
0.4886127674433998  0.9019077759899619  0.1483095813823629
0.5113522312116723  0.0980211078249436  0.8516635783491716
0.7644453353367745  0.9197259639960692  0.4818531736313411
0.5688615102395040  0.7469534641180319  0.1848221247898679
0.0799618953501574  0.8445427438632648  0.4817615160718375
0.2532894285527815  0.8221538107225145  0.1848446311113705
```

```
  0.1553109755591041  0.2353043846743440  0.4816649776095031
  0.1780746065096261  0.4314038999872922  0.1850113711713114
  0.4312582200918010  0.2531908926889253  0.8151044067008963
  0.2354089550819495  0.0801473228521363  0.5182271228949482
  0.7469407223716131  0.1781594029882931  0.8151355909204177
  0.9197301132833082  0.1551793476351334  0.5181967021086394
  0.8219601706299693  0.5688470817168554  0.8151565135341272
  0.8447004287258041  0.7644810841904824  0.5181754447080272
  0.9667192888685840  0.8638019216816487  0.3305877282705912
  0.0333116104720637  0.1362338565349809  0.6694313493973783
  0.1362511770393572  0.1029517953698479  0.3305743601908390
  0.8637243540371095  0.8970519587757748  0.6694285281760580
  0.8970834854538622  0.0333401003172905  0.3305729395106127
  0.1029245092017313  0.9666705980700770  0.6694258862842347
  0.6333451035387393  0.1970970972520039  0.6639020172218449
  0.6999507765749410  0.4695298220503277  0.0027454498051926
  0.8029418957682706  0.4362835106461940  0.6639044438962505
  0.5304241005979146  0.2303862588890538  0.0027583284159338
  0.5637408688640828  0.3666648711876024  0.6639069768644246
  0.7695810084458234  0.2999877045523316  0.0027620265099204
  0.3000585340678422  0.5304717686351895  0.9972481828999947
  0.3666204284872677  0.8028730367696296  0.3360976007832750
  0.4695839432975370  0.7696238392032571  0.9972407516138347
  0.1970959068778647  0.5637208017840167  0.3360930267597498
  0.2304156886200043  0.7000063701224550  0.9972398307847360
  0.4362470029068127  0.6333273061599923  0.3360930640274550
  0.0000075511458282  0.0000050259634098  0.2694475789634959
 -0.0000101464676951 -0.0000070384087740  0.7305553738871495
  0.6666712943394874  0.3333391283614260  0.6027779010008324
  0.6666593904958281  0.3333275096659416  0.0638855266906130
  0.3333428142977374  0.6666738176496161  0.9361135532455301
  0.3333262698947651  0.6666591147665759  0.3972216112734525
 -0.0000624254847209 -0.0000402109849951  0.3153589953893164
 -0.0000071147848527  0.0000001082983093  0.6846333976650362
  0.6666728511119869  0.3333313316756482  0.6486997904666483
  0.6667311383473116  0.3333767558194052  0.0179742849740949
  0.3332704495797786  0.6666311256621228  0.9820257089140632
  0.3334037952870552  0.6667049983240072  0.3513107673932021
```

A.4 KPOINTS

The same KPOINTS was set for all calculations with VASP:

```
Gamma-point only
```

```
 1        ! one k-point
rec       ! in units of the reciprocal lattice vector
 0 0 0 1  ! 3 coordinates and weight
```

A.5 POTCAR

The same POTCAR was used for all VASP calculations, which combined the PBE pseudopotential files for each atomic species in the specific version:

```
  PAW_PBE Fe 06Sep2000
   TITEL  = PAW_PBE Fe 06Sep2000
  PAW_PBE N 08Apr2002
   TITEL  = PAW_PBE N 08Apr2002
  PAW_PBE C 08Apr2002
   TITEL  = PAW_PBE C 08Apr2002
  PAW_PBE H 15Jun2001
   TITEL  = PAW_PBE H 15Jun2001
  PAW_PBE F 08Apr2002
   TITEL  = PAW_PBE F 08Apr2002
  PAW_PBE B 06Sep2000
   TITEL  = PAW_PBE B 06Sep2000
```

A.6 INCAR

A.6.1 Full relaxations under PBE-D3(BJ)+U

LS state

```
System = [Fe(ptz)6](BF4)2_LS

! Startparameter for this run:
PREC = normal !specifies the precision mode
ISPIN = 1 !non-spin polarized calculation
NCORE = 24 !the number of compute cores that work on an individual orbital

! Electronic Relaxation 1
ENCUT = 500 !cutoff energy for the plane-wave basis set (eV)
EDIFF = 1E-06 !stopping-criterion for ELM
LMAXMIX = 4 !max onsite mixed and CHGCAR, set to obtain fast convergence of d
↪  orbitals
LREAL = A !real-space projection

! Ionic relaxation
EDIFFG = -1E-02 !stopping-criterion for IOM
```

```
NSW = 1000 !number of steps for IOM
IBRION = 2 !ionic relaxation with conjugate gradient algorithm
ISIF = 3 !unit cell volume, cell shape, and ionic positions are relaxed
ISYM = 0 !switches off the use of symmetry

! VDW correction
IVDW = 12 !DFT-D3 method with Becke-Johnson damping function

! DOS related values:
ISMEAR = 0 !sets partial occupancies for each orbital using gaussian smearing
SIGMA = 0.1 !sets the width of smearing

! Write flags
LWAVE = T !writes WAVECAR, which provides predicted wavefunctions
LCHARG = F !does not write CHGCAR, which stores the PAW one-center
↪  occupancies the charge density
LVTOT = F !does not write LOCPOT, total local potential
LELF = F !does not write electronic localization function
LORBIT = 11 !writes the partial magnetization densities to the OUTCAR

! LDA+U
LDAU = T !switches on DFT+U
LDAUTYPE = 2 !Dudarev method is performed
LDAUL = 2 -1 -1 -1 -1 -1 !angular momentum for each species
LDAUU = 20.0 0 0 0 0 0 !U (eV) for each species
LDAUJ = 18.1 0 0 0 0 0 !J (eV) for each species
LDAUPRINT = 0 !no onsite occupancy matrix is written to the OUTCAR file

! Exchange correlation treatment
GGA = PE !Perdew-Burke-Ernzerhof (PBE)
```

HS state

```
System = [Fe(ptz)6](BF4)2_HS

! Startparameter for this run:
PREC = normal !specifies the precision mode
ISPIN = 2 !spin polarized calculation
NUPDOWN = 12 !difference between up and down spin electrons
MAGMOM = 4 4 4 318*0.0 !sets initial magnetic moment for each atom
NCORE = 24 !the number of compute cores that work on an individual orbital

! Electronic Relaxation 1
ENCUT = 500 !cutoff energy for the plane-wave basis set (eV)
EDIFF = 1E-06 !stopping-criterion for ELM
```

```
LMAXMIX = 4 !max onsite mixed and CHGCAR, set to obtain fast convergence of d
↪  orbitals
LREAL = A !real-space projection
ALGO = All !specifies the electronic minimization algorithm
TIME = 0.05 !controls the time step

! Ionic relaxation
EDIFFG = -1E-02 !stopping-criterion for IOM
NSW = 1000 !number of steps for IOM
IBRION = 2 !ionic relaxation with conjugate gradient algorithm
ISIF = 3 !unit cell volume, cell shape, and ionic positions are relaxed
ISYM = 0 !switches off the use of symmetry

! VDW correction
IVDW = 12 !DFT-D3 method with Becke-Johnson damping function

! DOS related values:
ISMEAR = 0 !sets partial occupancies for each orbital using gaussian smearing
SIGMA = 0.1 !sets the width of smearing

! Write flags
LWAVE = T !writes WAVECAR
LCHARG = F !does not write CHGCAR
LVTOT = F !does not write LOCPOT
LELF = F !does not write electronic localization function
LORBIT = 11 !writes the partial magnetization densities to the OUTCAR

! LDA+U
LDAU = T !switches on DFT+U
LDAUTYPE = 2 !Dudarev method is performed
LDAUL = 2 -1 -1 -1 -1 -1 !angular momentum for each species
LDAUU = 20.0 0 0 0 0 0 !U (eV) for each species
LDAUJ = 18.1 0 0 0 0 0 !J (eV) for each species
LDAUPRINT = 0 !no onsite occupancy matrix is written to the OUTCAR file

! Exchange correlation treatment
GGA = PE !Perdew-Burke-Ernzerhof (PBE)
```

A.6.2 Self-consistent calculations under PBE-D3(BJ)+U

LS state

```
System = [Fe(ptz)6](BF4)2_LS

! Startparameter for this run:
PREC = normal !specifies the precision mode
```

```
ISPIN = 1 !non-spin polarized calculation
NCORE = 24 !the number of compute cores that work on an individual orbital

! Electronic Relaxation 1
ENCUT = 500 !cutoff energy for the plane-wave basis set (eV)
EDIFF = 1E-06 !stopping-criterion for ELM
LMAXMIX = 4 !max onsite mixed and CHGCAR, set to obtain fast convergence of d
↪  orbitals
LREAL = A !real-space projection
ISYM = 0 !switches off the use of symmetry

! VDW correction
IVDW = 12 !DFT-D3 method with Becke-Johnson damping function

! DOS related values:
ISMEAR = 0 !sets partial occupancies for each orbital using gaussian smearing
SIGMA = 0.1 !sets the width of smearing

! Write flags
LWAVE = T !writes WAVECAR
LCHARG = F !does not write CHGCAR
LVTOT = F !does not write LOCPOT
LELF = F !does not write electronic localization function
LORBIT = 11 !writes the partial magnetization densities to the OUTCAR

! LDA+U
LDAU = T !switches on DFT+U
LDAUTYPE = 2 !Dudarev method is performed
LDAUL = 2 -1 -1 -1 -1 -1 !angular momentum for each species
LDAUU = 20.0 0 0 0 0 0 !U (eV) for each species
LDAUJ = 18.1 0 0 0 0 0 !J (eV) for each species
LDAUPRINT = 0 !no onsite occupancy matrix is written to the OUTCAR file

! Exchange correlation treatment
GGA = PE !Perdew-Burke-Ernzerhof (PBE)
```

HS state

```
System = [Fe(ptz)6](BF4)2_HS

! Startparameter for this run:
PREC = normal !specifies the precision mode
ISPIN = 2 !spin polarized calculation
NUPDOWN = 12 !difference between up and down spin electrons
MAGMOM = 4 4 4 318*0.0 !sets initial magnetic moment for each atom
NCORE = 24 !the number of compute cores that work on an individual orbital
```

```
! Electronic Relaxation 1
ENCUT = 500 !cutoff energy for the plane-wave basis set (eV)
EDIFF = 1E-06 !stopping-criterion for ELM
LMAXMIX = 4 !max onsite mixed and CHGCAR, set to obtain fast convergence of d
↪ orbitals
LREAL = A !real-space projection
ALGO = All !specifies the electronic minimization algorithm
TIME = 0.05 !controls the time step
ISYM = 0 !switches off the use of symmetry
SYMPREC = 1E-06 !determines the accuracy of positions specified in the POSCAR
↪ file

! VDW correction
IVDW = 12 !DFT-D3 method with Becke-Johnson damping function

! DOS related values:
ISMEAR = 0 !sets partial occupancies for each orbital using gaussian smearing
SIGMA = 0.1 !sets the width of smearing

! Write flags
LWAVE = T !writes WAVECAR
LCHARG = F !does not write CHGCAR
LVTOT = F !does not write LOCPOT
LELF = F !does not write electronic localization function
LORBIT = 11 !writes the partial magnetization densities to the OUTCAR

! LDA+U
LDAU = T !switches on DFT+U
LDAUTYPE = 2 !Dudarev method is performed
LDAUL = 2 -1 -1 -1 -1 -1 !angular momentum for each species
LDAUU = 20.0 0 0 0 0 0 !U (eV) for each species
LDAUJ = 18.1 0 0 0 0 0 !J (eV) for each species
LDAUPRINT = 0 !no onsite occupancy matrix is written to the OUTCAR file

! Exchange correlation treatment
GGA = PE !Perdew-Burke-Ernzerhof (PBE)
```

A.6.3 Phonon calculations under PBE-D3(BJ)+U

LS state

```
System = [Fe(ptz)6](BF4)2_LS

! Startparameter for this run:
PREC = accurate !specifies the precision mode
```

```
ISPIN = 1 !non-spin polarized calculation

! Electronic Relaxation 1
ENCUT = 500 !cutoff energy for the plane-wave basis set (eV)
EDIFF = 1E-06 !stopping-criterion for ELM
LMAXMIX = 4 !max onsite mixed and CHGCAR, set to obtain fast convergence of d
↪  orbitals

! Phonon
EDIFFG = -1E-02 !stopping-criterion for IOM
NSW = 1 !number of ionic steps
IBRION = 6 !calculation of phonon frequencies with finite differences
NFREE = 2 !central differences
POTIM = 0.015 !the width of the displacement of each ion to calculate the
↪  Hessian Matrix
ISYM = 0 !switches off the use of symmetry

! VDW correction
IVDW = 12 !DFT-D3 method with Becke-Johnson damping function

! DOS related values:
ISMEAR = 0 !sets partial occupancies for each orbital using gaussian smearing
SIGMA = 0.1 !sets the width of smearing

! Write flags
LWAVE = F !does not write WAVECAR
LCHARG = F !does not write CHGCAR
LVTOT = F !does not write LOCPOT
LELF = F !does not write electronic localization function
LORBIT = 11 !writes the partial magnetization densities to the OUTCAR

! LDA+U
LDAU = T !switches on DFT+U
LDAUTYPE = 2 !Dudarev method is performed
LDAUL = 2 -1 -1 -1 -1 -1 !angular momentum for each species
LDAUU = 20.0 0 0 0 0 0 !U (eV) for each species
LDAUJ = 18.1 0 0 0 0 0 !J (eV) for each species
LDAUPRINT = 0 !no onsite occupancy matrix is written to the OUTCAR file

! Exchange correlation treatment
GGA = PE !Perdew-Burke-Ernzerhof (PBE)
```

HS state

```
System = [Fe(ptz)6](BF4)2_HS
```

```
! Startparameter for this run:
PREC = accurate !specifies the precision mode
ISPIN = 2 !spin polarized calculation
NUPDOWN = 12 !difference between up and down spin electrons
MAGMOM = 4 4 4 318*0.0 !sets initial magnetic moment for each atom

! Electronic Relaxation 1
ENCUT = 500 !cutoff energy for the plane-wave basis set (eV)
EDIFF = 1E-06 !stopping-criterion for ELM
LMAXMIX = 4 !max onsite mixed and CHGCAR, set to obtain fast convergence of d
↪  orbitals
ALGO = All !specifies the electronic minimization algorithm
TIME = 0.05 !controls the time step

! Phonon
EDIFFG = -1E-02 !stopping-criterion for IOM
NSW = 1 !number of ionic steps
IBRION = 6 !calculation of phonon frequencies with finite differences
NFREE = 2 !central differences
POTIM = 0.015 !the width of the displacement of each ion to calculate the
↪  Hessian Matrix
ISYM = 0 !switches off the use of symmetry
SYMPREC = 1E-06 !determines the accuracy of positions specified in the POSCAR
↪  file

! VDW correction
IVDW = 12 !DFT-D3 method with Becke-Johnson damping function

! DOS related values:
ISMEAR = 0 !sets partial occupancies for each orbital using gaussian smearing
SIGMA = 0.1 !sets the width of smearing

! Write flags
LWAVE = F !does not write WAVECAR
LCHARG = F !does not write CHGCAR
LVTOT = F !does not write LOCPOT
LELF = F !does not write electronic localization function
LORBIT = 11 !writes the partial magnetization densities to the OUTCAR

! LDA+U
LDAU = T !switches on DFT+U
LDAUTYPE = 2 !Dudarev method is performed
LDAUL = 2 -1 -1 -1 -1 -1 !angular momentum for each species
LDAUU = 20.0 0 0 0 0 0 !U (eV) for each species
LDAUJ = 18.1 0 0 0 0 0 !J (eV) for each species
```

```
LDAUPRINT = 0 !no onsite occupancy matrix is written to the OUTCAR file

! Exchange correlation treatment
GGA = PE !Perdew-Burke-Ernzerhof (PBE)
```

A.6.4 On-the-fly training of MLFF

LS state

```
! Startparameter for this run:
PREC = normal !specifies the precision mode
ISPIN = 1 !non-spin polarized calculation
NCORE = 4 !the number of compute cores that work on an individual orbital

! Electronic Relaxation 1
ENCUT = 500 !cutoff energy for the plane-wave basis set (eV)
EDIFF = 1E-05 !stopping-criterion for ELM
LMAXMIX = 4 !max onsite mixed and CHGCAR, set to obtain fast convergence of d
↪ orbitals
ISYM = 0 !switches off the use of symmetry
NELM = 100 !sets the maximum number of electronic self-consistency steps
LREAL = A !real-space projection

! VDW correction
IVDW = 12 !DFT-D3 method with Becke-Johnson damping function

! DOS related values:
ISMEAR = 0 !sets partial occupancies for each orbital using gaussian smearing
SIGMA = 0.1 !sets the width of smearing

! MD
IBRION = 0 !ab-initio molecular dynamics with verlet algorithm
NSW = 5000 !number of time steps, continues increasing to reach the target
↪ configuration number
POTIM = 2.0 !md time step in fs
ISIF = 3 !computes stress tensor and changes box volume/shape
MDALGO = 3 !uses Langevin thermostat
PSTRESS = 0 !controls the external pressure for the Parinello-Rahman barostat
TEBEG = 300 !sets temperature in K, changes to 100 K for further training
POMASS = 55.847 14.001 12.011 4.000 18.998 10.811 !mass of ions in amu
LANGEVIN_GAMMA = 10.0 10.0 10.0 10.0 10.0 10.0 !friction
LANGEVIN_GAMMA_L = 10 !lattice friction

! Machine Learning
ML_LMLFF = T !uses machine learning force fields
ML_MODE = train !on-the-fly training
```

```
ML_MB = 3000 !sets the maximum number of basis functions in the kernel
ML_SCLC_CTIFOR = 0.6 !sets how many local-reference configurations are added
↪  to the sparse representation of the kernel
ML_MHIS = 4 !sets the number of previous Bayesian errors that are used for
↪  the update of ML_CTIFOR, which sets the threshold for the Bayesian error
↪  estimation on the force
ML_MCONF_NEW = 2 !sets the number of configurations that are stored
↪  temporarily as candidates for the training data
ML_CX = 0.35 !adjusts update of ML_CTIFOR, sets to default for 100K training

! Write flags
LWAVE = T !writes WAVECAR
LCHARG = F !does not write CHGCAR
LVTOT = F !does not write LOCPOT
LELF = F !does not write electronic localization function
LORBIT = 11 !writes the partial magnetization densities to the OUTCAR

! LDA+U
LDAU = T !switches on DFT+U
LDAUTYPE = 2 !Dudarev method is performed
LDAUL = 2 -1 -1 -1 -1 -1 !angular momentum for each species
LDAUU = 20.0 0 0 0 0 0 !U (eV) for each species
LDAUJ = 18.1 0 0 0 0 0 !J (eV) for each species
LDAUPRINT = 0 !no onsite occupancy matrix is written to the OUTCAR file

! Exchange correlation treatment
GGA = PE !Perdew-Burke-Ernzerhof (PBE)
```

HS state

```
System = [Fe(ptz)6](BF4)2_HS

! Startparameter for this run:
PREC = normal !specifies the precision mode
ISPIN = 2 !spin polarized calculation
NUPDOWN = 12 !difference between up and down spin electrons
MAGMOM = 4 4 4 318*0.0 !sets initial magnetic moment for each atom
NCORE = 4 !the number of compute cores that work on an individual orbital

! Electronic Relaxation 1
ENCUT = 500 !cutoff energy for the plane-wave basis set (eV)
EDIFF = 1E-05 !stopping-criterion for ELM
LMAXMIX = 4 !max onsite mixed and CHGCAR, set to obtain fast convergence of d
↪  orbitals
ISYM = 0 !switches off the use of symmetry
NELM = 100 !sets the maximum number of electronic self-consistency steps
```

```
LREAL = A !real-space projection
ALGO = All !specifies the electronic minimization algorithm
TIME = 0.05 !controls the time step

! VDW correction
IVDW = 12 !DFT-D3 method with Becke-Johnson damping function

! DOS related values:
ISMEAR = 0 !sets partial occupancies for each orbital using gaussian smearing
SIGMA = 0.1 !sets the width of smearing

! MD
IBRION = 0 !ab-initio molecular dynamics with verlet algorithm
NSW = 6000 !number of time steps, continues increasing to reach the target
↪  configuration number
POTIM = 2.0 !md time step in fs
ISIF = 3 !computes stress tensor and changes box volume/shape
MDALGO = 3 !uses Langevin thermostat
PSTRESS = 0 !controls the external pressure for the Parinello-Rahman barostat
TEBEG = 300 !sets temperature in K
POMASS = 55.847 14.001 12.011 4.000 18.998 10.811 !mass of ions in amu
LANGEVIN_GAMMA = 10.0 10.0 10.0 10.0 10.0 10.0 !friction
LANGEVIN_GAMMA_L = 10 !lattice friction

! Machine Learning
ML_LMLFF = T !uses machine learning force fields
ML_MODE = train !on-the-fly training
ML_MB = 3000 !sets the maximum number of basis functions in the kernel
ML_SCLC_CTIFOR = 0.6 !sets how many local-reference configurations are added
↪  to the sparse representation of the kernel
ML_MHIS = 4 !sets the number of previous Bayesian errors that are used for
↪  the update of ML_CTIFOR
ML_MCONF_NEW = 2 !sets the number of configurations that are stored
↪  temporarily as candidates for the training data
ML_CX = 0.35 !adjusts update of ML_CTIFOR

! Write flags
LWAVE = T !writes WAVECAR
LCHARG = F !does not write CHGCAR
LVTOT = F !does not write LOCPOT
LELF = F !does not write electronic localization function
LORBIT = 11 !writes the partial magnetization densities to the OUTCAR

! LDA+U
LDAU = T !switches on DFT+U
```

```
LDAUTYPE = 2 !Dudarev method is performed
LDAUL = 2 -1 -1 -1 -1 -1 !angular momentum for each species
LDAUU = 20.0 0 0 0 0 0 !U (eV) for each species
LDAUJ = 18.1 0 0 0 0 0 !J (eV) for each species
LDAUPRINT = 0 !no onsite occupancy matrix is written to the OUTCAR file

! Exchange correlation treatment
GGA = PE !Perdew-Burke-Ernzerhof (PBE)
```

A.7 Python Script for ML-Driven MD simulations

```
from ase.io import read, write
from ase.io.trajectory import Trajectory
from ase.calculators.vasp import Vasp
from ase.calculators.mixing import  MixedCalculator, MixedSCOCalculator
from ase import units
from ase.md.velocitydistribution import MaxwellBoltzmannDistribution,
    Stationary
from ase.md.npt import NPT
import numpy as np
import pandas as pd

timestep = 2.0  # fs
timescale = 20.0  # ps
nsteps = int(1000 * timescale / timestep)
temperature_list = list(range(50, 260, 10))  # Temperature in Kelvin, warm
    up from 50 to 260 K with increments of 10 K.
pressure = 1.0  # Enternal pressure in bar
ttime = 20.0  # Time constant in fs
pfactor = 2e6  # Barostat parameter in GPa

# Indexes of atoms
Fe2 = 1
N_indexes = [9, 10, 11, 12, 13, 14] # N7 to N12

# Set up the initial configuration
atoms = read('POSCAR')

# VASP Calculator
calcLS = Vasp(
        kpts=1,
        xc='PBE',
        prec='Normal',
        encut=500.0,
        ediff=1.0e-6,
        lreal='Auto',
        isym=0,
        ismear=0,
        sigma=0.1,
        ml_lmlff=True,
        ml_istart=2,
        lwave=False,
```

```
        lcharg=False,
        lvtot=False,
        lelf=False,
        lorbit=11,
        nsw=1,
        ibrion=-1,
        directory='./LS',
        txt='vasp.out')

calcIS = Vasp(
        kpts=1,
        xc='PBE',
        prec='Normal',
        encut=500.0,
        ediff=1.0e-6,
        lreal='Auto',
        algo='All',
        time=0.05,
        isym=0,
        ismear=0,
        sigma=0.1,
        ml_lmlff=True,
        ml_istart=2,
        lwave=False,
        lcharg=False,
        lvtot=False,
        lelf=False,
        lorbit=11,
        nsw=1,
        ibrion=-1,
        directory='./IS',
        txt='vasp.out')

calcHS = Vasp(
        kpts=1,
        xc='PBE',
        prec='Normal',
        encut=500.0,
        ediff=1.0e-6,
        lreal='Auto',
        algo='All',
        time=0.05,
        isym=0,
        symprec=1.0e-6,
        ismear=0,
        sigma=0.1,
        ml_lmlff=True,
        ml_istart=2,
        lwave=False,
        lcharg=False,
        lvtot=False,
        lelf=False,
        lorbit=11,
        nsw=1,
```

```
94          ibrion=-1,
95          directory='./HS',
96          txt='vasp.out')
97
98  calc = MixedCalculator(calcHS, calcIS, calcLS, 0.015)
99
100 for temperature in temperature_list:
101     # Set the momenta corresponding to temperature
102     MaxwellBoltzmannDistribution(atoms, temperature_K=temperature)
103     Stationary(atoms)
104
105     # Set up NPT dynamics
106     dyn = NPT(atoms,
107               timestep=timestep * units.fs,
108               temperature_K=temperature,
109               externalstress=pressure * units.bar,
110               ttime = ttime * units.fs,
111               pfactor = pfactor * units.GPa * (units.fs**2)
112               )
113
114     energy = []
115     structure = []
116
117     def save_energy(a=atoms):  # store energy and temperature to atoms in
    the definition.
118         """Function to save the temperature, potential, kinetic and total
    energy."""
119         imd = dyn.get_number_of_steps()
120         temp_K = a.get_temperature()
121         epot = a.get_potential_energy()
122         ekin = a.get_kinetic_energy()
123         etot = a.get_total_energy()
124         energy.append([imd, temp_K, epot, ekin, etot])
125
126     def save_structure(a=atoms):  # store structure to atoms in the
    definition.
127         """Function to save the lattice, volume and metal-ligand bond
    lengths."""
128         imd = dyn.get_number_of_steps()
129         lattice = a.get_cell_lengths_and_angles()
130         volume = a.get_volume()
131         MLbondlength = np.mean([a.get_distance(Fe2, N) for N in N_indexes])
132         structure.append([imd, lattice, volume, MLbondlength])
133
134     # Save trajectory
135     traj = Trajectory('md.traj', 'w', atoms)
136     dyn.attach(traj.write, interval=100)
137
138     # Now run the dynamics
139     for j in range(nsteps // 100):
140         atoms.calc = calc
141         dyn.run(100)
142         save_energy(atoms)
143         save_structure(atoms)
```

```
144         # Save POSCAR for each step
145         poscar = f'POSCAR_{j+1}_{int(temperature)}K'
146         write(poscar, atoms)
147 
148     # Convert energy and structure to DataFrame and save to CSV
149     energy_df = pd.DataFrame(energy, columns=['Steps', 'Temperature (K)', '
    Potential Energy (eV)', 'Kinetic Energy (eV)', 'Total Energy (eV)'])
150     structure_df = pd.DataFrame(structure, columns=['Steps', 'Lattice
    Parameters', 'Volume', 'Fe-N Bond Length'])
151     energy_df.to_csv(f'energy_{int(temperature)}K.csv', index=False)
152     structure_df.to_csv(f'structure_{int(temperature)}K.csv', index=False)
```

All theory, dear friend, is grey, but the golden tree of actual life springs ever green.

Johann Wolfgang von Goethe,
Faust